ARABIDOPSIS THALIANA SYTA AS A MODEL TO ADDRESS WHETHER SYNAPTOTAGMIN PROTEINS FUNCTION AS DIMERS OR TETRAMERS

A Dissertation
Presented to the Faculty of the Graduate School
Of Cornell University
In Partial Fulfillment of the Requirements for the Degree of
Doctor of Philosophy

By
Gregory Chandler Ray
May 2014

ARABIDOPSIS THALIANA SYTA AS A MODEL TO ADDRESS WHETHER SYNAPTOTAGMIN PROTEINS FUNCTION AS DIMERS OR TETRAMERS

Gregory Chandler Ray, Ph.D.

Cornell University, 2014

ABSTRACT

The *Arabidopsis thaliana* synaptotagmin SYTA (AT2G20990) regulates endocytosis at the plasma membrane and virus movement protein-mediated cell-to-cell movement. As with all synaptotagmin proteins, SYTA is predicted to consist of a transmembrane domain, a cytosolic variable domain, and two calcium/lipid binding domains (C_2A and C_2B) at its COOH-terminus. Deletion of the C_2B domain abolishes SYTA function. The C_2B deleted mutant of SYTA also acts as a dominant-negative mutant as evidenced by its interference with endogenous, wild-type SYTA. This finding is consistent with the unproven hypothesis that synaptotagmin proteins in animals potentially function as dimers or tetramers. However, the existence of a SYTA C_2B domain in plants that is functionally similar to those in animal synaptotagmins has been questioned by some research groups. In this project, I utilized molecular modeling to predict how a homodimer of SYTA may function, and cell-based functional assays and *in vitro* biochemical approaches to demonstrate the relevance of the model I created. I modeled SYTA-C_2B to explain how the C_2B domains from the individual proteins within a dimer could function to bind calcium. I demonstrated that key residues from this model (E430, D431, and E433) were functionally relevant by expressing alanine point mutants of each in protoplasts and observing that they did not localize to endosomes effectively. My research was consistent with the prediction that E430 and D431 are essential for SYTA function, possibly forming the core of a calcium-binding site. Although it is not essential in this activity, I also concluded that E433 may improve the calcium-sensing ability of C_2B. By utilizing dynamic and static light scattering, I observed that purified SYTA is a dimer, which indicated calcium binding via the C_2B domain is not required for the formation of this dimer. This research is the first direct observation of a synaptotagmin protein, plant or animal, forming a dimer.

BIOGRAPHICAL SKETCH

Gregory Ray was born and raised in Pittsburgh, Pennsylvania. He graduated from Shady Side Academy in 2004. Greg enrolled at Hamilton College in Clinton, New York and graduated in 2008 earning a Bachelor of Arts with a major in Biochemistry and Molecular Biology and a minor in Environmental Studies. As a component of his undergraduate studies, Greg attended the University of Limerick in Ireland and the University of Pittsburgh in Pennsylvania as a visiting student. In September 2008, Greg enrolled in the Biochemistry, Molecular and Cell Biology PhD program at Cornell University in Ithaca, NY and currently has an anticipated completion date of February 2014. Greg is continuing his education by pursuing an MBA from the Rotman School of Management at the University of Toronto in Canada.

ACKNOWLEDGEMENTS

This research project would not have been possible without the support and assistance of numerous individuals and resources largely at Cornell University. The following have all contributed significantly to this project: Sondra Lazarowitz (Research Advisor and Special Committee Member), Colin Parrish (Virology Training Grant and Special Committee Member), Volker Vogt (Special Committee Member), June Nasrallah (Special Committee Member), Asako Uchiyama (Postdoctoral Fellow, Lazarowitz Group), Harumi Shimada-Beltran (Postdoctoral Fellow, Lazarowitz Group), Amit Levy (Postdoctoral Fellow, Lazarowitz Group), Judy Zheng (Lab Technician, Lazarowitz Group), Daniel Rippol (Cornell Center for Advanced Computing), Carol Bayles (Microscopy and Imaging Facility), Gerald Feigenson (Technical and Procedural Support), Holger Sondermann (Technical and Procedural Support), Yuxin Mao (Technical and Procedural Support), Leila Toulabi (Technical and Procedural Support), FoSheng Hsu (Technical and Procedural Support), Timothy Huffaker (Technical and Procedural Support), Beth Lalonde (Technical and Procedural Support), Doug Ray (Graphics and Revision Support), Judith Ray (Revision Support) and Richard Ray (Revision Support).

TABLE OF CONTENTS

LIST OF FIGURES

LIST OF TABLES

LIST OF ABBREVIATIONS

C_2A	Synaptotagmin C_2A Domain
C_2B	Synaptotagmin C_2B Domain
Ca^{2+}	Soluble Calcium Ion
$CaCl_2$	Calcium Chloride
EGTA	Ethylene Glycol Tetraacetic Acid
ER	Endoplasmic Reticulum
ESCRT	Endosomal Sorting Complexes Required for Transport
FPLC	Fast Protein Liquid Chromatography
GFP	Green Fluorescent Protein
IPTG	Isopropyl β-D-1-Thiogalactopyranoside
LOMETS	Local Meta-Threading-Server
MP	Viral Movement Protein
NSP	Viral Nuclear Shuttling Protein
PD	Plasmodesmata
pKa	Acid Dissociation Constant
PM	Plasma Membrane
PS	Phosphatidylserine
RASP	Rapid Side-chain Predictor
RCSB	Research Collaboratory for Structural Bioinformatics
SCOP	Structural Classification of Proteins
SDS	Sodium Dodecyl Sulfate
SDS-PAGE	SDS Polyacrylamide Gel Electrophoresis
SNARE	Soluble N-Ethylmaleimide-Sensitive Factor Attachment Protein Receptor
SqLCV	Squash Leaf Curl Virus
SYT	Synaptotagmin
SYTA	*Arabidopsis* Synaptotagmin A
SYTC	*Arabidopsis* Synaptotagmin C
SYTE	*Arabidopsis* Synaptotagmin E

SYT1	Mammalian Synaptotagmin 1
SYT2	Mammalian Synaptotagmin 2
T-DNA	Transfer DNA from *Agrobacterium* tumor inducing (Ti) plasmid
TM	Transmembrane Domain
TMV	Tobacco Mosaic Virus
VD	Variable Domain

CHAPTER 1
Background and Significance

Introduction:

Plant viruses can cause many plant diseases, leading to billions of dollars in crop losses each year (Hull, 2009). The loss of crop yields could also be an underlying cause of humanitarian crises in developing and impoverished regions of the world, leading to famines and displacement of starving populations.

The more that is understood about how plant viruses function, the more plant viruses can be controlled. Presently, virus research at the cellular level is focused on viral-encoded proteins and on the host proteins that viruses hijack. Every protein and chemical reaction involved in the course of the infectious cycle of a virus has the potential to become the target of an antiviral strategy. Research and development of antiviral drugs for human and animal viruses have traditionally sought to disrupt viral processes and proteins (Emini & Fan, 1997). The same approach in plants has the potential to minimize the economic, political, and humanitarian issues caused by plant virus infections.

Synaptotagmin A (SYTA) from *Arabidopsis thaliana* (Thale Cress) is a plant protein involved in viral infections. Functional SYTA facilitates efficient viral translocation between adjacent cells through its interactions with viral movement proteins. The Lazarowitz research group has demonstrated the significance of this interaction with multiple distinct plant viruses (Lewis & Lazarowitz, 2010;

Uchiyama *et al*, 2010). Additionally, the Lazarowitz group has shown SYTA to be a regulator of both endocytosis at the plasma membrane and the recycling of endosomes to the plasma membrane in uninfected cells (Lewis & Lazarowitz, 2010). It is hypothesized that these viruses are piggybacking on SYTA as a means to reach the cell periphery.

Components of the virus are currently understood to move between cells by interacting with the host's SYTA protein as it is recycled to the plasma membrane within the context of endosome recycling (Lewis & Lazarowitz, 2010). In both viral movement and endocytic recycling of SYTA, evidence strongly suggests that the C_2B domain of SYTA is required for the protein to function (Littleton *et al*, 2001). Researchers, who have studied synaptotagmin proteins from other organisms, have disputed this requirement. A competing hypothesis proposes SYTA is fundamentally different in its function than the better studied synaptotagmins from other organisms (Schapire *et al*, 2008).

Plant viral disease:

The impact of plant virus infections can be quantified in terms of crop losses, which can reach billions of dollars. The consequences of these viruses have other broad social and environmental impacts as well (Anderson *et al*, 2004). An anticipated effect of increasing human population, particularly in countries with land issues, such as India and Egypt, is an increased strain on

affordable food supplies (Almeida, 2013). To meet the demand of feeding a global population, which is predicted to be over 9 billion by 2050, either the productivity of lands that are currently arable needs to increase or undeveloped land must be converted from a natural to arable state, which may be a particular challenge as low lying lands are also at risk of being lost to rising seas (Japan Times, 2013). Should no improvements be made in food production, a higher percentage of the human population will be forced to subsist on an insufficient diet. Mitigating the impact of plant viruses through control or containment is a means to increase the productivity of the agricultural industry.

By using antiviral strategies to aid in minimizing a significant global threat, researchers need to understand how plant viruses function and how they interact with their hosts. Targets could be identified and techniques could be developed that restrict plant viruses. The development of these targets and techniques could lead to the commercial production of chemicals and/or disease-resistant genetically-modified plants, which would assist agriculturists in defending against crop failure caused by plant viruses.

Currently, the presence of viruses in plants is detected by either the appearance of one or more specific symptoms or by an assay for viral material. Viral symptoms, such as distortion of leaves, stunted growth, or abnormal fruiting are easily observable on the infected host plants and can render entire harvests

inedible or worthless (Hull, 2009). The potential benefits of host-virus interaction research include the mitigation or prevention of viral symptoms and the resultant crop loss.

Plant virus infection:

Many different families and species of plant viruses exist. Most of these viruses share similar strategies to successfully infect a plant cell. Plant viruses must find a way to bypass the rigid cell wall, which is a physical barrier to viruses moving between adjacent plant cells (Benitez-Alfonso *et al*, 2010). Without a means of egress, the plant cell is analogous to a prison cell for a virus. Another major obstacle for plant viruses is to reach and infect new host plants. Because of the stationary nature of plants, two hosts are unlikely to come into contact to spread a virus directly. Instead, another agent is necessary for this transmission.

Figure 1-1 details a simplified course of viral infection. While the specific details vary from one virus to another, some key features are common among many viruses. A plant virus can be physically introduced into a cell of a host plant by a biological vector (e.g. insect) or by mechanical means (e.g. gardening tool). In the case of insect transmission, the virus may simply be carried in the mouthparts of the insect. However, the vector-virus interaction can be more complex for several virus-vector pairs. Some viruses will enter the gut of vectors and ultimately localize to and accumulate in the vector's salivary glands. From

these glands, the virus will be introduced with sufficient titer to infect a new host (Blanc *et al*, 2011). Some viruses, including plant Rhabdoviruses, are particularly noteworthy because research has shown these viruses are able to replicate in both the host plant and in the insect vector (Jackson *et al*, 2005). Viruses spread from host to host with great diversity and specificity. The prevention of viral spread may also be diverse and specific through use of effective pesticides to halt vector transmission and by good agricultural practices to inhibit manual transmission.

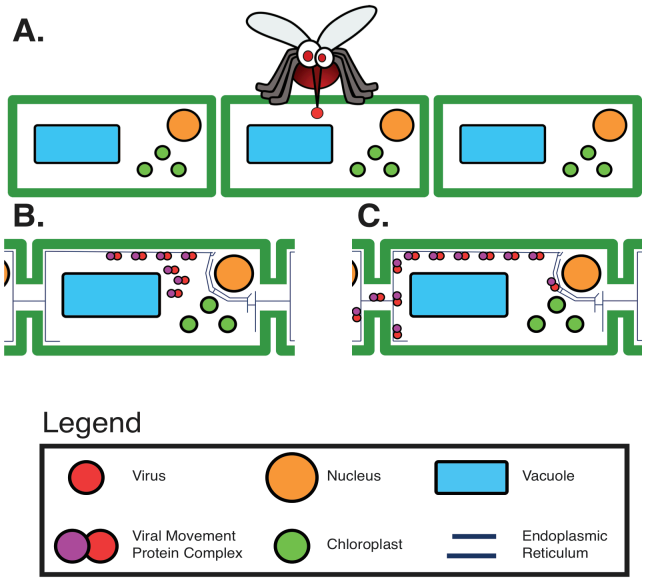

Figure 1-1: **Simplified plant virus infection**. (A) An insect vector introduces a virus into a host cell by penetrating the cell wall with the vector's mouthparts. Some viruses are introduced by mechanical means, such as a garden tool, instead of by vector. (B) Once in the cell, the virus is uncoated and replicates at a site of viral replication in the cell specific to that virus. Viral genome-encoded proteins will be expressed. (C) The virus moves locally from one cell to an adjacent cell by using various membrane compartments (ER and endosomes have been implicated) in the plant cell to localize to plasmodesmata. The virus then exploits plasmodesmata, to move into the adjacent cell, thereby creating a local infection. Once the virus reaches vascular tissue, the infection can become systemic.

After transmission, the virus uncoats in the newly infected host cell. The viral genome utilizes the host cell's biosynthesis machinery, including the use of nucleic acid polymerases, to begin replicating and expressing its genes in a highly regulated manner in order to copy genomes and produce messenger RNA (mRNA). Further, the host's ribosomes synthesize viral proteins from these mRNA transcripts. Depending on the specific virus and the requirements for its replication, the virus may localize within the cytosol or the nucleus (Morozov & Solovyev, 2003; Ingham *et al*, 1995; Citovsky, 1999). Some viruses, including Geminiviruses, rely on DNA replication and transcription machinery in the nucleus. Other viruses, such as Potexviruses, will create inclusions within the cell that aid in their ability to replicate in the cytosol. These complexes are hypothesized to shelter the replicating virus from the host cell's defense response (Tilsner *et al*, 2011). While these "X-bodies" have long been observable (Kassanis, 1939), high-resolution imaging has only recently been able to suggest how viral and host proteins may interact to facilitate replication within a viral replication complex (Solovyev *et al*, 2012). Specifically, in the case of Potato Virus X, the core of the X-body contains rearranged endoplasmic reticulum and viral proteins implicated in replication (TGB2 and TGB3). These X-bodies are surrounded by both viral RNA and encapsulated virions that are proposed to protect the site of replication (Linnik *et al*, 2013). Because of the diversity in viral replication, replication is likely difficult to target without knowing the replication strategy of a virus.

Following replication and in order to spread the infection, a virus must be able to travel to and infect new host cells. The walls that separate adjacent plant cells act as physical barriers to the spread of viruses and other pathogens. To overcome this barrier to virus movement, plant viruses encode and express one or more movement proteins that allow the virus to exploit the small transwall pores, plasmodesmata (PD), that connect adjacent cells (Zambryski & Crawford, 2000; Schoelz *et al*, 2011; Ueki & Citovsky, 2011). Because cell-to-cell movement is a common feature of plant viruses, cell-to-cell movement is a desirable process to target in order to inhibit plant virus infections.

In healthy plants, PD are gated in a highly regulated manner. Although the maximum size of particles that can pass through PD is somewhat variable, PD do have a fairly small size exclusion limit of approximately 50 kDa (Oparka *et al*, 1999). This size limitation means that PD must be actively regulated to facilitate the transfer of macromolecules between cells. For comparison, a TMV genome has a molecular weight of 2.2 MDa (Caspar, 1963), which is 2 orders of magnitude greater than the size limit of the PD. Without assistance, it would be impossible for an unmodified virion to pass through an average PD.

In addition to molecular weight, hydrodynamics influence the ability of macromolecules to pass through PD (Oparka & Roberts, 2001). Specifically,

molecules that have lower surface area relative to molecular weight (are more spherical) will be more restricted in their ability to move. An unstructured (linear) molecule (nucleic acid or protein) would find less resistance to movement than a folded (globular) molecule. This is analogous to threading a needle: an unknotted thread will pass through the eye; however, introducing a knot will make the thread too big to pass through the eye. Unfolded proteins are not favorable and can lead to aggregation and protein degradation (Kurepa & Smalle, 2008). Were a virus to unfold proteins associated with its genome, the infected cell might become severely stressed. From the perspective of a virus, this would be a particularly risky proposition because stress can also trigger the innate immune response of the plant cell (Dangl & Jones, 2001) resulting in an additional obstacle to viral movement. Because of the limitations on the size and hydrodynamics, all plant viruses must modify the PD in order to move between cells, and one function of the viral cell-to-cell movement proteins is to modify the PD for the benefit of the virus.

Viral genomes must be able to localize to the modified PD to utilize modified PD to spread infection locally. Because the volume of a plant cell is orders of magnitude larger than a nucleoprotein complex, it is inefficient for the virus to rely on free diffusion as opposed to facilitated diffusion along ER. Evidence suggests that, at least in the case of TMV, that the viral cell-to-cell movement protein is responsible for allowing the facilitated diffusion along ER in

addition to modifying the PD (Epel, 2009). To spread a local infection, plant viruses travel to and penetrate the PD with the aid of the movement proteins (MPs)[1] that they encode. Without the aid of MPs, exiting a plant cell would be a Herculean task for viruses.

At or near the site of replication, the replicating virus will form either a complete virion or a viral nucleoprotein complex that consists of a genome and proteins necessary for propagating infection including, but not limited to the cell-to-cell MP. Geminiviruses, for example, encode two movement proteins in their genome. One movement protein facilitates the cell-to-cell movement. The other, NSP (formerly BR1) allows the DNA genome to enter and exit the nucleus for DNA replication in the new host cell (Sanderfoot *et al*, 1996). Regardless of form, such a complex establishes an infection in the adjacent cells with the necessary help of its MP(s), ultimately leading to the local spread of the virus within the tissue. Once a plant virus spreads as far as the vascular tissue, the virus can disseminate throughout the plant resulting in a systemic infection (Hull, 2009; Harries & Ding, 2011). As the systemic infection spreads within a plant, it is more likely to be acquired by another viral vector, allowing the virus to spread throughout the population. Without the action of the MP, a virus would not be able do too much damage to the host and ultimately to the population. MP-directed

[1] In this report "MP" will specifically refer to the cell-to-cell movement proteins of plant viruses. Some plant viruses encode other movement proteins that are necessary for other virus translocation events, such as nuclear shuttling.

cell-to-cell movement through the PD is an important potential target to combat plant viruses.

The plasmodesmata:

Plasmodesmata are important direct connections between adjacent plant cells. Evidence of plant viruses exploiting them to move has been available for decades (De Zoeten & Gaard, 1969). More recent studies established that PD are actively regulated connections and have established the extent to which they are active (Oparka *et al*, 1999). The current consensus is that PD regulate the exchange of various macromolecules, small molecules, and ions between adjacent cells. The resulting molecular gradient is necessary for essential plant functions including growth, development, and defense (Maule *et al*, 2011; Xu & Jackson, 2010). PDs are formed when a plant cell divides but maintains a continuous ER connection between the resulting daughter cells at the time of division (Zambryski, 2004). New cell walls are deposited around the ER connections after division. A simplified, but unproven, model of PD formation could be described as portions of ER that remain attached at the cell plate when two cells divide. When a cellulose cell wall is deposited between the two daughter cells, the leftover portions of ER create a pore that becomes a plasmodesma. This model fails to explain the complexity and branching seen in many PD; other, perhaps more accurate, models are yet to be tested (Maule *et al*, 2011; Faulkner *et al*, 2008).

Regardless of conditions of PD formation, PD consist of three essential components. First, a continuous PM connection between the cells creates a continuous membrane connection between the cells establishing an ongoing cytosolic connection. Second, a central rod, known as the desmotubule, is derived from the ER when the PD forms. Third, the rigid cell wall surrounding the PD exerts size constraints on the PD (Maule, 2008; Zambryski, 2004) (Figure 1-2). In addition to these three components, other structural proteins are present at PD, although their functions at the PD are generally not well understood.

Movement proteins:

Viral movement proteins are essential for plant viruses to spread from an infected cell to an adjacent cell. MPs, such as the 30K protein from *Tobacco mosaic virus* (TMV), are able to facilitate the movement of a plant virus by targeting viral genomes to PD and changing the regulation or relative functional impact of proteins at PD (Guenoune-Gelbart *et al*, 2008). Among the suggested PD modifications that may increase the permeability of PD is the depletion of callose in the neck region of the PD by β-1,3-glucanase (Ueki *et al*, 2010). Some uncertainty exists regarding the role of the desmotubule in PD gating (Zavaliev *et al*, 2011; Ueki *et al*, 2010; Botha & Cross, 2000; Iglesias & Meins, 2000). Ueki *et al*. demonstrated that the 30K MP of TMV co-localized with an ankyrin repeat containing protein (ANK) at PD, and that when both were expressed, activity of β-

1,3-glucanase increased and levels of callose at PD decreased (Ueki *et al*, 2010). Further, plants without β-1,3-glucanase, and, therefore, permanent callose deposits are less susceptible to viral disease (Beffa *et al*, 1996). Expanding on this work, it is possible that movement proteins alter the function or relative activity of many proteins at the PD.

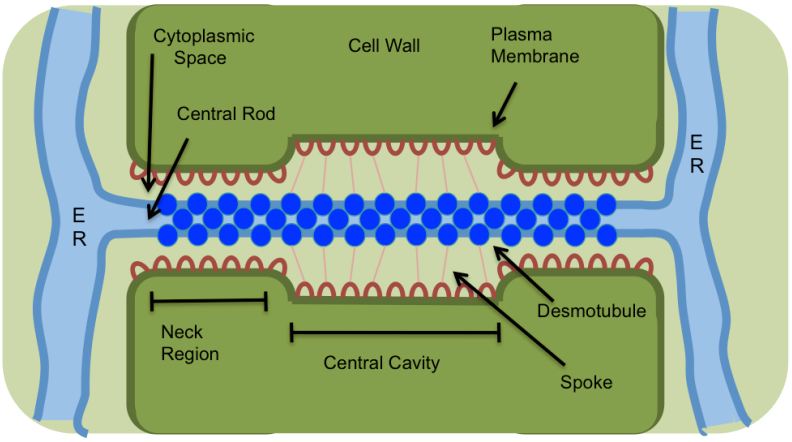

Figure 1-2: **Plasmodesmata are direct connections between adjacent plant cells**. Plasmodesmata are symplasmic connections between two adjacent cells. PD allow for the transport of both small molecules and macromolecules between the cells to occur. The ER of the two cells is connected by the desmotubule in the core of the PD. While PD have direct ER connections (central rod), the majority of exchange is thought to pass through the cytosolic space around these connections. Virus movement proteins for cell-to-cell movement target PD. The specific interactions between viral movement proteins and PD that allow viruses to exploit PD remain unclear. Based on Zambriski, 2004.

Having evolved at only limited recombination, MPs do not represent a single family of proteins but instead are distinct to specific different clades of plant viruses (Mushegian & Koonin, 1993). For example, the 30K movement protein of TMV, a positive-sense (+)RNA Tobamovirus, is not closely related to either of the two movement proteins (MP or NSP) of the DNA Geminiviruses. These movement proteins include those of *Cabbage leaf curl virus* (CaLCuV),

which were mentioned in this report (Mushegian & Koonin, 1993). The Tobamovirus and Geminivirus movement proteins are distinct in sequence when compared to the triple gene block (TGB) proteins that originate from the Potyvirus family, Potexvirus family, and other virus families (Schoelz *et al*, 2011; Taliansky *et al*, 2008; Morozov & Solovyev, 2003). Taken as a group, the MPs from DNA and RNA plant viruses are an example of either or both recombination and convergent evolution. This occurs when proteins of unrelated origin have gained like function over many generations and/or when ancient recombinations have diverged significantly (Mushegian & Koonin, 1993). In addition to the movement proteins that play a role in translocation across the cell wall, some viruses, such as the Geminiviruses, encode additional movement proteins to facilitate intracellular translocation. In the DNA Geminiviruses, the nuclear shuttle protein (NSP) cycles the viral genome between the nucleus, where it replicates using the host DNA replication machinery, and the cytosol, adding two additional steps to their viral lifecycles, specifically, the transit of viral genomes into and out of the nucleus (Sanderfoot *et al*, 1996; Ward & Lazarowitz, 1999). NSP and MP interact in the cytoplasm of Geminivirus-infected cells. As a consequence of MP interaction with other cellular macromolecules, MP ensures that NSP-ssDNA complexes are actively trafficked to the cell periphery and are translocated into an adjacent cell through PD (Sanderfoot *et al*, 1996).

Because there are distinct viral movement proteins, it is not a given that all movement proteins should target an identical set of host proteins. Still, because these movement proteins do have functional overlap, it is not surprising that there are host proteins that are targeted by many viral movement proteins (Ding, 2009; Harries & Ding, 2011). Because diverse viruses target the PD for cell-to-cell movement, proteins involved with PD structure or function should be common viral targets. To be able to develop strategies to broadly inhibit infection by a range of plants viruses, finding common host proteins to target is necessary. Various research groups have undertaken screening for interactions between movement and host proteins.

Synaptotagmin A interacts with diverse movement proteins:

Lewis and Lazarowitz identified a fragment of the Synaptotagmin A (SYTA) protein from *Arabidopsis thaliana* as having a direct interaction with the cell-to-cell movement protein of CaLCuV in a yeast SRS screen. They demonstrated, using an *in vitro* GST-SYTA$^{\Delta TM}$ pull-down assay, that the cell-to-cell movement proteins from two Geminiviruses, CaLCuV and *Squash leaf curl virus* (SqLCV), bind directly with SYTA. The GST- SYTA$^{\Delta TM}$ pulled down both of these cell-to-cell movement proteins but had no effect on the luciferase control. This observation indicated that binding with SYTA was a general feature of Geminivirus family cell-to-cell movement proteins. Further, they showed that SYTA and the 30K MP from TMV also directly bind with each other using the

same GST- SYTA$^{\Delta TM}$ pull-down assay (Lewis & Lazarowitz, 2010). This finding suggested that unrelated families of viruses could have converged upon and exploited the same pathway to spread infection.

Given the potential of being a broad viral target, SYTA is a particularly favorable candidate for functional study. Lewis and Lazarowitz assayed the effect of SYTA on systemic viral infection to demonstrate the biological relevance of the SYTA-MP interaction. In their assay, an *Arabidopsis* T-DNA insertion line (*syta-1*) was infected with various viruses. The *syta-1* line is about 90% knocked down in its expression of SYTA. In *syta-1* a premature stop on the C-terminal side of the C_2B domain of SYTA exists (Figure 1–3). However, even with the truncation and only 10% expression, *syta-1* homozygote plants had no obvious phenotype under normal short and long day growth conditions (Lewis & Lazarowitz, 2010). Still, no null (knockout) line of SYTA is available (Lewis & Lazarowitz, 2010). The absence of a null mutant allowed Lewis and Lazarowitz to conclude that SYTA is an essential *Arabidopsis* protein and that the *syta-1* protein may be able to fill the same essential role in development. They measured the viral infectivity within the *syta-1* line and compared it to the infectivity in wild-type *Arabidopsis* with 100% endogenous SYTA expression level. The appearance of systemic symptoms caused by the Geminivirus, Tobamovirus, and Potyvirus family viruses were delayed and attenuated in the *syta-1* mutant plants as compared with the wild-type *Arabidopsis* control line (Col-0*)* indicating a differential response to viral

stress. When *syta-1* was assayed with a *Caulimovirus*, the delay and attenuation of symptoms was not observed (Lewis & Lazarowitz, 2010; Uchiyama *et al*, 2014). This data further implicated SYTA as playing an important role in the lifecycle of many unrelated plant viruses.

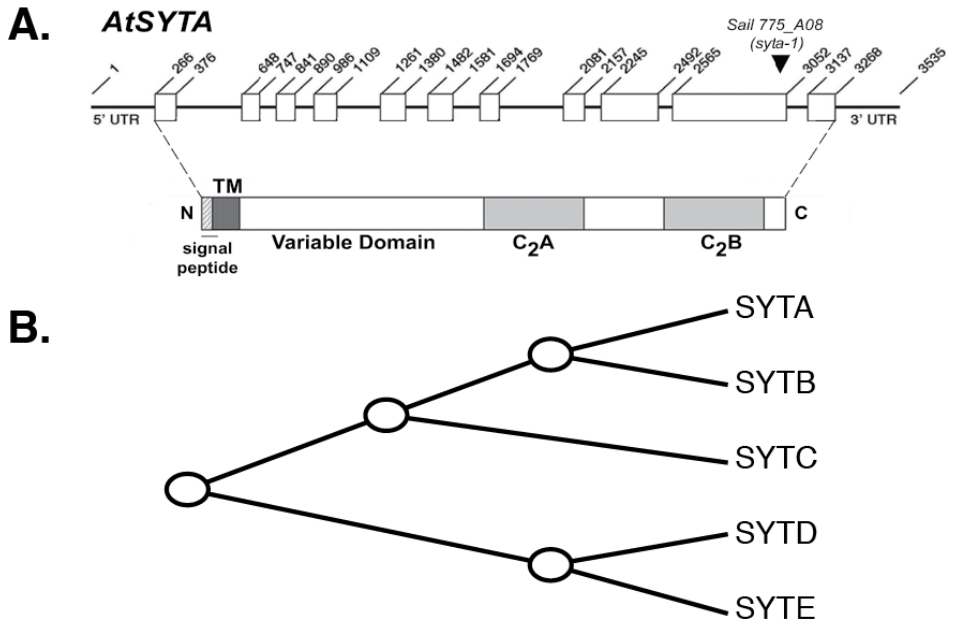

Figure 1-3: ***Arabidopsis* synaptotagmin genes and proteins**. (A) *At*SYTA gene schematic showing the relative size and arrangement of the exons (boxes) that form coding sequence. The position of the T-DNA insert in the C-terminal region of the *syta-1* mutant line is indicated above the 3' end of the gene with an arrow. Below the gene is a diagram of SYTA protein. The protein model shows the relative positions of the domains that define SYTA as being a synaptotagmin Specifically, the structure consists of an uncleaved N-terminal signal peptide, a single transmembrane domain (TM), a cytosolic variable domain, and two Ca^{2+}-lipid binding domains, C_2A and C_2B, at the C-terminal. From Lewis and Lazarowitz, 2010. (B) Paralog tree based upon the homology within the *Arabidopsis* synaptotagmin gene family. There are five *Arabidopsis* synaptotagmin genes, SYTs A–E, that are named based upon their similarity to SYTA.

Observing the effect of the SYTA knockdown on systemic infection indicated that SYTA has a role in viral infection. However, the assay was not sufficient to answer the question of where in the viral lifecycle SYTA was

interacting with the virus and where the virus was stymied. Given that SYTA directly interacted with distinct MPs, the hypothesis was that the scarcity of SYTA was limiting cell-to-cell movement. Lewis and Lazarowitz employed a cell-to-cell MP movement assay to observe the local spread of GFP-tagged MPs from TMV and from CaLCuV in agro-infiltrated *Nicotiana benthamiana* leaves to confirm that the SYTA-MP interactions are biologically relevant for cell-to-cell movement (Lewis & Lazarowitz, 2010). In this assay, the MP was co-infiltrated with wild-type SYTA, or with one of two potential dominant-negative SYTA mutants.

The first SYTA mutant had the N-terminal transmembrane domain removed (ΔTM), the hypothesis being that it would mislocalize to the cytosol and competitively inhibit MP. By binding competitively to the overexpressed $SYTA^{\Delta TM}$, the MP would be prevented from localizing to the cell periphery through its interactions with the endogenous membrane bound SYTA. The other potential mutant tested was a C-terminal C_2B domain deleted (ΔC2B) truncation mutant of the protein. The design of this mutant was created by research on animal synaptotagmins that demonstrated the C_2B domain was a regulator of some SYT functions in animal systems (Littleton *et al*, 2001). This SYTA mutant was designed based on the studies in animal systems, it was utilized because the CaLCuV MP interacted with a C-terminal fragment of SYTA in the initial screen and the possibility existed that the C_2B domain is functionally analogous to the same domain in the animal systems.

In their movement assay, Lewis and Lazarowitz observed that the foci of MP transient expression were statistically more often found to be two or more cells in size when the fluorescently labeled movement protein was co-expressed with wild-type SYTA, SYTA$^{\Delta TM}$, or an empty vector (only endogenous SYTA) indicating that movement of the MP was occurring normally in both cases. This also indicated that the SYTA$^{\Delta TM}$ was not inhibiting the function of endogenous SYTA in cell-to-cell movement. The wild-type SYTA or the SYTA$^{\Delta TM}$ forms of SYTA were significantly different from the SYTA$^{\Delta C2B}$ with which the majority of foci were limited to a single cell (Lewis & Lazarowitz, 2010). Single cell foci are indicative of a failure of the movement protein to function normally in translocation through PD and across the cell wall.

Lewis and Lazarowitz concluded that the defect in the SYTA$^{\Delta C2B}$ prevented the MP from functioning normally. Ultimately, this assay showed that SYTA is a regulator of movement protein-directed cell-to-cell movement for two families of plant viruses. SYTA$^{\Delta C2B}$ functioned as a dominant-negative in the assay as it interfered with the function of the endogenous SYTA in the cells. Lewis and Lazarowitz conducted a bombardment assay using the cell-to-cell MP and *syta-1* knockdown line to affirm their conclusion by demonstrating that functional SYTA is a necessity of MP function in cell-to-cell movement.

The Arabidopsis synaptotagmin family:

The gene encoding SYTA was identified as a synaptotagmin gene because computer-based sequence alignments of the Arabidopsis genome to the library of known genes predicted it to encode a protein with the conserved domain structure that defines the synaptotagmin proteins based on sequence similarity to synaptotagmins from animals (Initative, 2000; Craxton, 2001). Synaptotagmins are defined based on having an uncleaved N-terminal signal peptide that partially overlaps a single transmembrane domain (TM), followed by a cytosolic variable domain (VD), and two cytosolic calcium/lipid-binding domains (so-called C_2 domains) near the C-terminal (Craxton, 2001; Lewis & Lazarowitz, 2010; Perin *et al*, 1991a). Before sequenced genomes of plants were available, synaptotagmins were thought to be limited to animal cells, where they were named based upon the role and conservation of SYT1 (formerly p65) in the exocytosis of neurotransmitters in animals (Perin *et al*, 1991b). The sequencing of the *Arabidopsis* genome revealed five protein-encoding genes with predicted domain structures matching the definition of a synaptotagmin (Fukuda, 2003; Craxton, 2004). The five genes, named SYT A, B, C, D, and E based upon their sequence similarity to the SYTA gene, are all expressed (Figure 1–3 and Table 1-1) (Lewis & Lazarowttz, 2010; Fukuda, 2003). Given that overlapping or redundant functions between the SYTs may exist, the effect of other *Arabidopsis* SYTs on viral infectivity has been investigated for SYTB and SYTC. The Lazarowitz group has shown that neither SYTB nor SYTC is redundant with

SYTA and that neither regulates virus cell-to-cell movement. Unlike SYTA, neither SYTB nor SYTC is ubiquitously expressed in the *Arabidopsis* plant; SYTB is expressed in siliques, stems, flowers, and anthers and SYTC is specific to stomatal guard cells (Uchiyama *et al*, 2010; Lazarowitz *et al*, 2010; Uchiyama *et al*).

Table 1-1. ***Arabidopsis* synaptotagmin gene family**. The *Arabidopsis* synaptotagmin gene family consists of five genes, SYT A–E, which are named based upon their similarity to SYTA. From Lewis and Lazarowitz, 2010.

Gene	Locus	Product Size	Similarity to SYTA			Expressed
			Protein	C2A	C2B	
SYTA	At2g20990	541	-	-	-	Yes
SYTB	At1g20080	535	66%	62.4%	72.6%	Yes
SYTC	At5g04220	540	50%	52.9%	56.3%	Yes
SYTD	At5g11100	574	29%	40.2%	28.4%	Yes
SYTE	At1g05500	560	31%	40.2%	28.1%	Yes

SYTA function:

Since research interests were not of a viral nature, the first published reports about SYTA examined its role in uninfected *Arabidopsis* plants and did not consider SYTA's role in viral disease,. These studies implicated SYTA as having a role in the recovery of a plant from osmotic and freezing stresses (Yamazaki *et al*, 2008; Schapire *et al*, 2008). Schapire et al. showed that homozygous *syta-1* seedlings of *Arabidopsis* are more sensitive to the addition of NaCl in concentrations greater that 50 mM to growth media than wild-type seedlings, based upon comparisons of root lengths (Schapire *et al*, 2008).

Yamazaki et al. demonstrated that initiation of an RNA silencing response to SYTA lowered the freezing tolerance of *Arabidopsis* (Yamazaki *et al*, 2008). Neither of these groups showed where nor how SYTA functioned in plant tolerance to these stresses, although their results were consistent with their suggestion of SYTA having a role in membrane dynamics analogous to that of SYT7 from *Drosophila* (Andrews & Chakrabarti, 2005). Lewis and Lazarowitz investigated both the subcellular localization and cellular functions of SYTA (Lewis & Lazarowitz, 2010). Lewis and Lazarowitz showed that GFP-tagged SYTA (SYTA-GFP) localizes to plasma membrane-derived endosomes by demonstrating SYTA-GFP co-labeling with the membrane dye FM 4–64. FM 4-64 labels plasma membrane derived endosomes when labeling times are less than 20 minutes (Vida & Emr, 1995). When the C_2B domain is deleted, the SYTA mutant protein ($SYTA^{\Delta C2B}$) does not localize to endosomes, but, rather, this protein localizes to the plasma membrane and, as a consequence of overexpression, can accumulate through the endoplasmic reticulum network (Lewis & Lazarowitz, 2010). Expressing cellular compartment markers together with $SYTA^{\Delta C2B}$ showed that $SYTA^{\Delta C2B}$ does not observably alter the secretory pathway. In leaf epidermal cells transiently expressing $SYTA^{\Delta C2B}$, FM 4-64 dye labeling demonstrates the formation of early endosomes at the plasma membrane is inhibited. This result helped Lewis and Lazarowitz conclude that SYTA is a regulator of early endosome formation at the plasma membrane (Lewis & Lazarowitz, 2010).

The SYTA$^{\Delta C2B}$ mutant acts as a dominant-negative mutant, which means the endogenous SYTA (expressed from the genome of the transfected cell) is no longer functional when SYTA$^{\Delta C2B}$ is expressed. Specifically, when the SYTA$^{\Delta C2B}$ mutant is expressed, it acts as an antagonist to the endogenous functional SYTA in the cell. Within a multiprotein complex, interactions cause this dominant-negative phenotype (Alberts *et al*, 2002). When the SYTA$^{\Delta C2B}$ deletion mutant is expressed *in vivo*, it localizes to the PM and interferes with the endogenous wild-type SYTA, abolishing its function (Lewis & Lazarowitz, 2010). This effect strongly suggests a direct interaction occurs between the defective SYTA$^{\Delta C2B}$ mutant and endogenous SYTA protein. To determine if the deleterious effects of the SYTA$^{\Delta C2B}$ mutant were not do to free Ca^{2+} being fully sequestered in a cell, Lewis and Lazarowitz also tested the SYTA$^{\Delta TM}$ mutant. That the SYTA$^{\Delta TM}$ mutant, lacking a transmembrane domain, did not disrupt SYTA function, indicated that SYTA$^{\Delta C2B}$ specifically is a dominant negative mutant and that the SYTA$^{\Delta C2B}$ phenotype was not the result of over expression of a mutant as the SYTA$^{\Delta TM}$ did not inhibit function (Lewis & Lazarowitz, 2010).

In addition to establishing that SYTA regulates early endosome formation, Lewis and Lazarowitz also demonstrated that SYTA regulates endosome recycling at the plasma membrane. They showed that when the recycling endosome marker RabF1-GFP is co-expressed with SYTA$^{\Delta C2B}$, RabF1–GFP

labeled endosomes accumulated at the PM without fusing. This accumulation indicated that endosomes were unable to recycle (Lewis & Lazarowitz, 2010). From this experiment, Lewis and Lazarowitz concluded that when SYTA$^{\Delta C2B}$ is expressed not all proteins that should be recycled to the PM can reach the PM in the same way they would in a healthy cell. The conclusion that SYTA$^{\Delta C2B}$ blocks endosome recycling is also relevant to viral MPs as it suggests that MPs take advantage of SYTA recycling back to the plasma membrane.

The interaction of wild-type SYTA and SYTA$^{\Delta C2B}$ would be predicted to create a heterodimer that is strongly favored over an endogenous functional homodimeric complex of wild-type SYTA due to the overexpression of SYTA$^{\Delta C2B}$. Because of the overexpression of SYTA$^{\Delta C2B}$, a homodimeric form of this mutant would also be expected to be present. Overexpressing SYTA$^{\Delta C2B}$ results in the formation of SYTA complexes lacking at least one intact C_2B domains from the two expected to be in a complex, in the presence of endogenous SYTA. Lewis and Lazarowitz showed with their SYTA$^{\Delta C2B}$ mutant that having an intact C_2B domains in a complex is necessary for SYTA function. Because the loss of SYTA function prevents the formation of PM derived endosomes, assaying for mutants of SYTA-GFP that do not form endosomes (such as SYTA$^{\Delta C2B}$–GFP) in protoplasts can be used as an assay to determine if that mutation will abolish function in endocytosis.

Even with the understanding that SYTA regulates early endosome formation and endosome recycling, little is agreed upon about how endocytosis from the plasma membrane functions or what are the pathways in plant cells (Baluska & Wan, 2012; Ueda *et al*, 2012). Differing models of what events and compartments, with insufficient direct evidence to derive strong conclusions, are involved having made plant endocytosis a controversial area of study. Evidence exists to suggest that plants do have homologs to some ESCRT proteins (Winter & Hauser, 2006). Endocytosis has been more thoroughly studied in yeast and animal systems than in plant systems (Yamashita, 2012). In the present model of SYTA in endocytosis, SYTA regulates the formation and uptake of early endosomes into the cell at the plasma membrane. These endosomes will either recycle directly back to the plasma membrane or be trafficked to another endomembrane compartment where both endosomal proteins and endosomal cargoes could be sorted. Such a compartment, while not currently demonstrated, could potentially be the trans-Golgi network or an endocytic recycling complex [possibly analogous to the ESCRT complex found in other eukaryotes (Otegui *et al*, 2012)]. If such a compartment exists, it will be expected to sort SYTA so that it is recycled back to the plasma membrane (Figure 1–4). Because SYTA localizes to and regulates both endosome formation and recycling to the PM, SYTA and SYTA mutants have potential to become useful tools in elucidating the details of plant endocytosis and endomembrane trafficking.

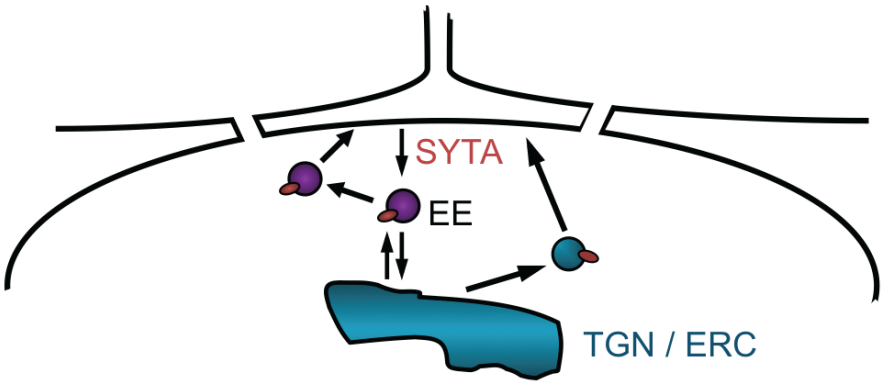

Figure 1–4: **Model of possible SYTA trafficking in endocytosis.** SYTA regulates the formation of plasma membrane-derived early endosomes (EE). SYTA also regulates the recycling of endosomes back to the plasma membrane. Viral MPs are proposed to exploit the recycling of endosomes to the PM as a pathway to reach the PD for cell-to-cell movement. How endosomes are trafficked within a cell is unclear. This model diagrams how SYTA-labeled endosomes may directly recycle back to the plasma membrane (left – purple) or be trafficked to another compartment before recycling to the PM (right – blue). However, no evidence favoring the existence the intermediate compartment has been published. If such a compartment exists, the compartment may be related to the trans–Golgi network (TGN) or an endocytic recycling complex (ERC).

Synaptotagmins beyond Arabidopsis:

Genes that encode synaptotagmin proteins have been identified in the genomes of all complex animals, including mammals, fish, nematodes, and flies when their respective genomes have been sequenced (Craxton, 2001; 2004; Fukuda, 2003). The synaptotagmin proteins were first isolated in cells of rat brain extracts (Perin *et al*, 1991a). Researchers were interested in identifying proteins involved in neuronal function when they identified SYT1. At the time, the SYT1 was initially named p65.

While synaptotagmins are conserved in animals, they were not found in the genome of a budding yeast, *Saccharomyces cerevisiae*, when it was

sequenced. The absence of a SYT in yeast fueled speculation that SYTs were related to the nervous systems of animals and to synaptic function. When SYTs were found in the genomes of both *Arabidopsis* and *Oryza* (rice), it became clear that SYTs were more broadly distributed among eukaryotes and that SYTs may have evolved to become the tricalbins of *Saccharomyces* sometime in evolutionary history (Craxton, 2004). The tricalbins are similar in structure to SYTs except they contain more than two C_2 domains. Studies of different SYTs in animals revealed that some SYT family proteins play a more general role in membrane dynamics than does SYT1 (Sudhof, 2001). One of these roles is the maintenance of membrane homeostasis in response to stresses (Andrews & Chakrabarti, 2005).

An in-depth look at the *Saccharomyces* genome revealed the presence of a class of similar proteins known as “tricalbins,” which is short for “triple calcium binding” (Craxton, 2004). Instead of containing two C_2 domains, these proteins contain three or more C_2 domains and therefore do not meet the classic definition of a synaptotagmin (Creutz *et al*, 2004; Schulz & Creutz, 2004). Given the similarity of tricalbins to SYTs, they may have evolved from SYTs in yeast’s ancestors by providing and maintaining some specific function(s). These tricalbin proteins seem to have a broadly redundant function with SYTs that are involved in regulating cellular membrane dynamics. Manford et al. have revealed that they are necessary for tethering ER to the PM and are involved in the regulation of

phosphoinositide signaling. They demonstrated that when all tricalbins are deleted PI4P accumulates at the PM (Manford *et al*, 2012). This finding is significant because PI4P aids in cellular trafficking to the PM; the loss of ER-PM contact may indicate defective recycling from the PM into the cell. Future studies may reveal the extent to which the tricalbins and synaptotagmins share equivalent functions.

Similarly to plant SYTs, animal SYTs are membrane-anchored Ca^{2+}–lipid-binding proteins. SYTs bind to lipids in response to elevated concentrations of Ca^{2+} ions in the cytosol (Chapman, 2008), which means they sense influxes of free Ca^{2+} in the cytosol. The best studied example of a synaptotagmin is the mammalian SYT1, which functions in the exocytosis of neurotransmitter and synaptic vesicle homeostasis in the synapses between nerve cells (Pang & Südhof, 2010). As Ca^{2+} gradients drive neurotransmitter release, the popular opinion is that SYT1 is responsible for sensing the change in Ca^{2+} during a signaling event.

While it is clear that SYT1 functions in exocytosis, the exact order of events in exocytosis remains an enigma. Researchers have proposed at least six models of regulated exocytosis (Kasai *et al*, 2012). One of the models, diagrammed in Figure 1–5, has garnered some broader use because of its relative simplicity; this model does not reflect any interactions with SNARE

proteins as the nature and timing of the interactions remains a subject of debate (Kochubey *et al*, 2011; van den Bogaart *et al*, 2011; Parisotto *et al*, 2012; Kasai *et al*, 2012). I have chosen this specific model because there is some indirect evidence of vesicles with defective SYTs being able to dock at the synapse (Desai *et al*, 2000; Littleton *et al*, 2001).

According to this model, the cellular trafficking machinery localizes a synaptic vesicle loaded with neurotransmitter near the plasma membrane. With the vesicle in close proximity to this membrane, the SNARE complex assembles and primes the vesicle for fusion. An electrical potential along the nerve stimulates an influx of Ca^{2+} into the cell through voltage-gated Ca^{2+} channels. In response to the surge in free Ca^{2+} ions, the SYT1 anchored to the synaptic vesicle binds simultaneously to the free Ca^{2+} ions and the target membrane. This results in bringing the vesicle near enough to the plasma membrane to facilitate fusion of the vesicular membrane to the plasma membrane, which leads to the release of neurotransmitters into the extracellular space of the synapse (Chapman, 2008; Kasai *et al*, 2012; Catterall, 2011). Much of the uncertainty among models of synaptotagmin function center on the specific mechanism of synaptotagmins in exocytosis and how they relate to other proteins involved both physically and temporally (Südhof, 2013).

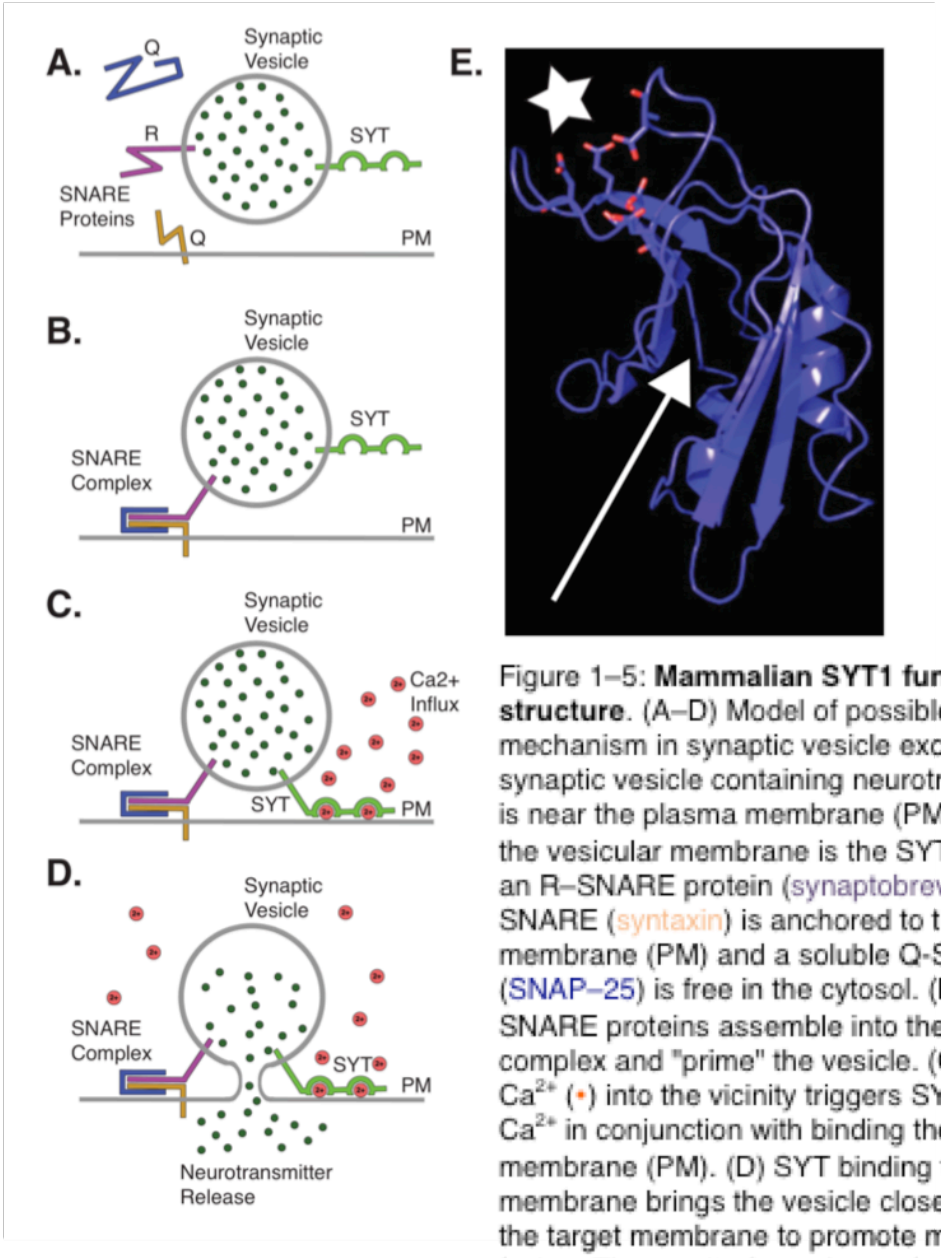

Figure 1–5: **Mammalian SYT1 function and structure**. (A–D) Model of possible SYT1 mechanism in synaptic vesicle exocytosis. (A) A synaptic vesicle containing neurotransmitters (•) is near the plasma membrane (PM). Anchored in the vesicular membrane is the SYT protein and an R–SNARE protein (synaptobrevin). A Q-SNARE (syntaxin) is anchored to the target membrane (PM) and a soluble Q-SNARE (SNAP–25) is free in the cytosol. (B) The SNARE proteins assemble into the SNARE complex and "prime" the vesicle. (C) An influx of Ca^{2+} (•) into the vicinity triggers SYT to bind to Ca^{2+} in conjunction with binding the target membrane (PM). (D) SYT binding to the membrane brings the vesicle close enough to the target membrane to promote membrane fusion. The result of membrane fusion is the release of neurotransmitter molecules into the synapse. A-D adapted from Chapman 2008 and Zhang 2009. (E) The structure of the C_2A domain of *Rn*SYT1 with the common C_2 beta sandwich fold indicated with an arrow. The active site (★) is enriched with acidic amino acids that facilitate the mutual binding of Ca^{2+} and membrane. E adapted from Shao, 1998.

After the neurotransmitter has been released, fully fused synaptic vesicles will rapidly reform and take in free neurotransmitter molecules from the synapse (Smith *et al*, 2008). This new formation allows both vesicles and neurotransmitters to be recycled for an additional signaling event and allows for the role of SYT1 in exocytosis and endocytosis to be uncoupled (Yao *et al*, 2012). Observations of electrical potentials across the neuronal membrane should be expected to reveal the rate of each process. SYT1 mutants can be used to see what domains of SYT1 are involved in either process. It is more difficult to uncouple these processes in other animal cell types, where electron potential has not been correlated with either process. However, studies of proteins, such as the intersectins, that can link functions may provide new tools in uncoupling the processes (Gubar *et al*, 2013).

Research on SYT1 and other animal SYTs has been focused on the two C_2 domains, C_2A and C_2B. These two domains are of interest because they are responsible for sensing Ca^{2+} and are the most highly conserved between SYT proteins. Most *in vitro* work has used constructs that only consist of the separated two domains. Occasionally, researchers do use both C_2 domains joined by the linker region between them. This linker region approach limits the relevance of studies where one of the omitted domains plays a role in function (MacArthur *et al*, 1994), but since it greatly simplifies and increases yield in purifications, this approach has been useful to researchers. Most synaptotagmin

researchers operate under the assumption that SYTs function as dimers or tetramers, but no conclusive evidence of native dimer formation has been published. Occasional reports of dimer-like artifacts derived from denatured SYT proteins have been published (Vrljic *et al*, 2011; Perin *et al*, 1991a). To conclude that a dimer forms, native protein will have to be utilized to eliminate the possibility that an aggregate or a biologically irrelevant protein complex is observed.

The C_2 domains from a handful of synaptotagmins have been crystallized and structures of these domains have been published. No structure corresponding to any other domain of any animal synaptotagmin has been deposited in the Research Collaboratory for Structural Bioinformatics (RCSB) protein data bank. The 3-D structures reveal that the two animal SYT C_2 domains are very similar in their structural motifs. Both C_2 domains consist of a beta-sandwich motif and a highly negatively charged binding site at one end of that motif (Figure 1–5 E) (Sutton *et al*, 1995; 1999; Fuson *et al*, 2007; Shao *et al*, 1998). In conjunction with function studies, the mechanisms by which SYTs bind Ca^{2+} and lipids have been hypothesized. The strong negative charge of the Ca^{2+}-binding site is caused by the presence of acidic residues (aspartic acids and glutamic acids), which are capable of stabilizing the strong positive charge of multiple Ca^{2+} ions in conjunction with the protein interacting with the negatively charged membrane leaflet. Given the similarity between the two Ca^{2+}-binding

domains, C_2A and C_2B, one may suspect that their functions are equivalent. However, studies with both SYT1 and SYT2 show that the C_2B domain is dominant and essential for the function of animal SYTs in exocytosis and endosome recycling (Littleton *et al*, 2001; Desai *et al*, 2000). *Drosophila* SYT1 loses the ability to interact with clathrin, a core part of the endocytosis machinery, when C_2B is deleted. Specific C_2B deletions were demonstrated to abolish interactions with the SNARE proteins (Littleton *et al*, 2001). The observation that the C_2B domain is necessary for function is also the case for SYTA from *Arabidopsis* (Lewis & Lazarowitz, 2010).

Do Arabidopsis *SYTs have a true C_2B domain?*

Alignments of the primary protein sequence of the C_2B domain of SYTA from *Arabidopsis* to the C_2B domain of SYT1 from *Rattus norvegicus* (laboratory rat) suggest that four of the five acidic residues in the active site of SYT1 are not conserved in SYTA. The loss of these residues, illustrated as black triangles in Figure 1–6 A, led other research groups to hypothesize that SYTA is not capable of stabilizing Ca^{2+} ions with its C_2B domain. By extension, they argued that the C_2B domain of SYTA should be of little or no functional importance and therefore not a C_2 domain at all. (Schapire *et al*, 2008; Yamazaki *et al*, 2010). However, the hypothesis that SYTA is fundamentally different than the synaptotagmins from animals is limited to those research groups. Figure 1–6 B shows the interactions

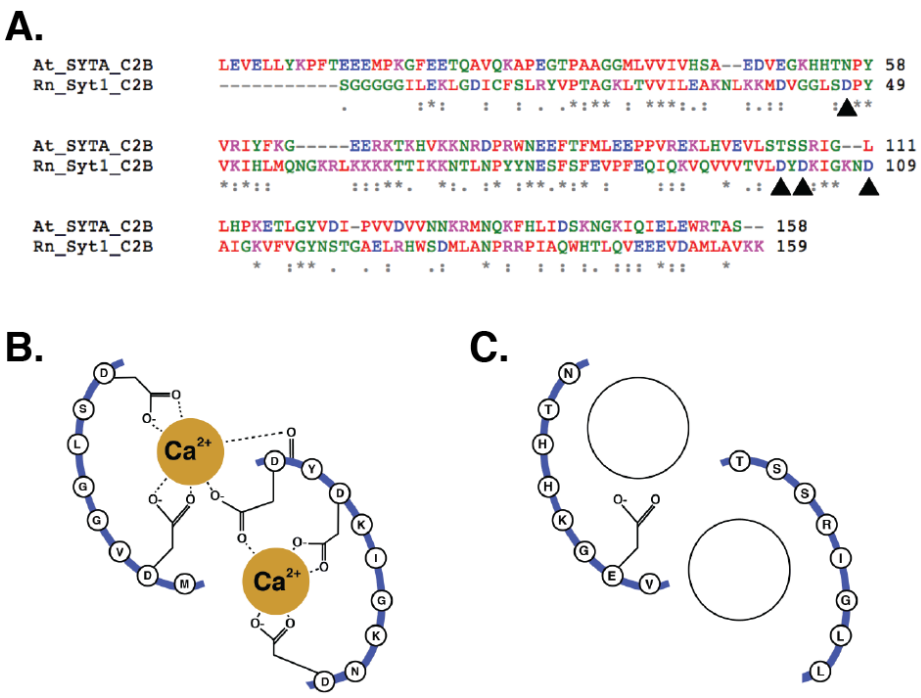

Figure 1–6: **Comparison of primary structures of C_2B domains between plant and animal synaptotagmins**. (A) Primary sequence alignment indicates that four of the acidic residues responsible for calcium binding by rat SYT1 (*Rn*SYT1) C_2B domain are not conserved in *Arabidopsis* SYTA (*At*SYTA), as indicated by black arrowheads. Only one acidic residue (E499 in *Arabidopsis*) is conserved between the two proteins in this region of the C_2B domain. (B) The interactions by which a single rat SYT1 C_2B domain stabilizes calcium ions. Note that two loops are involved in the stabilization of Ca^{2+}. Copied from Bhalla, 2008. (C) The homologous loops of a single *At*SYTA C_2B domain aligning with those shown in B highlight the insufficient negative charge available for Ca^{2+} binding in this site.

by which a single rat SYT1 C_2B domain is able to stabilize to Ca^{2+} ions. Both bound Ca^{2+} ions are stabilized by multiple partial negative charges in addition to the negative charge that is provided by the target membrane. SYTA is not capable of the same stabilization because the available negative charge in the binding site is a mere -1 charge (Figure 1–6 C).

Lewis and Lazarowitz demonstrated that the C_2B domain is functional and dominant in SYTA function (Lewis & Lazarowitz, 2010). Their strong evidence that $SYTA^{\Delta C2B}$ acts as a dominant-negative mutant to interfere with endogenous SYTA would be problematic for the model proposed by Schapire and Yamazaki (Yamazaki *et al*, 2010; 2008; Schapire *et al*, 2008). To more thoroughly refute their model of SYTA, it is necessary to address the question of how the C_2B domain functions without the accepted Ca^{2+}-binding site present.

Hypothesis:

Based on the dominant-negative behavior of the $SYTA^{\Delta C2B}$ in functional studies and consistent with the hypothesis for animal synaptotagmins, I propose that SYTA from *Arabidopsis thaliana* forms a biologically active dimer or tetramer. I further propose that dimerization is necessary to form the Ca^{2+}-binding site of the C_2B domain. This hypothesis, as tested in this project, would be the first direct evidence confirming whether the dimer or tetramer exists, aiding research on SYTA and impacting the larger synaptotagmin field.

Project overview:

By creating a predictive model of its 3-D structure as a dimer, I addressed the question of how the SYTA C_2B domain is likely to function as part of a dimer or tetramer. The structure of the model proposes that a novel Ca^{2+}-binding site would be created when two SYTA C_2B domains are properly aligned within a

SYTA dimer. Based on the model's predictions, I tested this binding site for biological relevance by mutational analyses using an *in vivo* functional cell-based protoplast expression assay. After demonstrating the functional importance of key mutants, I demonstrated the formation of a SYTA protein dimer and examined the stability of this dimer by means of laser light scattering. Finally, I began the investigation of the interaction between SYTA and phospholipids.

WORKS CITED

Alberts, B. *et al.* "*Molecular Biology of the Cell*." (Garland Science, New York, 2002).

Almeida, I. "High Food Prices Seen by Olam CEO as Result of Population Growth." *bloomberg.com* (2013). at <http://www.bloomberg.com/news/2013-02-04/high-food-prices-seen-by-olam-ceo-as-result-of-population-growth.html>.

Anderson, P. K. *et al.* "Emerging infectious diseases of plants: pathogen pollution, climate change and agrotechnology drivers." *Trends Ecol. Evol. (Amst.)* **19,** 535–544 (2004).

Andrews, N. W. & Chakrabarti, S. "There's more to life than neurotransmission: the regulation of exocytosis by synaptotagmin VII." *Trends Cell Biol.* **15,** 626–631 (2005).

Arabidopsis Genome Initiative. "Analysis of the genome sequence of the flowering plant *Arabidopsis thaliana*." *Nature* **408,** 796–815 (2000).

Baluska, F. & Wan, Y. L. in "*Endocytosis in Plants"* (Samaj, J.) pp. 123–149 (Springer Berlin Heidelberg, 2012).

Beffa, R. S. *et al.* "Decreased susceptibility to viral disease of β-1,3-glucanase-deficient plants generated by antisense transformation." *Plant Cell* **8,** 1001–1011 (1996).

Benitez-Alfonso, Y. *et al.* "Plasmodesmata: gateways to local and systemic virus infection." *Mol. Plant Microbe Interact.* **23,** 1403–1412 (2010).

Blanc, S. *et al.* "New research horizons in vector-transmission of plant viruses." in "*Host—microbe interactions: fungi/parasites/viruses"* **14,** 483–491 (2011).

Botha, C. E. & Cross, R. H. "Towards reconciliation of structure with function in plasmodesmata-who is the gatekeeper?" *Micron* **31,** 713–721 (2000).

Caspar, D. L. "Assembly and Stability of the Tobacco Mosaic Virus Particle." *Adv. Protein Chem.* **18,** 37–121 (1963).

Catterall, W. A. "Voltage-gated calcium channels." *Cold Spring Harb. Perspect. Biol.* **3,** 1-23 (2011).

Chapman, E. R. "How does synaptotagmin trigger neurotransmitter release?" *Annu. Rev. Biochem.* **77,** 615–641 (2008).

Citovsky, V. “Tobacco mosaic virus: a pioneer of cell-to-cell movement.” *Philos. Trans. R. Soc. Lond., B, Biol. Sci.* **354,** 637–643 (1999).

Craxton, M. “Genomic analysis of synaptotagmin genes.” *Genomics* **77,** 43–49 (2001).

Craxton, M. “Synaptotagmin gene content of the sequenced genomes.” *BMC Genomics* **5,** 43-56 (2004).

Creutz, C. E. *et al.* “Characterization of the yeast tricalbins: membrane-bound multi-C_2-domain proteins that form complexes involved in membrane trafficking.” *Cell. Mol. Life Sci.* **61,** 1208–1220 (2004).

Dangl, J. L. & Jones, J. D. G. “Plant pathogens and integrated defense responses to infection.” *Nature* **411,** 826–833 (2001).

Desai, R. C. *et al.* The C_2B domain of synaptotagmin is a Ca^{2+}-sensing module essential for exocytosis.” *J. Cell Biol.* **150,** 1125–1136 (2000).

De Zoeten, G. A. & Gaard, G. “Possibilities for inter- and intracellular translocation of some icosahedral plant viruses.” *J. Cell Biol.* **40,** 814–823 (1969).

Ding, B. “The biology of viroid-host interactions.” *Annu. Rev. Phytopathol.* **47,** 105–131 (2009).

Emini, E. A. & Fan, H. Y. “Immunological and Pharmacological Approaches to the Control of Retroviral Infections” in “*Retroviruses”* (eds Coffin J.M. *et al*). (Cold Spring Harbor Laboratory Press, Cold Spring Harbor, NY, 1997).

Epel, B. L. “Plant viruses spread by diffusion on ER-associated movement-protein-rafts through plasmodesmata gated by viral induced host β-1,3-glucanases.” *Semin. Cell Dev. Biol.* **20,** 1074–1081 (2009).

Faulkner, C. *et al.* “Peeking into pit fields: a multiple twinning model of secondary plasmodesmata formation in tobacco.” *Plant Cell* **20,** 1504–1518 (2008).

Fukuda, M. “Molecular cloning, expression, and characterization of a novel class of synaptotagmin (Syt XIV) conserved from *Drosophila* to humans.” *J. Biochem.* **133,** 641–649 (2003).

Fuson, K. L. *et al.* “Structure of human synaptotagmin 1 C_2AB in the absence of Ca_{2+} reveals a novel domain association.” *Biochemistry* **46,** 13041–13048 (2007).

Gubar, O. *et al.* “Intersectin: The Crossroad between Vesicle Exocytosis and Endocytosis.” *Front. Endocrinol. (Lausanne)* **4,** (article 109) 1-5 (2013).

Guenoune-Gelbart, D. *et al.* “Tobacco mosaic virus (TMV) replicase and movement protein function synergistically in facilitating TMV spread by lateral diffusion in the plasmodesmal desmotubule of *Nicotiana benthamiana*.” *Mol. Plant Microbe Interact.* **21,** 335–345 (2008).

Harries, P. & Ding, B. “Cellular factors in plant virus movement: at the leading edge of macromolecular trafficking in plants.” *Virology* **411,** 237–243 (2011).

Hull, R. “*Comparative Plant Virology*.” (Elisevier, Amsterdam, 2009).

Iglesias, V. A. & Meins, F. J. “Movement of plant viruses is delayed in a β-1,3-glucanase-deficient mutant showing a reduced plasmodesmatal size exclusion limit and enhanced callose deposition.” *Plant J.* **21,** 157–166 (2000).

Ingham, D. J. *et al.* “Both bipartite *geminivirus* movement proteins define viral host range, but only BL1 determines viral pathogenicity.” *Virology* **207,**191–204 (1995).

Jackson, A. O. *et al.* “Biology of plant rhabdoviruses.” *Annu Rev Phytopathol* **43,** 623–660 (2005).

japantimes.co.jp., Kitazume, T. (ed.). “Climate change feared to create global food crisis” at <http://www.japantimes.co.jp> (4 April 2013).

Kasai, H. *et al.* “Distinct initial SNARE configurations underlying the diversity of exocytosis.” *Physiol Rev* **92,** 1915–1964 (2012).

Kassanis, B. “Intranuclear Inclusions in Virus Infected Plants.” *Ann. Applied Biology* **26,** 705–709 (1939).

Kochubey, O. *et al.* Regulation of transmitter release by Ca^{2+} and synaptotagmin: insights from a large CNS synapse.” *Trends Neurosci.* **34,** 237–246 (2011).

Kurepa, J. & Smalle, J. A. “To misfold or to lose structure?: Detection and degradation of oxidized proteins by the 20S proteasome.” *Plant Signal Behav.* **3,** 386–388 (2008).

Lazarowitz, S. G. *et al.* “*Arabidopsis* synaptotagmins: Non-redundant functions in plant development.” in *21St International Conference On Arabidopsis Research* (2010).

Lewis, J. D. & Lazarowitz, S. G. “*Arabidopsis* synaptotagmin SYTA regulates endocytosis and virus movement protein cell-to-cell transport.” *Proc. Natl. Acad. Sci. U.S.A.* **107,** 2491–2496 (2010).

Linnik, O. *et al.* “Unraveling the structure of viral replication complexes at super-resolution.” *Front. Plant Sci.* **4,** (article 6) 1-13 (2013).

Littleton, J. T. *et al.* “Synaptotagmin mutants reveal essential functions for the C_2B domain in Ca^{2+}-triggered fusion and recycling of synaptic vesicles *in vivo*.” *J. Neurosci.* **21,** 1421–1433 (2001).

MacArthur, M. W. *et al.* “NMR and crystallography – complementary approaches to structure determination.” *Trends Biotechnol.* **12,** 149–153 (1994).

Manford, A. G. *et al.* “ER-to-plasma membrane tethering proteins regulate cell signaling and ER morphology.” *Dev. Cell* **23,** 1129–1140 (2012).

Maule, A. J. “Plasmodesmata: structure, function and biogenesis.” *Curr. Opin. Plant Biol.* **11,** 680–686 (2008).

Maule, A. J. *et al.* “Plasmodesmata – membrane tunnels with attitude.” *Curr. Opin. Plant Biol.* **14,** 683–690 (2011).

Morozov, S. Y. & Solovyev, A. G. “Triple gene block: modular design of a multifunctional machine for plant virus movement.” *J. Gen. Virol.* **84,** 1351–1366 (2003).

Mushegian, A. R. & Koonin, E. V. “Cell-to-cell movement of plant viruses. Insights from amino acid sequence comparisons of movement proteins and from analogies with cellular transport systems.” *Arch. Virol.* **133,** 239–257 (1993).

Oparka, K. J. *et al.* “Simple, but not branched, plasmodesmata allow the nonspecific trafficking of proteins in developing tobacco leaves.” *Cell* **97,** 743–754 (1999).

Oparka, K. J. & Roberts, A. G. “Plasmodesmata. A not so open-and-shut case.” *Plant Physiol.* **125,** 123–126 (2001).

Otegui, M. S. *et al.* in “*Endocytosis in Plants”* (Samaj, J.) 249–270 (Springer Berlin Heidelberg, 2012).

Pang, Z. P. & Südhof, T. C. “Cell biology of Ca^{2+}-triggered exocytosis.” *Curr. Opin. Cell Biol.* **22,** 496–505 (2010).

Parisotto, D. *et al.* “SNAREpin assembly by Munc18-1 requires previous vesicle docking by synaptotagmin 1.” *J. Biol. Chem.* **287,** 31041–31049 (2012).

Perin, M. S. *et al.* “Structural and functional conservation of synaptotagmin (p65) in *Drosophila* and humans.” *J. Biol. Chem.* **266,** 615–622 (1991).

Sanderfoot, A. A. *et al.* “A viral movement protein as a nuclear shuttle. The *geminivirus* BR1 movement protein contains domains essential for interaction with BL1 and nuclear localization.” *Plant Physiol.* **110,** 23–33 (1996).

Schapire, A. L. *et al.* “*Arabidopsis* synaptotagmin 1 is required for the maintenance of plasma membrane integrity and cell viability.” *Plant Cell* **20,** 3374–3388 (2008).

Schoelz, J. E. *et al.* “Intracellular transport of plant viruses: finding the door out of the cell.” *Mol Plant* **4,** 813–831 (2011).

Schulz, T. A. & Creutz, C. E. “The tricalbin C2 domains: lipid-binding properties of a novel, synaptotagmin-like yeast protein family.” *Biochemistry* **43,** 3987–3995 (2004).

Shao, X. *et al.* “Solution structures of the Ca^{2+}-free and Ca^{2+}-bound C_2A domain of synaptotagmin 1: does Ca^{2+} induce a conformational change?” *Biochemistry* **37,** 16106–16115 (1998).

Smith, S. M *et al.* “Synaptic vesicle endocytosis: fast and slow modes of membrane retrieval.” *Trends Neurosci.* **31,** 559–568 (2008).

Solovyev, A. *et al.* “Recent advances in research of plant virus movement mediated by triple gene block.” *Front. Plant Sci.* **3,** (article 276) 1-8 (2012).

Südhof, T. C. “Synaptotagmins: Why So Many?” *J. Biol. Chem.* **277,** 7629–7632 (2001).

Südhof, T. C. “Neurotransmitter release: the last millisecond in the life of a synaptic vesicle.” *Neuron* **80,** 675–690 (2013).

Sutton, R. B. *et al.* Structure of the first C_2 domain of synaptotagmin 1: a novel Ca^{2+}/phospholipid-binding fold.” *Cell* **80,** 929–938 (1995).

Sutton, R. B. *et al.* “Crystal structure of the cytosolic C_2A-C_2B domains of synaptotagmin III. Implications for Ca^{2+}-independent snare complex interaction.” *J. Cell Biol.* **147,** 589–598 (1999).

Taliansky, M. *et al.* “Role of plant virus movement proteins.” *Methods Mol. Biol.* **451,** 33–54 (2008).

Tilsner, J. *et al.* “Plasmodesmata viewed as specialized membrane adhesion sites.” *Protoplasma* **248,** 39–60 (2011).

Uchiyama, A. *et al.* "*Arabidopsis* synaptotagmin SYTA has a key role in regulating the cell-to-cell movement of diverse plant viruses." in *21St International Conference On Arabidopsis Research* (2010).

Uchiyama, A. *et al.* "*Arabidopsis* SYTC." *In preparation*

Ueki, S. *et al.* "ANK, a host cytoplasmic receptor for the Tobacco mosaic virus cell-to-cell movement protein, facilitates intercellular transport through plasmodesmata." *PLoS Pathog.* **6,** e1001201 (2010).

Ueki, S. & Citovsky, V. "To gate, or not to gate: regulatory mechanisms for intercellular protein transport and virus movement in plants." *Mol. Plant* **4,** 782–793 (2011).

Ueda, T. *et al.* in "*Endocytosis in Plants"* (Samaj, J.) pp. 201–216 (Springer Berlin Heidelberg, 2012).

van den Bogaart, G. *et al.* "Synaptotagmin-1 may be a distance regulator acting upstream of SNARE nucleation." *Nat. Struct. Mol. Biol.* **18,** 805–812 (2011).

Vida, T. A. & Emr, S. D. A new vital stain for visualizing vacuolar membrane dynamics and endocytosis in yeast. *J. Cell Biol.* **128,** 779–792 (1995).

Vrljic, M. *et al.* "Post-translational modifications and lipid binding profile of insect cell-expressed full-length mammalian synaptotagmin 1." *Biochemistry* **50,** 9998–10012 (2011).

Ward, B. M. & Lazarowitz, S. G. "Nuclear export in plants. Use of *geminivirus* movement proteins for a cell-based export assay." *Plant Cell* **11,** 1267–1276 (1999).

Winter, V. & Hauser, M. T. "Exploring the ESCRTing machinery in eukaryotes." *Trends Plant Sci.* **11,** 115–123 (2006).

Xu, X. M. & Jackson, D. "Lights at the end of the tunnel: new views of plasmodesmal structure and function." *Curr. Opin. Plant Biol.* **13,** 684–692 (2010).

Yamashita, T. "Ca^{2+}-dependent regulation of synaptic vesicle endocytosis." *Neurosci. Res.* **73,** 1–7 (2012).

Yamazaki, T. *et al.* "Calcium-dependent freezing tolerance in *Arabidopsis* involves membrane resealing via synaptotagmin SYT1." *Plant Cell* **20,** 3389–3404 (2008).

Yamazaki, T. *et al.* “Arabidopsis synaptotagmin SYT1, a type I signal-anchor protein, requires tandem C_2 domains for delivery to the plasma membrane.” *J. Biol. Chem.* **285,** 23165–23176 (2010).

Yao, J. *et al.* “Uncoupling the roles of synaptotagmin I during endo- and exocytosis of synaptic vesicles.” *Nat. Neurosci.* **15,** 243–249 (2012).

Zambryski, P. & Crawford, K. “Plasmodesmata: gatekeepers for cell-to-cell transport of developmental signals in plants.” *Annu. Rev. Cell Dev. Biol.* **16,** 393–421 (2000).

Zambryski, P. “Cell-to-cell transport of proteins and fluorescent tracers via plasmodesmata during plant development.” *J. Cell Biol.* **164,** 165–168 (2004).

Zavaliev, R. *et al.* “Biology of callose (β-1,3-glucan) turnover at plasmodesmata.” *Protoplasma* **248,** 117–130 (2011).

CHAPTER 2

Structural Modeling of Synaptotagmin A C2B Domain

Introduction:

To determine if the plant synaptotagmin SYTA could have a functional C_2B domain, I proposed testing to learn if the C_2B function in binding Ca^{2+} was a consequence of dimerization. However, because the proposed Ca^{2+}-binding site of rat SYT1 is not thought to be conserved to *Arabidopsis* SYTA, I first needed to identify where cations would bind with SYTA. I started by modeling the SYTA C_2 domains. Modeling of the C_2B domain might lead to visualization of the sites where direct interactions with Ca^{2+} could occur either in an individual C_2B domain or between C_2B domains within a homodimer.

To create the SYTA-C_2B dimer model and reveal insights into the inter-domain interaction at the molecular level, the standard approach is using the coordinates of one known structure as a framework to build a homology model. Because the homology between SYTA and the available solved structures of animal synaptotagmins was below 20% sequence identity (Craxton, 2004), I could not use that approach with SYTA. The low homology meant that any model that I created based on overlaying sequences would not be expected to reliably predict the structure of SYTA-C_2B. A threshold of about 50% residue identity is generally required for this approach to be informative (Arnold *et al*, 2006). When the homology between two proteins is less than 50%, the modeled protein's structural elements within may not align accurately with the real structure, which

is unknown, of the modeled protein. This concept was demonstrated by comparing the percent conservation of protein structure data with the percentage sequence identity between the same proteins (Chothia & Lesk, 1986). The study demonstrated that proteins with at least 50% sequence identity have at least 90% structural similarity. Proteins with sequence identities of about 20% have structural similarities of between 42% and 98%. Proteins with low structural similarity would not have comparable intra-molecular interactions. In the case of SYTA, any predicted interactions derived from a homology model could be unreal and misleading. Therefore, in the case of SYTA, the homology modeling approach is not an informative test of possible C_2B dimer function. To overcome the limitations of homology modeling, I chose to employ a more in-depth modeling technique that considers more than a primary sequence alignment when creating a model.

With an abundance of resources available to understand and analyze proteins *in silico*, numerous tools exist to compare protein and peptide sequences and simple alignments. These specific tools are useful because not all changes in amino acid residues are equivalent; different changes will have different impacts on protein structure and function (Yutani *et al*, 1985). Using tools that can test for a protein's building blocks properties should produce a better-differentiated protein model. Among the specific protein properties that one can consider in the creation of 3-D protein models are secondary structure,

possible local interactions, steric hindrance, and structural motifs. Attempting to resolve too much information in a computational model makes the refinement of the individual peptides difficult and will result in diminishing improvements to models (Ginalski, 2006). One does not need to invest the time to run all available computational tests on a protein of interest; there is a certain point when additional computational insights will not change the resultant model appreciably. Even though the limited computational power currently available for computational research and modeling systems necessitates a constraint on the size of peptide that can be modeled, reasonable models can be produced. The most significant challenges in protein structural modeling are the selection of the templates and the alignment of the query sequence to these templates (Ginalski, 2006). I modeled both C_2 domains of SYTA using two different approaches: LOMETS threading and secondary structure-driven threading. Both methods produced informative models, and the secondary structure-directed model proved most useful in making functional predictions about Ca^{2+} binding in a SYTA C_2B domain dimer.

LOMETS modeling:

The first method I used to model SYTA was the *ab initio* local meta-threading-server (LOMETS) method. In this method, the protein sequence is broken into small fragments of a few residues in length. These sets of residues are treated independently as microdomains. In order to determine the most likely

structure, software analyzes and optimizes each microdomain for lowest energy confirmations. The LOMETS software then reassembles microdomains into a structural template akin to a draft structure. The template may have some steric hindrance and unrealized intermolecular interactions. To make the template into a relevant model, the software optimizes for its lowest energy structure, a process that can takes hours or even days depending on the query sequence. The model is then compared to a protein structure database to classify the likely fold of the domain (Zhang, 2008; Roy *et al*, 2010). I should have been able to define the possible binding sites in the modeled domains after generating this model. This approach to protein modeling could be considered to be analogous to modular construction, where small features are assembled independently and then are brought together to make the final product.

As my query sequences, I submitted to a LOMETS server the sequences of the SYTA C_2B domain, and the C_2A-C_2B domains including both domains and the linker. Each query sequence had approximately one week of LOMETS server time allotted toward assembly and optimization of each model. The LOMETS server returned five individual models of each submission from the many models evaluated by the LOMETS server. Within each set of the five models, the C_2B domains all exhibited the same topology. Figure 2–1 shows a model of the C_2A and C_2B domains of SYTA.

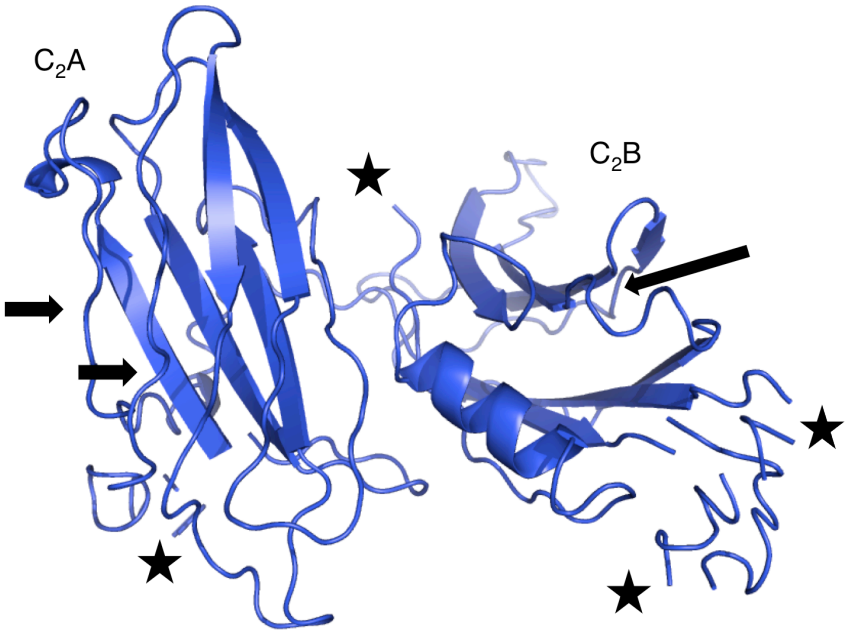

Figure 2-1: **LOMETS model of SYTA C_2A-C_2B**. This model reveals that both C_2 domains of SYTA are predicted to have the defined C_2 β-sandwich fold that correlates with calcium lipid binding. However, some of the predicted beta-strands are modeled as random coil (➔). This model cannot reliably predict the surface structure, including the loops at the ends of the beta-strands (★). C_2A is on the left, C_2B on the right. This model was created from a query sequence corresponding to both C_2A and C_2B domains

The LOMETS modeling predicted that both of the queried SYTA domains have the C_2 domain fold. Given that SYTA is proposed to be a synaptotagmin, this was the expected outcome. However, while the beta sandwich structure that defines C_2 domains is largely apparent in the LOMETS structure, the LOMETS models do not offer reliable predictions of the loops at the ends of the C_2 domain. Some of discontinuities in the models are indicated in Figure 2-1 (★). These discontinuities decrease confidence in using the residues in the loop to draw any conclusions.

The LOMETS models of the C_2 fold in SYTA C_2B predict that SYTA C_2B has the same structural fold as its animal homologs. This structural similarity allows for some comparisons to be made between the models. When I visually compared the C_2 domains in the LOMETS model (Figure 2-1) to a solved structure (Figure 1-5E), I noticed that the LOMETS model does predict that some residues are expected to be components of the beta sheet based on primary alignment to SYT1. These residues are instead modeled as random coil. Because the LOMETS model focuses heavily on local interactions[2], the software tends to undervalue the contribution of distal residues on stabilizing the structure. Considering the microdomains before assembling the structural motif and because of the order of events in model building, LOMETS modeling is prone to give structuring of the microdomains disproportionate importance in creating its models (Zhang, 2008). This phenomenon occurs despite the thorough consideration of interactions between residues that are physically closely situated but are actually located within distant peptide sequences. Were the programmer of the LOMETS model to change its constraints on evaluating distance, the models it produced could be improved (Paluszewski & Karplus, 2009). However, to do so would also require a significant increase in available computational power or computational time. Such an increase would not be likely to change the conclusion of the fold type.

[2] Here, "local" defined as nearby within the primary sequence, not nearby in 3-D space.

The major deficiency of the LOMETS modeling was the inability to reliably model the turns at either end of the C_2 domains. The LOMETS server only displayed fragments of random coil where they can be projected, but the LOMETS model omitted the residues it could not model confidently. This is represented by the presence of small, disconnected fragments of peptide (★) in Figure 2–1. Because of computational limitations, the LOMETS software uses only 620 so-called "benchmark proteins" in its algorithms, meaning that all LOMETS predictions are based on observations of how these 620 proteins are folded. The software is also prone to being uncertain about how to deal with obscure microdomains. The small set of "benchmark proteins" could create biases in the microdomains that lead to unrealistic confirmations. There can be great structural variability among small identical peptides (5 residues). Comparisons to the wrong set of proteins may model some microdomains incorrectly (Kabsch & Sander, 1984). The models were weakest at the periphery, which is probably an effect of the periphery being the least structured part of each domain.

The LOMETS model was successful in revealing the fold of both SYTA C_2 domains, but it was ineffective at modeling the periphery of these domains. Because of this limitation, the LOMETS model could not be used to make predictions about the residues that are likely to be involved in the Ca^{2+} binding

potential of SYTA. Since surface residues where C_2B domains interact could be assumed to be responsible for C_2B binding to Ca^{2+}, the inability of the LOMETS method to reliably model these domains, given the available reference data, indicates the LOMETS method is unreliable in creating a predictive model of a dimer. Because of the limitations of LOMETS modeling, not one of the ten LOMETS models I created from the SYTA query sequences were effective at modeling the SYTA-C_2B dimer to make a binding prediction.

Secondary structure-based threading model:

Because the LOMETS modeling procedure proved to be unsatisfactory, I chose to employ a different approach based upon secondary structure predictions. An important consideration in this alternative modeling approach was utilizing a method that did not require the SYTA sequence to be fragmented to the extent necessitated by LOMETS modeling. I created these models with the assistance and guidance of Dan Ripoll of the Cornell Center for Advanced Computing. To begin, this approach required us to determine the structural fold of each C_2 domain (Jones, 1999). With this information, we could predict the secondary structure for each residue of each domain computationally, and then align the corresponding sequences to the 3-D structures of the previously crystallized proteins with the most fold similarity to our SYTA query sequence. Finally, the coordinates of our models were energetically optimized with an optimization potential energy function (Liwo *et al*, 1999; Pillardy *et al*, 2001). After

the optimization, the modeled domains could be aligned and queried for potential Ca^{2+} binding sites.

Our secondary structure prediction revealed that both the SYTA C_2A and SYTA C_2B domains consisted of alternating beta-strands and unstructured coiled regions (Figure 2–2). Our predictions were congruent with the protein topology of C_2 domains. This finding was expected given the hypothesis that SYTA is a synaptotagmin.

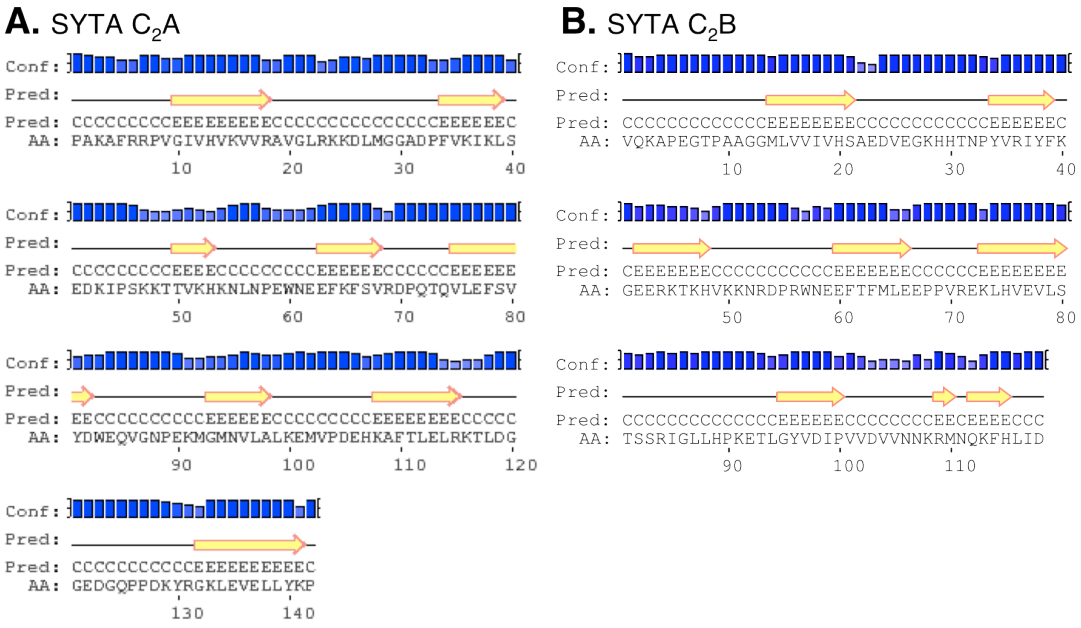

Figure 2-2: **Predicted secondary structure of SYTA C_2 domains**. The secondary structure predictions of the (A) SYTA C_2A domain and (B) SYTA C_2B domain propose that both consist of 8 β-strands (E) (yellow arrows) with confidence (large blue bars). Regions of coiled structure (C) are also predicted with confidence.

To determine the framework on which we would overlay the secondary structure of SYTA C_2A and C_2B, we queried the proteins deposited in the Research Collaboratory for Structural Bioinformatics (RCSB) protein database for

similarity to the SYTA C_2A and C_2B primary sequences. These queries, and therefore this modeling approach, considered all deposited protein structures. In 2009, this database held over 50,000 structures (Berman *et al*, 2013). Unlike the LOMETS modeling where the coordinate data available to aid in modeling is limited to 620 benchmark proteins, this secondary structure driven approach is not limited to the same constraints on reference data. Table 2–1 lists the highest sequence similarity results in order of their respective jury scores. This jury score compares the similarity in terms of primary sequence and the likelihood of structural similarity. A high jury score indicates a significant likelihood that two domains will share the same fold (Ginalski *et al*, 2003). The Structural Classification of Proteins (SCOP) map is the defined structural fold within the

Table 2-1: **Similarity of SYTA C_2 domains to proteins in the RCSB Protein Data Bank (PDB)**. Similarity between SYTA and proteins with structures deposited in the protein databank sorted based on jury score (likelihood of similarity). The PDB hit is the code for the matching PDB structure. The SCOP map b.7.1 represents a comparison to a C_2 domain from another protein. Listed protein functions are based upon RCSB-PDB annotation.

Organism	PDB Hit	Protein	Model	Jury Score	Raw Score	Fssp Map	Scop Map	Protein Function (PDB)
R. rattus	1dqvA	SYT3	PSIB_01	132.4	2.00E-32	223.7.1	b.7.1	Endocytosis/Exocytosis
R. rattus	1dqv_A	SYT3	FFA3_02	117.8	-71.5	223.7.1	b.7.1	Endocytosis/Exocytosis
H. sapiens	2r83A	SYT1	PSIB_02	116	4.00E-32		b.7.1	Endocytosis/Exocytosis
R. rattus	1dqv_A	SYT3	ESY1_01	113.4	0	223.7.1	b.7.1	Endocytosis/Exocytosis
H. sapiens	2r83A	SYT1	ST02_01	112.8	4.05E-39		b.7.1	Endocytosis/Exocytosis
R. rattus	1dqvA	SYT3	BASI_02	112.6	218.89	223.7.1	b.7.1	Endocytosis/Exocytosis
R. rattus	1dqvA	SYT3	RPSB_02	107.4	2.00E-24	223.7.1	b.7.1	Endocytosis/Exocytosis
R. rattus	1dqv_A	SYT3	MGTH_01	105	84.866	223.7.1	b.7.1	Endocytosis/Exocytosis
H. sapiens	2r83_A	SYT1	FFA3_01	103.8	-76		b.7.1	Endocytosis/Exocytosis
H. sapiens	2r83A	SYT1	BASI_01	99.6	227.79		b.7.1	Endocytosis/Exocytosis
H. sapiens	2r83A	SYT1	RPSB_01	98.6	6.00E-26		b.7.1	Endocytosis/Exocytosis
R. norvegicus	1rsy_A	SYT1	FFA3_05	86	-50.1		b.7.1	Calcium/Phospholipid Binding Protein
R. norvegicus	1rsyA	SYT1	ST02_05	85	7.14E-24		b.7.1	Calcium/Phospholipid Binding Protein
H. sapiens	2d8k_A	SYT7	FFA3_03	84.2	-52.4		b.7.1	Endocytosis/Exocytosis
R. norvegicus	1rsyA	SYT1	BASI_06	84.2	127.71		b.7.1	Calcium/Phospholipid Binding Protein
R. norvegicus	1bynA	SYT1 Ca2+ bound	ST02_03	81	3.35E-24	223.7.1	b.7.1	Endocytosis/Exocytosis
R. norvegicus	1digA	PLC-delta1	PSIB_04	80.4	5.00E-19	223.7.1	c.1.18	Lipid Degradation
H. sapiens	2enp_A	SYT17	FFA3_07	80.2	-48.6		b.7.1	Transport Protein
H. sapiens	2d8kA	SYT7	BASI_05	79.2	127.78		b.7.1	Endocytosis/Exocytosis
H. sapiens	2enpA	SYT17	BASI_10	78.4	124.61		b.7.1	Transport Protein

known protein structure that matches to the query sequence (Andreeva *et al*, 2008). The b.7.1 SCOP map is associated with the sixteen best jury score matches to the SYTA C_2B query sequence. This SCOP map represents the C_2 domain fold in the SCOP database (Andreeva *et al*, 2008).

The functions of each of the proteins with the highest jury score are in endocytosis/exocytosis or calcium/phospholipid binding (Sutton *et al*, 1995; Shao *et al*, 1998; Sutton *et al*, 1999; Fuson *et al*, 2007). The jury score matches are similar to domains with similar functions, and this finding coincides with the hypothesis that SYTA functions the same way as a true synaptotagmin.

Single domain models:

With the computational assistance of the Cornell Center for Advanced Computing's high performance computing system, we assembled models of each of the C_2A and C_2B domains based upon the secondary structure and the highest jury score models. Both domains (Figure 2–3) exhibited the canonical C_2 domain fold. The beta-sandwich was the most obvious feature in the structural model. An additional consequence of this modeling approach was a complete prediction of the arrangement of all residues in each domain. Modeling the entirety of each domain meant that employing this secondary structure-based method could overcome the most significant limitation of the LOMETS method. Because these models are structured at their periphery, testable hypotheses about the functions

of residues in the loops and less structured regions of each domain could be made.

Having a complete model of SYTA C_2B allowed me to make comparisons between the Ca^{2+}-binding sites as predicted in the SYTA C_2B monomer and dimer models. Alignment of the our predicted SYTA C_2B domain monomer 3-D structure to the crystal structure of rat SYT1-C_2B (Cheng *et al*, 2004) agrees with the prediction from the primary sequence alignment (Figure 1-6) that the Ca^{2+}-binding site of the monomer is not conserved between animal synaptotagmins and *Arabidopsis* SYTA. Our model of SYTA C_2B has a negative charge at the homologous site that is not of enough significance to bind and stabilize Ca^{2+} ions.[3] When superimposing the Ca^{2+} ions of the rat SYT1 C_2B model onto our SYTA C_2B model, there is only one acidic amino acid, glutamic acid residue 499 (E499), that contributes a negative charge where Ca^{2+} ions are modeled to bind. However, in our model, located a few positions away from the first loop of SYTA C_2B that aligns with the Ca^{2+}-binding site of the animal SYTs, is a surface region with a strong negative charge. This region consists of three closely packed amino acids, all three with negative charges. Two of these amino acids, glutamic acid 430 (E430) and aspartic acid 431 (D431), are adjacent to one another. These two residues make up the most electronegative region among the solvent-exposed area of the SYTA C_2B domain. Due to a low pKa, the localized strong

[3] The negative charge needed to bind Ca^{2+} is provided by the presence of aspartic and glutamic acid residues within a potential binding site.

charge makes this site a prime candidate for interactions with cations in the cytosol. While the region of the SYTA C_2B domain that aligns with the Ca^{2+}-binding site of animal SYT C_2B domains lacks the necessary negative charge to stabilize Ca^{2+}, it does have a generally polar character, which may be caused by the tendency of proteins to favor having polar residues exposed on cytosolic surfaces. Having these polar residues exposed likely contributes to the solubility of SYTA C_2B domains in the cytosol.

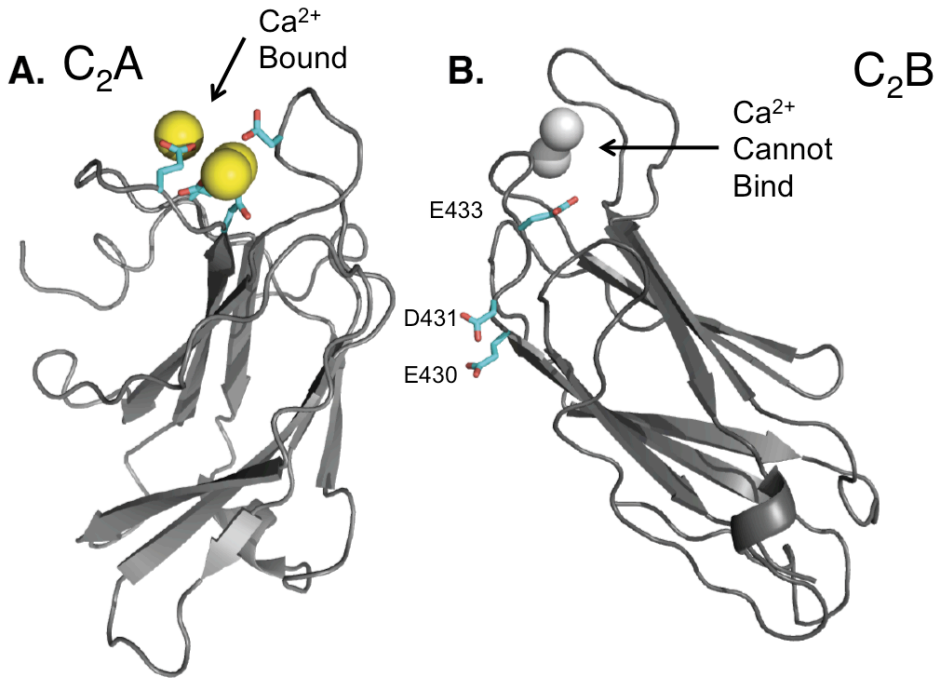

Figure 2-3: **Threading models of individual SYTA C_2 domains**. (A) The model of the SYTA C_2A domain suggests that the necessary residues are present to stabilize Ca^{2+} in the same arrangement as animal SYTs. (B) The model of the SYTA C_2B domain shows that the acidic residues necessary for Ca^{2+} stabilization, as demonstrated in animal SYTs, are not present in SYT C_2B. Therefore, Ca^{2+} cannot bind (indicated by grey spheres). The C_2B domain is predicted to contain an acidic region (E430, D431, & E433) on the surface. The acid rich region comprised of these three residues is highlighted in Figure 2-4. A close-up on these three C_2B residues of interest is in Figure 3-1.

When my SYTA C_2A model was aligned with the C_2A domain from rat SYT1, it became apparent that in the SYTA C_2A domain monomer Ca^{2+} binding could occur through a similar coordination mechanism to that of rat SYT1 (Shao *et al*, 1998). Both C_2A domains have acidic residues arranged such that the side chains of these residues are equivalent. This equivalent arrangement of acidic amino acid residues suggests that the charge interactions that drive Ca^{2+}-lipid binding are conserved between SYTA C_2A and the rat SYT1 C_2A domain. This conclusion coincides with the model that the C_2A domains are comparable between these plant and animal synaptotagmins (Yamazaki *et al*, 2010). This conclusion fits with the model that the C_2A domains can have equivalent interactions with Ca^{2+} in both plant and animal synaptotagmins (Yamazaki *et al*, 2010).

C_2B domain dimer model:

After observing that the SYTA$^{\Delta C2B}$ mutant was defective in endocytosis and functioned as a dominant-negative, Lewis and Lazarowitz hypothesized that SYTA functions as a component of a multiprotein complex, such as a dimer (Lewis & Lazarowitz, 2010). Created protein mutations when overexpressed, can disrupt the function of endogenous wild type protein through either direct interaction or substrate limitation (Herskowitz, 1987). Because overexpression of the presumed substrate (Ca^{2+}) binding SYTA$^{\Delta TM}$ mutant did not impair SYTA function, substrate limitation of endogenous SYTA was ruled out as the likely

cause of the dominant negative effect (Lewis & Lazarowitz, 2010). Instead, Lewis & Lazarowitz's evidence supported a SYTA multimer that formed through interactions between individual SYTAs. Their model argues that dimer formation would not be dependent on the C_2B domain, but the phenotype associated with $SYTA^{\Delta C2B}$ highlighted the importance of that domain for function.

Modeling the SYTA C_2B domain as a dimer could be expected to predict interactions between individual C_2B domains that can be tested for a role in SYTA function. Identifying and confirming the presence of such interactions would support my hypothesis that C_2B, and therefore SYTA, functions as a dimer. While it is possible to freely align two C_2B monomer models to create a dimer, I incorporated additional available data to create a scaffold for my dimer model. I built the dimer structure by alignment to structures of C_2 domains deposited in the RCSB protein databank where the unit cell contains multiple identical C_2 domains (Schrödinger LLC, 2010).

While not necessarily of biological relevance, unit cells formed during *in vitro* crystallization studies will favor one low energy spatial arrangement over other arrangements. Should no arrangement be favored, that peptide unit cell would be subject to twinning, which is the formation of heterologous crystals. These structures cannot be delineated at high resolution with X-ray crystallography because they lack the homogeneity to produce a clear diffraction

pattern (Yeates, 1997). Thus, proteins that are subject to twinning are not represented in the protein database. Among the C_2 domain structures with multiple C_2 domains in the unit cell, the RCSB-PDB structure 2UZP, a human C_2 Ca^{2+}-binding domain (Pike *et al*, 2007), has the most homology with SYTA C_2B, and with the highest scoring animal synaptotagmins used in modeling based upon jury scores (Table 2-1).

I created the model of a C_2B dimer by aligning a SYTA C_2B domain model to the individual C_2 domains of the 2UZP unit cell. The alignment function I used within the PyMOL software aligned the domain structures based on sequence, structure and low energy (Schrödinger LLC, 2010). The low energy optimization prevented me from creating a model where domains overlapped. My dimer model (Figure 2–4) had negatively charged acidic side chains of each C_2B domain as the nearest contacts between the two domains. These two domains appear to create a highly negatively-charged binding site between the two SYTA C_2B monomers for a cation (presumably Ca^{2+}). My model predicts that this binding site forms from the four acidic side chains of glutamic acid residue 430 (E430) and aspartic acid residue 431 (D431) from each of the C_2B domains. The E430 and D431 residues together can provide the C_2B domain with an adequate localized

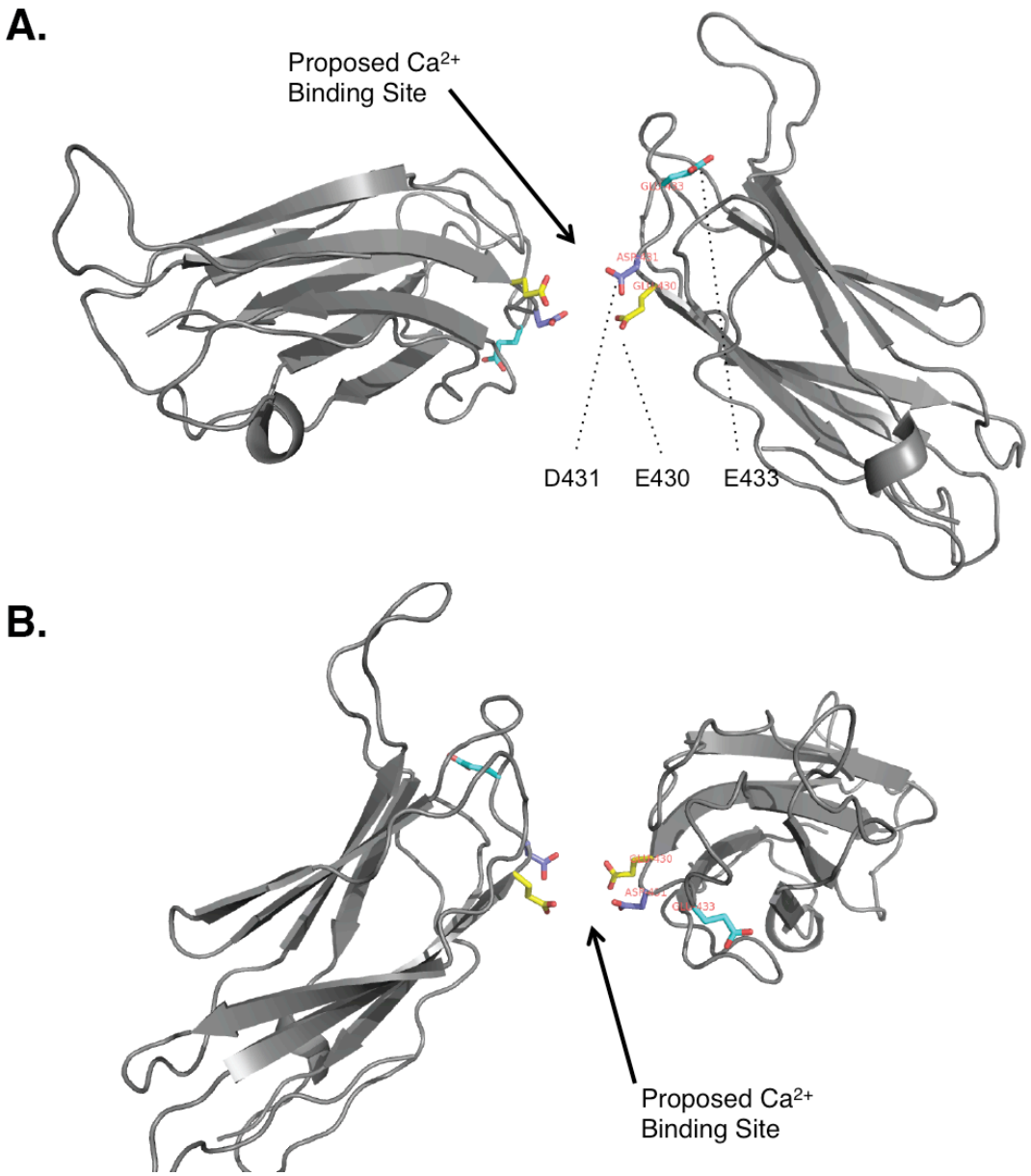

Figure 2-4: **SYTA C_2B modeled as a dimer**. When two C_2B domains are modeled as though a dimer had been formed, a negatively charged region of C_2B (residues E430, D431, and E433), as shown in Figure 2-3 B, is predicted to align between the two C_2B domains. Specifically, this model hypothesizes that in the event that two SYTA molecules dimerize, a Ca^{2+} binding site is created between glutamic acid residue E430 (yellow) and aspartic acid residue D431 (violet) of the two C_2B domains. The glutamic acid residue E433 is nearby and could contribute additional local negative charge to this C_2B dimer binding site through electrostatic effects. A and B are front and back views of the same model. A close-up zooming in on the residues of interest is in Figure 3-1.

negative charge to bind Ca^{2+} ions. Based on the alignment, I postulated that a negative charge, provided by the conformational flexibility of the nearby glutamic acid residue 433 (E433), would either aid in the binding of Ca^{2+} at this site, or, at least, help to recruit Ca^{2+} to the site. The arrangement of the E433 in the model may refine my hypothesis for the relevance of E433, but repeated modeling of side chains to confirm this hypothesis is expensive. Further, common methods, such as RASP, are designed to model side chains to avoid steric effects between side chains (Miao *et al*, 2011). Because E433 is on the surface and potentially solvent exposed, clashes with other side chains in the C_2B domain are unlikely. Recently, new algorithms have become available that consider much of the rotameric data in the RCSB in modeling side chains (Joonghyun & Deok-Soo, 2013). In either instance, the algorithms are not refined enough to be applied to a protein complex and, therefore, I did not utilize them.

Regardless of the specific role of E433, its proximity to the other two residues at the core of this predicted binding site suggests that its negative charge may contribute to the function of E430 and D431. The electrostatic effects of a charged residue can have influence at distances up to about 12Å, which is roughly equivalent to three residues away in the primary sequence of a protein (Mehler & Solmajer, 1991). E433 meets this criterion for both E430 and D431. Of particular interest, the predicted dimer binding site for Ca^{2+} would be accessible to the cytosol, which suggests that either the exchange of Ca^{2+} into and out of the

site has the potential to be extremely dynamic or that Ca^{2+} bound here may play an important role in the interaction of SYTA with cellular membranes.

Summary:

Taking into account functional studies of the $SYTA^{\Delta C2B}$ dominant-negative mutant (Lewis & Lazarowitz, 2010), which provided *in vivo* evidence consistent with SYTA functioning as a dimer or as a tetramer (which is also proposed for animal synaptotagmins), I modeled the SYTA C_2B domain. My model predicted the method by which the SYTA C_2B domain could function to bind Ca^{2+} in a dimer. A threading model, based upon sequence alignment and secondary structure prediction, predicted a novel Ca^{2+}-binding site that would exist between two SYTA-C_2B domains in a dimer. Because $SYTA^{\Delta C2B}$ functions as a dominant-negative, perhaps another domain or domains catalyzes the dimerization. While the formation of a SYTA dimer is likely promoted by the VD and/or C_2A domains, a SYTA dimer may be strengthened further by the C_2B interactions. Considering the functional studies, the interactions I modeled between the C_2B domains is most likely to be important for promoting interaction between C_2B and cytosolic Ca^{2+} ions. In the next chapter, I will explain the results of testing my model experimentally for functional relevance.

METHODS:

LOMETS Modeling

Coordinate files were constructed using sequences of SYTA representing the C_2A-C_2B (residues 230-541) and C_2B (residues 407-525) domains using the I-Tasser server (http://zhanglab.ccmb.med.umich.edu/I-TASSER/) as described (Zhang, 2008; Roy *et al*, 2010). Once uploaded to the server, the SYTA queries were fragmented into small peptides. Each peptide was queried against the structures in the RCSB protein databank for complementary structures. The complementary structures were then assembled into a model. The server produced 200 models per query and evaluated each model to determine the lowest energy structures. Multiple rounds of optimization were utilized, with the least favorable structures being removed after each round of optimization, until the lowest energy model reflecting the fragment predictions remained (Zhang, 2008; Roy *et al*, 2010). Coordinate files were viewed and processed with PyMol (Schrödinger LLC).

Secondary Structure and Jury Score Prediction

Secondary structure and alignment to RCSB Protein Data Bank (PDB) structures (http://www.rcsb.org/pdb/home/home.do) was created with the BioInfoBank meta server (http://meta.bioinfo.pl/submit_wizard.pl). Sequences of SYTA representing the C2A-C2B region of the SYTA protein or the C_2B domain alone were uploaded to the server. Once uploaded to the server, each SYTA fragment was used in a

PSI-Blast query (Altschul *et al*, 1990) to identify any related proteins. The related proteins in conjunction with the secondary structure prediction tool were used to assign structural predictions to residues of SYTA with low confidence scores (Ginalski *et al*, 2004). The server predicted the secondary structure by integrating the predictions for the individual residues into a model of the full query sequence (McGuffin *et al*, 2000). The structural databases were queried using the secondary structure prediction (but not the confidence scores) to predict the protein fold (SCOP Map) and to generate a list of homologous structures which were ranked by their 3D-jury scores and used to build the model. (Grotthuss *et al*, 2003; Ginalski *et al*, 2003; Paś *et al*, 2011).

3-D Modeling

Each atomic structural model for the SYTA query sequences was built using MODELLER and the information from the BioInfoBank meta server by threading the SYTA sequence onto the predicted fold and optimizing for lowest energy (Šali & Blundell, 1993; Šali *et al*, 1995). The proteins with high jury scores were utilized by the software as a resource in making decisions on how to optimize the structure. Coordinate files were viewed, aligned and processed with PyMol (Schrödinger LLC). Aligning one SYTA C2B model twice, once each to two C2 domains from RCSB PDB structure 2UZP, created the dimer model.

WORKS CITED

Altschul, S. F. *et al.* “Basic local alignment search tool.” *J. Mol. Biol.* **215,** 403–410 (1990).

Andreeva, A. *et al.* “Data growth and its impact on the SCOP database: new developments.” *Nucleic Acids Res.* **36,** 419–425 (2008).

Arnold, K. *et al.* “The SWISS-MODEL workspace: a web-based environment for protein structure homology modeling.” *Bioinformatics* **22,** 195–201 (2006).

Berman, H. M. *et al.* “*RCSB PDB - Content Growth Report*.” (rcsb.org, 2013).

Cheng, Y. *et al.* “Crystallographic identification of Ca^{2+} and Sr^{2+} coordination sites in synaptotagmin I C_2B domain.” *Protein Sci.* **13,** 2665–2672 (2004).

Chothia C. & Lesk A. M. “The relation between the divergence of sequence and structure in proteins.” *EMBO J.* **5,** 823 (1986).

Craxton, M. “Synaptotagmin gene content of the sequenced genomes.” *BMC Genomics* **5,** 43-56 (2004).

Fuson, K. L. *et al.* “Structure of human synaptotagmin 1 C_2AB in the absence of Ca^{2+} reveals a novel domain association.” *Biochemistry* **46,** 13041–13048 (2007).

Ginalski, K. *et al.* “3D-Jury: a simple approach to improve protein structure predictions.” *Bioinformatics* **19,** 1015–1018 (2003).

Ginalski, K. *et al.* “Detecting distant homology with Meta-BASIC.” *Nucleic Acids Res.* **32,** W576–81 (2004).

Ginalski, K. “Comparative modeling for protein structure prediction.” *Curr. Opin. Struct. Biol.* **16,** 172–177 (2006).

Herskowitz, I. “Functional inactivation of genes by dominant negative mutations.” *Nature* **329,** 219–222 (1987).

Jones, D. T. “Protein secondary structure prediction based on position-specific scoring matrices.” *J. Mol. Biol.* **292,** 195–202 (1999).

Joonghyun, R. & Deok-Soo, K. “Protein structure optimization by side-chain positioning via beta-complex.” *J. of Global Optim.* **57,** (2013).

Kabsch, W. & Sander, C. “On the use of sequence homologies to predict protein structure: identical pentapeptides can have completely different conformations.” *Proc. Natl. Acad. Sci. U.S.A.* **81,** 1075–1078 (1984).

Lewis, J. D. & Lazarowitz, S. G. "*Arabidopsis* synaptotagmin SYTA regulates endocytosis and virus movement protein cell-to-cell transport." *Proc. Natl. Acad. Sci. U.S.A.* **107,** 2491–2496 (2010).

Liwo, A. *et al.* "Protein structure prediction by global optimization of a potential energy function." *Proc. Natl. Acad. Sci. U.S.A.* **96,** 5482–5485 (1999).

McGuffin, L. J. *et al.* "The PSIPRED protein structure prediction server." *Bioinformatics* **16,** 404–405 (2000).

Mehler, E. L. & Solmajer, T. "Electrostatic effects in proteins: comparison of dielectric and charge models." *Protein Eng.* **4,** 903–910 (1991).

Miao, Z. *et al.* "RASP: rapid modeling of protein side chain conformations." *Bioinformatics* **27,** 3117–3122 (2011).

Paluszewski, M. & Karplus, K. "Model quality assessment using distance constraints from alignments." *Proteins* **75,** 540–549 (2009).

Paś, J. *et al.* "GRDB – Gene Relational Database." *BioInfoBank Library Acta.* **11,** 2659–2659 (2011).

Pike, A. C. W. *et al.* "Crystal structure of the C_2 domain of human protein kinase C gamma." *rcsb.org* (2007). doi:10.2210/pdb2uzp/pdb.

Pillardy, J. *et al.* "Recent improvements in prediction of protein structure by global optimization of a potential energy function." *Proc. Natl. Acad. Sci. U.S.A.* **98,** 2329–2333 (2001).

Roy, A. *et al.* "I-TASSER: a unified platform for automated protein structure and function prediction." *Nat. Protoc.* **5,** 725–738 (2010).

Šali, A. & Blundell, T. L. "Comparative protein modeling by satisfaction of spatial restraints." *J. Mol. Biol.* **234,** 779-815 (1993).

Šali, A. *et al.* "Evaluation of comparative protein modeling by MODELLER." *Proteins* **23,** 318–326 (1995).

Shao, X. *et al.* "Solution structures of the Ca^{2+}-free and Ca^{2+}-bound C_2A domain of synaptotagmin I: Does Ca^{2+} induce a conformational change?" *Biochemistry* **37,** 16106–16115 (1998).

Sutton, R. B. *et al.* "Structure of the first C_2 domain of synaptotagmin 1: a novel Ca^{2+}/phospholipid-binding fold." *Cell* **80,** 929–938 (1995).

Sutton, R. B. *et al.* “Crystal structure of the cytosolic C_2A-C_2B domains of synaptotagmin III. Implications for Ca^{2+}-independent SNARE complex interaction.” *J. Cell Biol.* **147,** 589–598 (1999).

von Grotthuss, M. “Application of 3D-Jury, GRDB, and Verify3D in fold recognition.” *Proteins* **53,** 418–423 (2003).

Yamazaki, T. *et al.* “*Arabidopsis* synaptotagmin SYT1, a type I signal-anchor protein, requires tandem C_2 domains for delivery to the plasma membrane.” *J. Biol. Chem.* **285,** 23165–23176 (2010).

Yeates, T. O. in “*Macromolecular Crystallography Part A”* (ed. Carter, J.) **V 276,** 344–358 (Academic Press, Waltham, MA, 1997).

Yutani, K. *et al.* “Effect of amino acid substitutions on conformational stability of a protein.” *Adv. Biophys.* **20,** 13–29 (1985).

Zhang, Y. “I-TASSER server for protein 3D structure prediction.” *BMC Bioinformatics* **9,** 40 (2008).

CHAPTER 3
In vivo analysis of Synaptotagmin A mutants

Introduction:

In an attempt to better understand how the C_2B domain of SYTA functions, I predicted the existence of a Ca^{2+}-binding site in SYTA by creating a model of the C_2B domain as a dimer. This proposed binding site would be formed between two SYTA C_2B domains when the whole SYTA protein forms a dimer or tetramer. My model is consistent with the hypothesis established by Lewis and Lazarowitz that SYTA functions as a dimer or tetramer (Lewis & Lazarowitz, 2010). My C_2B dimer model predicts that residues E430 and D431 from each SYTA protein in the dimer align to form a Ca^{2+}-binding site, which is predicted to be involved in C_2B functions. The negative charge of the Ca^{2+}-binding site would be enhanced by the negative charge of the nearby E433 residue of each SYTA protein because the E433 residue is proximal to the binding site. Such a phenomenon has been observed in other proteins (Mehler & Solmajer, 1991). The E433 residues could act to promote Ca^{2+} binding by increasing the electronegativity of the binding site, thereby helping the binding site to recruit Ca^{2+} ions. The increase in electronegativity and Ca^{2+} binding could make the Ca^{2+}-SYTA interaction more favorable and, consequently, make SYTA more sensitive to Ca^{2+} concentrations.

My SYTA C_2B dimer model led me to two important questions that could be tested experimentally: first, whether the predicted Ca^{2+}-binding site in the

dimer model is necessary for SYTA function; and, second, if the section of the primary sequence of SYTA C_2B that aligns to the Ca^{2+}-binding site in mammalian SYT1 C_2B is dispensable for function. My determination of which residues in SYTA corresponded to SYT1 was based on both the primary sequence alignments and 3D modeling. By integrating my model with the previously available data, I hypothesized that the proposed binding site would be necessary for SYTA function in endocytosis and that the residues corresponding to the mammalian SYT1 C_2B active site were not essential in endocytosis.

To answer these two questions and test my SYTA C_2B dimer model to demonstrate its functional relevance, I introduced alanine missense mutations into the SYTA C_2B domain. Alanine was selected because it is nonpolar and nonreactive with polar ions and molecules. Alanine is also less likely to inhibit protein folding because it is a relatively small residue and lacks side chain bulk. Making a physical disruption of folding highly unlikely, the methyl group side chain of alanine still maintains the chirality of each residue. While glycine is smaller than alanine, glycine is achiral and therefore too flexible to guarantee proper SYTA folding. Employing a residue with a small side chain mitigates the effect of reduced polarity on protein solubility as less of the nonpolar side chain is solvent exposed (Chatellier *et al*, 1995; Gaffaney *et al*, 2008). I tested these mutants for SYTA function in an *in vivo* assay. Specifically targeting my alanine point mutations to the residues that merited interest in my model, mutations were

generated to both the predicted SYTA C_2B Ca^{2+}-binding site and the loops of SYTA C_2B that align with the rat SYT1 C2B active site.

I predicted that, if the Ca^{2+}-binding site was functionally relevant, the expression of alanine mutants of the core E430 and D431 residues in the predicted C_2B Ca^{2+}-binding site would mimic the defective phenotype of $SYTA^{\Delta C2B}$ in an *in vivo* assay of SYTA for protoplasmic endocytosis. Specifically, in this assay endosomes would be predicted to not form at the plasma membrane. Further, I predicted that alanine point mutants targeting residues independent of the proposed SYTA C_2B Ca^{2+}-binding site would exhibit the wild-type SYTA phenotype when tested in the same functional assay. The formation of endosomes at the plasma membrane would prove this prediction.

Mutagenesis:

To test the predictions of the SYTA C_2B dimer model, fourteen different SYTA residues were mutated by site-directed mutagenesis to alanine. Four of these residues were in the C_2A domain and the remaining ten key residues were in the C_2B domain. Site-directed mutagenesis was used because it is an effective way to alter or eliminate charged molecules that are of interest in understanding intermolecular interactions. I chose site-directed mutagenesis as an approach because it would best attribute phenotypes to specific amino acid residues. I chose mutating to alanine over mutating to a positively-charged

residue, such as arginine or lysine, to avoid the possibility of creating a charge interaction in the proposed active site that may have made results difficult to interpret. Modification to alanine mitigated concerns about the bulk of the side chain. Unlike alanine, which only has a β-carbon in its side chain, both arginine and lysine have side chains that stretch beyond a δ-carbon. Alanine mutagenesis was effective in identifying residues essential for the function of rat SYT1 C_2B, which also justifies its being a reasonable approach in addressing SYTA function (Gaffaney *et al*, 2008).

The fourteen residues chosen for mutagenesis fall into three sets based on how they fit within the SYTA model (Table 3–1). The first set, set A (as in C_2**A**), consisted of the four acidic residues in the Ca^{2+}-binding site of the C_2A domain. Based on animal synaptotagmin studies, C_2A may be necessary for SYTA function in endocytosis from the plasma membrane. However, the point mutations in the C_2A domain Ca^{2+}-binding site were not predicted to have a marked effect on protein function in a test for endocytic function in the protoplast assay because the mutation of any single acidic amino acid was not predicted to remove enough negative charge to prevent Ca^{2+} binding. The second set, set D (as in **d**imer), consists of the three acidic residues that form my predicted Ca^{2+}-binding site when the SYTA C_2B domain is part of a homodimer, as modeled in Figure 2-4. The alanine mutations of the set D residues

Table 3-1: **Site-Directed SYTA Alanine Missense Mutants**. Residues from three models were mutated to alanine by making the following codon modifications. Group "A" mutants modified residues in the C_2A domain involved in predicted Ca^{2+} binding based on the model of C_2A in Figure 2-3 A. Group "D" mutants modified acidic residues important for the predicted C_2B dimer model in Figure 2-4. Groups "C" mutants modified polar residues that are relevant in the SYTA C_2B monomer model that is predicted not to bind Ca^{2+}.

Domain	Residue	Native Codon	Alanine Codon	
C2A	Asp 282	GAT	GCT	A
C2A	Asp 332	GAC	GCC	
C2A	Glu 334	GAA	GCA	
C2A	Glu 340	GAG	GCG	
C2B	Glu 430	GAG	GCG	D
C2B	Asp 431	GAT	GCT	
C2B	Glu 433	GAA	GCA	
C2B	His 436	CAC	GAC	C
C2B	His 437	CAT	GAT	
C2B	Thr 438	ACC	GCC	
C2B	Asn 439	AAT	GCT	
C2B	Ser 487	AGC	GCC	
C2B	Ser 489	TCT	GCT	
C2B	Glu 499	GAA	GCA	

are predicted to yield a SYTA protein that would fail to function in the same protoplast assay. The third set, set C (as in the **c**anonical C_2 binding site), consists of the seven charged and polar residues that are modeled as residing in the coils that align to the Ca^{2+}-binding site of the mammalian SYT1 C_2B domain (Figure 3–1). Mutations to the set C residues in SYTA C_2B are predicted not to affect the function of SYTA. As residues on the homologous loops are predicted to function in some animal SYTs, the analogous mutations in those systems would be predicted to inhibit the homologous SYT function in endocytosis and

exocytosis for other organisms (including some mammalian SYT1 proteins where this has been demonstrated) (Gaffaney *et al*, 2008).

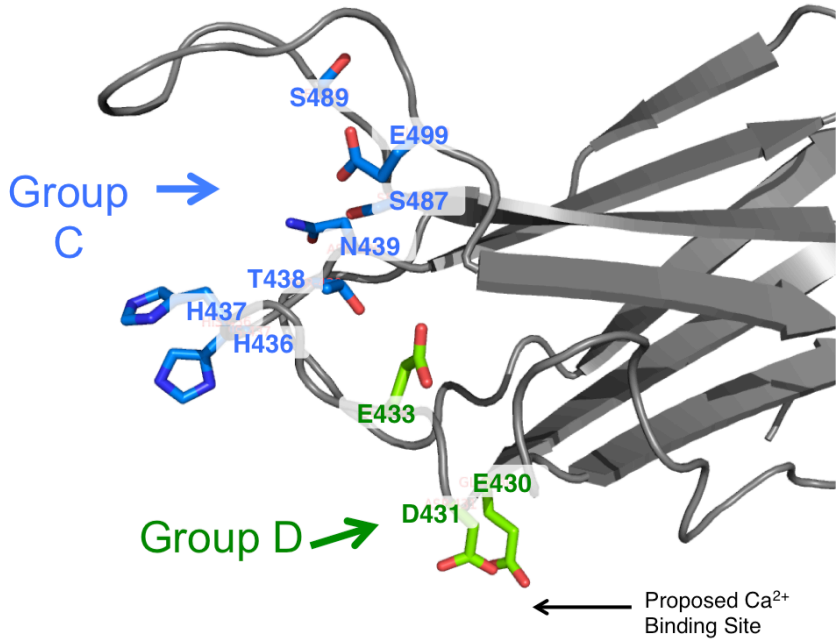

Figure 3-1: **SYTA C_2B residues investigated with alanine missense mutations**. These ten SYTA C_2B domain residues were individually mutated to alanine to create site-directed point mutants. The residues from SYTA C_2A and C_2B that were mutated were selected based on threading models of SYTA C_2 domains (Figures 2-3 & 2-4). The SYTA C_2B mutated residues are grouped based on the model for C_2B Ca^{2+} binding which they are designed to test. Individual mutant details are listed in Table 3-1.Group C (blue) mutants are mutations that disrupt the polar residues that directly align with the active site of rat SYT1 C_2B protein. Group D (green) mutants are predicted to participate in the creation of the Ca^{2+}-binding site identified in the dimer model (Figure 2-4).

I tested SYTA alanine missense mutants using an *in vivo* functional assay in protoplasts to determine which mutants, if any, were defective in function and acted like $SYTA^{\Delta C2B}$. To carry out this assay, I isolated protoplasts from the leaves of 6-8 week old *Nicotiana benthamiana* plants and transfected them with a SYTA mutant of interest with a C-terminus GFP fusion (SYTA-GFP). After approximately 20 hours, I was able to determine if either the mutation was

functional based on whether the SYTA-GFP had regulated the formation of PM derived endosomes, which would have been labeled with the SYTA-GFP, or if the mutant was defective in endocytosis as indicated by SYTA-GFP localized elsewhere in the protoplast. I predicted that the set D mutants would not localize to endosomes because Ca^{2+} binding had been abolished. In addition to testing the relevance of the predicted C_2B dimer site, screening for function in protoplasts eliminates the need to focus on all fourteen mutants in subsequent assays. Mutants with wild-type function would not need further consideration; the only exception would be if I were to use them as future controls.

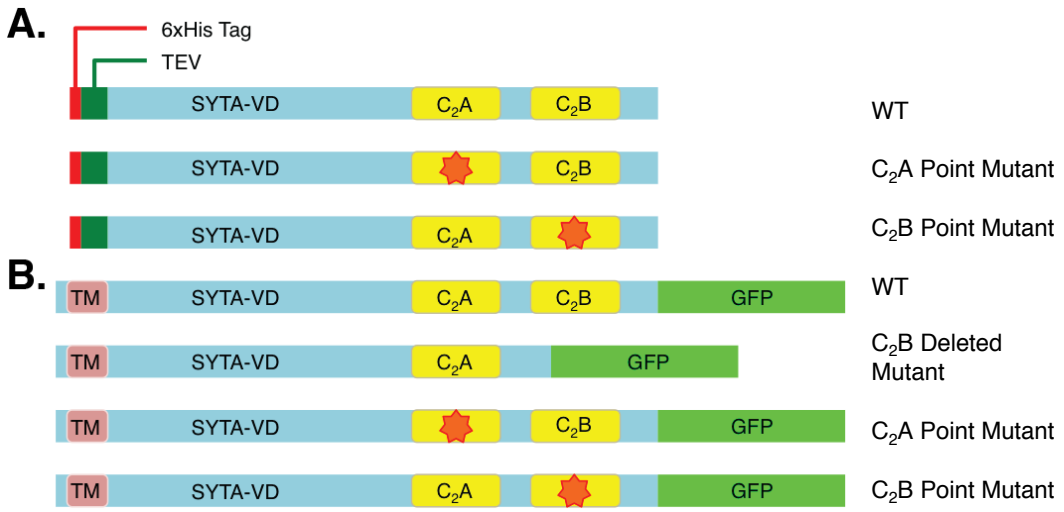

Figure 3-2: **SYTA constructs used in this study**. (A) $SYTA^{\Delta TM}$ constructs had residues 1-32 replaced with a histidine metal affinity binding site (6xHis) and *Tobacco Etch Virus* (TEV) protease cleavage site. Missense mutations (orange ✸) were introduced into the C_2A or C_2B domains by site-directed mutagenesis. (B) SYTA-GFP constructs have a GFP fluorophore fused at the C-terminus to allow imaging of the protein. $SYTA^{\Delta C2B}$-GFP had the C_2B domain deleted.

I generated the SYTA point mutations by directing specific targeted DNA replication errors changing codons of interest into alanine codons. I created the mutants with a pET28a-$SYTA^{\Delta TM}$ plasmid through a modified polymerase chain

reaction. The pET28a-SYTA$^{\Delta TM}$ plasmid is a 6.8 kb *E. coli* expression vector that includes the gene for a mutant of SYTA where the signal peptide and transmembrane domain (TM) were deleted (SYTA$^{\Delta TM}$). I chose this plasmid as a template because smaller templates are more reliably mutagenized in mutagenic PCR than larger plasmids (Kunkel 1985). Among the SYTA constructs used in this study, pET28a-SYTA$^{\Delta TM}$ was the smallest. For *in vivo* protoplast expression studies, I subcloned each individual mutation into a pTEX-GFP vector. Sub-cloning of the mutants created a series of fluorescently-labeled SYTA alanine point mutants, each with a GFP fluorophore at the COOH-terminal (Figure 3–2) (Frederick *et al*, 1998). The SYTA mutant pET28a vectors were constructed for expression from an *E. coli* expression system. The mutants in the pTEX vector were designed for *in vivo* transient expression studies in plant cells and protoplasts.

Protoplast transient expression:

To test each of the SYTA alanine missense mutants for function, I employed the previously mentioned protoplast transient expression assays. The basis for these functional assays was the studies of SYTA by Lewis and Lazarowitz (Lewis & Lazarowitz, 2010). Lewis and Lazarowitz demonstrated that the ability of SYTA to function in endocytosis could be inferred from the subcellular localization of fluorescently-labeled SYTA. Lewis and Lazarowitz demonstrated that the loss of function mutant, SYTA$^{\Delta C2B}$-GFP, did not

accumulate on endosomes in protoplasts, but, instead, SYTA was concentrated at the plasma membrane and was prone to backing up within the secretory system into the endoplasmic reticulum. Lewis and Lazarowitz proposed that the presence of SYTA$^{\Delta C2B}$ in the ER was caused by a combination of overexpression and buildup of protein at the PM, which inhibits the processing of the protein through the secretory system (Lewis & Lazarowitz, 2010). When untagged SYTA$^{\Delta C2B}$ was expressed in leaf epidermal cells, both endocytosis at the plasma membrane and endosome recycling to the plasma membrane failed to occur. This failure indicated that SYTA is a regulator of both functions (Lewis & Lazarowitz, 2010). All three phenotypes are a feature of the deletion of C_2B from SYTA on endocytosis, and, as a result, we assume that these phenotypes are linked: a mutant that causes one is likely to cause the other two.

SYTA mutations that have the same phenotype as the wild-type SYTA are presumed to be functional. Specifically, the formation of endosomes in my *in vivo* protoplast assay demonstrated that a mutant retained its functionality and therefore the mutated residue was not essential for the endocytic function of SYTA at the plasma membrane. In my assay, alanine point mutants that exhibit the same localization pattern as SYTA$^{\Delta C2B}$ show that endocytosis is not occurring normally at the cell surface. By extension, the phenotypic change can be attributed to the necessity of the residue that had been mutated for SYTA function in endocytosis.

Wild-type SYTA-GFP and each of the SYTA alanine missense mutants were transiently expressed in protoplasts derived from *Nicotiana benthamiana* leaf tissue (Carvalho & Lazarowitz, 2004). As Lewis and Lazarowitz previously demonstrated, wild-type SYTA localizes to endosomes (Lewis & Lazarowitz, 2010). This localization indicates that endocytosis is functioning normally and that SYTA is functional in endocytosis (Figure 3-3 A). SYTA$^{\Delta C2B}$ localized to the plasma membrane and not to the endosomes, which indicates that this mutant was not functioning properly in endocytosis. In addition to localizing to the PM, SYTA$^{\Delta C2B}$ did accumulate to varying extents in the ER (Figure 3–3 B) (Lewis & Lazarowitz, 2010).

The C_2A mutants (set A) behaved like wild-type SYTA in the protoplast assay. Each of the alanine missense mutants in set A localized to endosomes at ~20 hours and at ~40 hours post transfection (Figure 3–3 C, D). The localization of the set A mutants indicates their functionality in endocytosis. The alanine missense mutants targeting the residues comprising the canonical C_2B Ca^{2+}-binding site (set C) also localized to endosomes at both ~20 hours and ~40 hours post-transfection (Figure 3–3 E, F). As is the case with the set A mutants, the localization pattern of the set C mutants shows that they function in endocytosis. The three mutants that I predicted to form the C_2B Ca^{2+}-binding site in the SYTA dimer model (set D), all localized to the plasma membrane and did not localize to

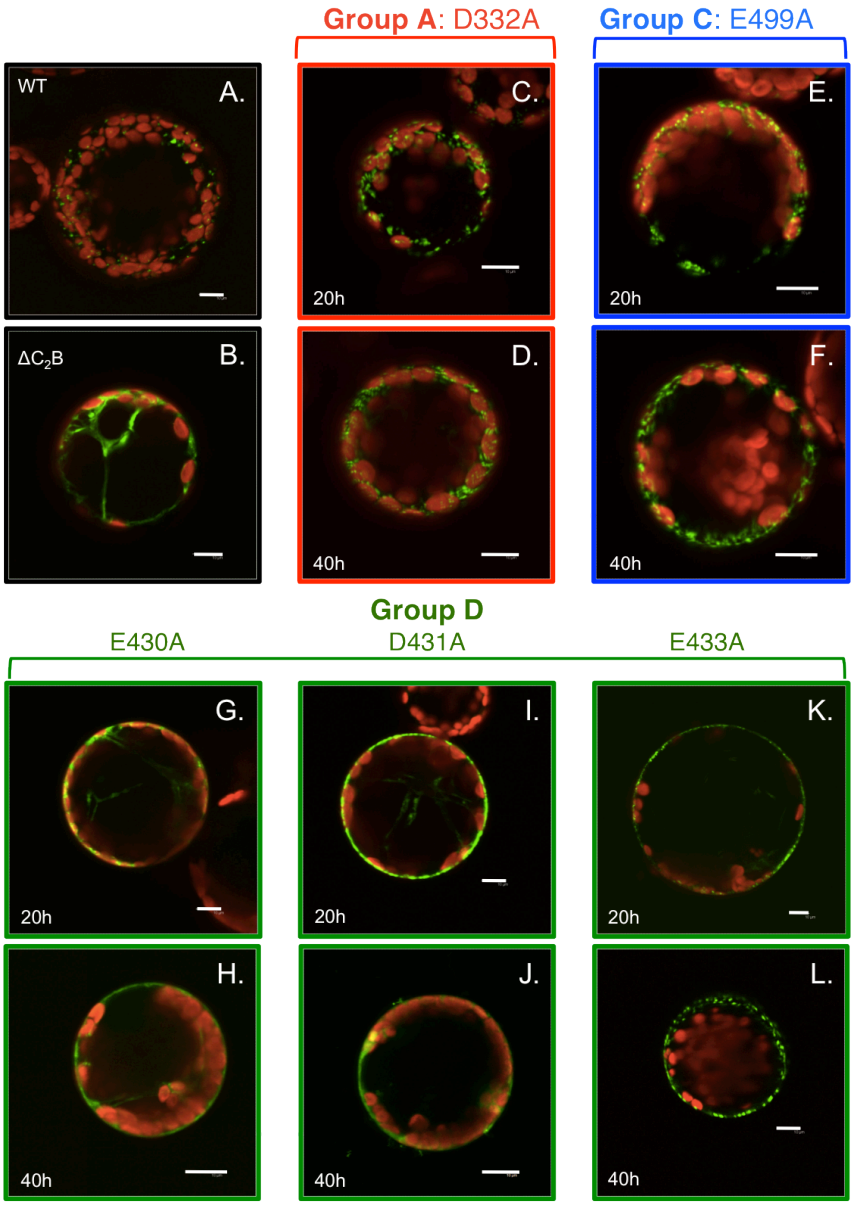

Figure 3-3: **Localization of wild type and mutant SYTA-GFP fusions in protoplasts**. Projected confocal light scanning microscopy (CLSM) Z-series of (A) wild type and (B-L) mutant SYTA-GFP in *N. benthamiana* protoplasts at ~20h and ~40h post transfection. (A) WT SYTA-GFP localizes to endosomes and (B) $SYTA^{\Delta C2B}$-GFP remains at the plasma membrane and backs up into the ER. (C-D) C_2A domain mutant E332A (group "A") localizes to endosomes at both ~20h and ~40h post transfection. (E-F) The E499A C_2B missense mutant (group "C") localizes to endosomes at both ~20h and ~40h post transfection. Mutants in the key residues in the dimer model (group "D"), (G-H) E430A and (I-J) D431A localize to the plasma membrane and ER. The localization of the E433A mutant is (K) at the plasma membrane at ~20h post transfection and (L) to endosomes at ~40h post transfection. Images shown for group "A" (red, C-D) and group "C" (blue, E-F) are representative of those groups. GFP is shown in green and chlorophyll autofluorescence is shown in red in all panels. Scale bars 10 µm.

endosomes at ~20 hours post transfection, as had the SYTA$^{\Delta C2B}$-GFP mutant (Figure 3–3 G, I, K). At ~40 hours post-transfection, both the E430A and D431A mutants were still localized to the plasma membrane (Figure 3–3 H, J). Among all the mutants, the SYTA^{E433A}-GFP mutant was unique. Although not localized to endosomes at ~20 hours post transfection, the E433A mutant did localize to endosomes at ~40 hours post transfection (Figure 3–3 L).

The localization of the SYTA mutants when expressed in protoplasts (as shown in Figure 3–3) is summarized in Table 3–2. Alanine missense mutants in both the SYTA C_2A domain (set A) and the non-conserved loop region of the SYTA C_2B domain corresponding to the rat SYT1 C_2B active site (set C) localized to endosomes (the same as wild-type SYTA-GFP). This localization indicates that each of these mutants functioned in the same way as wild-type SYTA. The set D mutants were defective in SYTA function. In localizing to the plasma membrane, the SYTA^{E430A}-GFP and SYTA^{D431A}-GFP missense mutants localized identically to SYTA$^{\Delta C2B}$-GFP indicating a loss of function in endocytosis. This loss of function is consistent with their proposed role in the dimer model. The SYTA^{E433A}-GFP mutant was delayed in localizing to endosomes, suggesting that this mutant retained some endocytic function, but was not fully effective as a regulator of endocytosis.

Table 3-2: **Summary of SYTA-GFP mutant localization in protoplasts**. Both WT and ΔC_2B proteins localized as previously observed (Lewis & Lazarowitz, 2010). Group "A" (red) and group "C" (blue) mutants replicated the wild-type phenotype of endosome localization. The group "D" mutants were defective in localization, replicating the ΔC_2B phenotype; only the E433A mutant was able to localize to endosomes after 24 hours, indicating a delay in observed function. The fully defective E430A and D431A mutants form the core of the proposed Ca^{2+}-binding site in the dimer model.

SYTA	Domain	Localization	
WT	C_2A+C_2B	endosomes	
ΔC_2B	C_2B	plasma membrane + ER	
Group A	C_2A	endosomes	
Group C	C_2B	endosomes	
E430A	C_2B	plasma membrane + ER	*dimer*
D431A	C_2B	plasma membrane + ER	
E433A	C_2B	delayed (>24 h) to endosomes	

Subcellular compartment-specific markers:

In order to verify the subcellular localization of the SYTA alanine missense mutants, I co-expressed each mutant with compartment-specific markers in *Nicotiana benthamiana* mesophyll protoplasts. To observe the co-expression, I individually co-transfected protoplasts with a SYTA-GFP construct and a mCherry-tagged compartment marker for each of the plasma membrane, the Golgi, and the peroxisomes (Nelson *et al*, 2007). I imaged the protoplasts at approximately 20 hours and approximately 40 hours post-transfection. With the exception of the transfection of an additional plasmid, the experimental setup was identical to the previous protoplast localization assay. Co-transfection with the

plasma membrane marker confirmed that both SYTA$^{\Delta C2B}$-GFP and SYTA^{E430A}-GFP localized to the plasma membrane. Wild-type SYTA did not localize to the plasma membrane (Figure 3–4 A, C, E).

To show whether endosomes labeled with SYTA-GFP were distinct from other membrane compartments, I co-expressed SYTA-GFP with compartment markers for the Golgi apparatus and peroxisomes. Co-localization with the Golgi apparatus marker was tested because the trans-Golgi network has been suggested as a target of endosomes and a sorting compartment for endosomes. This hypothesis is not agreed upon within the research community (Viotti *et al*, 2010). Were it to be shown that some fraction of SYTA-GFP were to localize to the Golgi, it would provide circumstantial evidence supporting a role for the Golgi in the SYTA regulated endocytic pathway.

Because Schapire *et al.* showed that SYTA influences plasma membrane dynamics in *Arabidopsis* (Schapire *et al*, 2008), I tested the co-localization of SYTA-GFP with peroxisomes. Because peroxisomes are involved in the catabolism of fatty acids, they could be a destination for endosomes when a cell uses endocytosis to maintain membrane homeostasis (Kindl, 1993). SYTA-GFP did not co-localize with either of these two compartment-specific markers (Figure 3–4 G, I). This data indicates that the SYTA-GFP-labeled endosomes, the Golgi apparatus, and the peroxisomes are distinct. The distribution of the chloroplasts

within the protoplasts is visualized by chlorophyll auto-fluorescence recolored blue (Figure 3–4 B, D, F, H, J). The distinct localization of SYTA-GFP means that it could be developed as a useful marker in studying plant endocytosis.

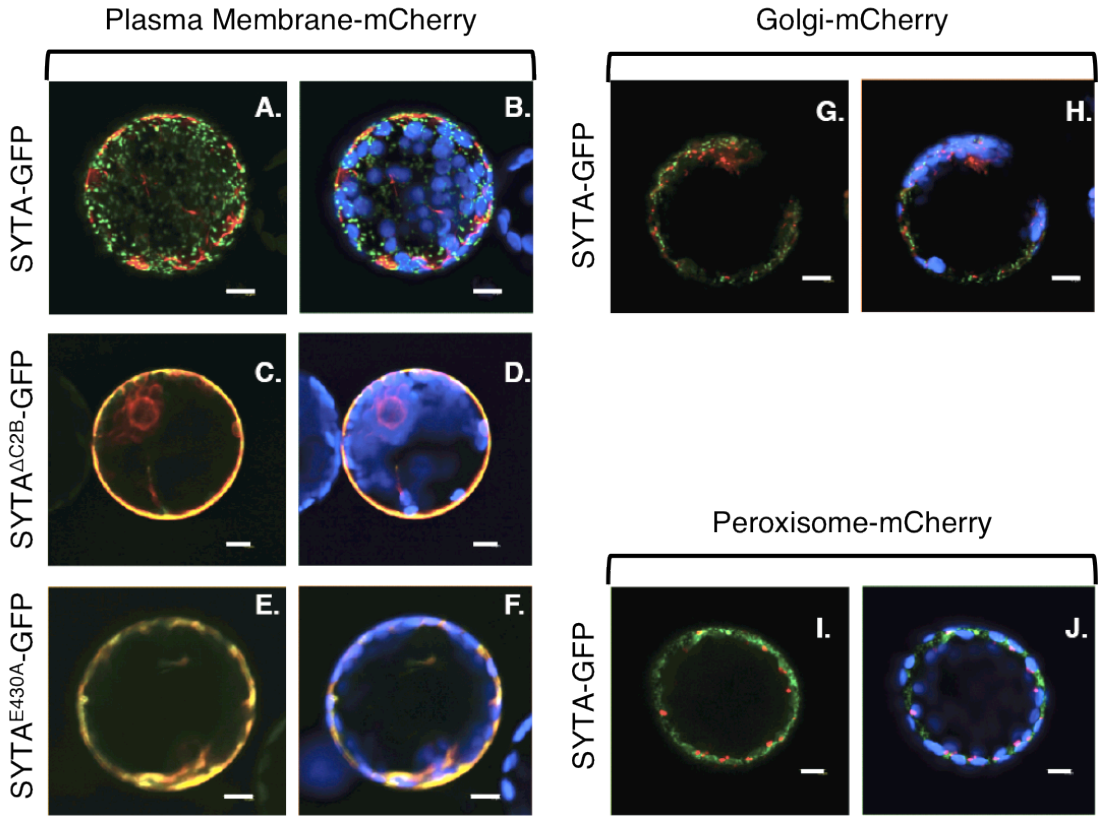

Figure 3-4: **Co-localization of SYTA and compartment-specific membrane markers.** Projected CLSM Z-series of transiently expressed (A-B, G-J) wild-type SYTA-GFP, (C-D) SYTA$^{\Delta C2B}$-GFP, and (E-F) SYTA^{E430A}-GFP co-expressed with (A-F) a plasma membrane marker mCherry fusion protein, (G-H) Golgi marker mCherry fusion protein and (I-J) peroxisome marker mCherry fusion protein in *N. benthamiana* protoplasts. GFP is shown in green and mCherry is shown in red in all panels. Chlorophyll autofluorescence is shown in blue in panels B, D, F, H and J. (A-B, G-J) SYTA-GFP labeled endosomes are distinct from the (A-B) plasma membrane (~20h post transfection), (G-H) Golgi (~20h post transfection), and (I-J) peroxisomes (~40h post transfection). (C-D) SYTA$^{\Delta C2B}$-GFP (~40h post transfection) and (E-F) SYTA^{E430A}-GFP (~20h post transfection) both localized to the plasma membrane, as indicated by co-localization (yellow). The plasma membrane marker is full-length *At*PIP2A, the Golgi marker is the transmembrane domain (residues 1-49) of *Gm*Man1, and the peroxisome marker is a peroxisomal targeting signal (Ser-Lys-Leu) (Nelson *et al,* 2007). Scale bars 10 µm.

Summary:

My protoplast expression studies showed that residues, that were predicted to be Ca^{2+}-binding in my SYTA C_2B dimer model, are functional and are consistent with my model. These expression studies concur with my hypothesis that when SYTA forms a dimer or tetramer, these residues create a functional C_2B Ca^{2+}-binding site.

This observation shows that the residues corresponding to these point mutants are essential for SYTA function. Each of the three point mutants to the proposed Ca^{2+}-binding site of the SYTA C_2B dimer model was not functional in endocytosis. The results of the protoplast transient expression assay confirm the prediction from my SYTA C_2B dimer model that the Ca^{2+}-binding site should be necessary for function. Alanine missense mutants that targeted the two residues $SYTA^{E430A}$-GFP and $SYTA^{D431A}$-GFP were proposed to be the core of my Ca^{2+}-binding site based upon their negative charge density. At the tested time points, these missense mutants localized to the PM based upon co-labeling and were defective in endocytosis function. The defective function of these specific point mutants in endocytosis suggests that residues E430 and D431 fit my model's prediction of their function.

My protoplast assay demonstrated that $SYTA^{E433A}$-GFP was also defective in endocytic function. Instead of a total loss of function, the formation of

endosomes is slowed or delayed. This observation suggests that E433 may be an effector of Ca^{2+}-binding at the proposed dimer site. Given the predicted peripheral location of residue E433 relative to the two other residues in the Ca^{2+}-binding site of the SYTA C_2B dimer model (Figure 2–4), both the model of the dimer and the protoplast data suggest that the negative charge provided by the SYTA residue E433 could help to recruit Ca^{2+} to the core of the binding site. My model proposes that E433 is close enough (within 12 Å) to affect both E430 and D431 (Mehler & Solmajer, 1991). Should my hypothesis be correct, the E433 residue would likely function to increase the affinity of the SYTA C_2B for binding Ca^{2+}.

In the case of the predicted Ca^{2+}-binding residues of SYTA C_2A (set A), mutating any acidic residue would likely not remove enough negative charge to prevent Ca^{2+} from binding in the C_2A domain, although, given the evidence of a functional role for C_2A in some animal SYTs, this is conjecture. Within the limitations of my protoplast assay, the C_2A domain is not predicted to be essential for SYTA function in endocytosis. Abolishing the interaction of individual C_2A acidic residues and Ca^{2+} does not prevent endocytosis; it still may have another consequence that was not observed with this assay. This non-essential function is indicated by animal SYT studies. When the SYT1 C_2A domain is removed from SYT1, the SYT1 C_2B domain is capable of promoting membrane clustering. In the opposite case, where SYT1 C_2B is removed, SYT C_2A is not

able to bring membranes into close proximity. When assayed for function in neurotransmitter release, SYT1$^{\Delta C2B}$ was not functional and SYT1$^{\Delta C2A}$ retained function, but SYT1$^{\Delta C2A}$ was partially impaired in recovery (Littleton *et al*, 2001; Xue *et al*, 2008; Yao *et al*, 2012). Further, at least one SYT1 C_2A point mutant to the SYT1 C_2 domain fragment (C_2AB-D178N) showed a significant decrease in the ability of the fragment to mix lipids as compared to the wild type (C_2AB) fragment (Xue *et al*, 2008). If the function of SYTA was impaired by any of the SYTA C_2A missense mutants, the protoplast assay was probably not the appropriate assay to observe it.

My mutants of SYTA C_2B that targeted the canonical C_2B Ca^{2+}-binding site, based upon alignment with rat SYT1 (set C), functioned the same as wild-type SYTA. The retention of function when these residues were mutated to alanine indicated that this site was not necessary for SYTA-regulated endocytosis. While it is possible that these polar residues do interact with ions, an equally likely suggestion is that their polar character is most significant in adding to the cytosolic solubility of the C_2B domain. The most likely candidate to play a role in Ca^{2+}-binding if the C_2B monomer model were to bind Ca^{2+} as predicted based on its -1 charge would be E499, the only acidic residue among set C (Figure 1-6 C). However the SYTA^{E499A}-GFP mutant retains wild-type SYTA function, which indicates either that any interaction that may occur with E499 is not essential for

SYTA function in endocytosis or that it creates a phenotype that my protoplast assay is not designed to observe.

While the results in this section agree with the hypothesis that the SYTA C_2B domain functions as a dimer or tetramer, they do not distinguish between SYTA being either a dimer or a tetramer. The next chapter demonstrates that, as I have hypothesized, a SYTA dimer can and does form.

METHODS

Mutagenesis

Mutagenic PCR primers were designed with the site-directed mutagenesis primer design tool, Quick Change Primer Design, from Stratagene (now Agilent Technologies) (http://www.genomics.agilent.com/primerDesignProgram.jsp) in order to create alanine codons that are compatible with the codon bias in higher eukaryotes, as opposed to the codon usage of *E. coli*. The alanine codons utilized are listed in Table 3-1. Primer pairs for each mutant are listed in Table 3-3. These oligonucleotides were used for mutagenic PCR of a SYTA coding DNA sequence (CDS) from which the transmembrane domain and signal peptide had previously been deleted (SYTA$^{\Delta TM}$) when the CDS was cloned into a pET28a vector (Rosenberg *et al*, 1987; Lewis & Lazarowitz, 2010). A Dpn1 restriction digest of the PCR product was utilized to eliminate non-mutagenized DNA. Dpn1 (New England Biolabs) distinguishes between the methylated template DNA, which it digests, and the non-methylated mutagenic PCR product (Agilent, 2008). Each PCR product was transformed into DH5α *E. coli* competent cells by electroporation and plated on LB agar with kanamycin selection to generate colonies (Sambrook & Russell, 2001). Colonies were selected and their pET28a-SYTA$^{\Delta TM}$ was sequenced to confirm if the desired mutant had been created. The colonies were inoculated and grown to high density in LB culture media at 37°C, and plasmid DNA was purified with the QIAamp DNA Mini Kit (Qiagen). A fragment of the gene containing the desired mutation was sequenced with an

Applied Biosystems 3730xl capillary system (Cornell BRC Genomics Lab). After confirming the presence of a desired mutation, the entire gene coding DNA region of pET28a-SYTA$^{\Delta TM}$ (insertion site and inserted gene) was sequenced to confirm that only the codon of interest had been mutated. As each mutant was generated, it could be cloned into other vectors for any assay testing the mutant.

Table 3-3: **Oligonucleotide pairs utilized in mutagenic PCR of SYTA**. Each of the fourteen SYTA missense mutants was created by mutagenic PCR using a forward and reverse mutagenic primer for each mutant. The forward oligonucleotide corresponds to the coding sequence of SYTA and the reverse oligonucleotide corresponds to the reverse compliment sequence of SYTA. Mutated nucleotides are labeled in bold font.

SYTA Residue	**Forward Oligonucleotide**	**Reverse Oligonucleotide**
Asp 282	GGGGCAG**C**TCCATTCGTG	CACGAATGGA**G**CTGCCCC
Asp 332	CAGTGTGTATG**C**CTGGGAACAG	CTGTTCCCAG**G**CATACACACTG
Glu 334	GTGTATGACTGGG**C**ACAGGTTG	CAACCTGT**G**CCCAGTCATACAC
Glu 340	GGAATCCCG**C**GAAGATGGG	CCCATCTTC**G**CGGGATTCC
Glu 430	CATTCGGCTG**C**GGATGTTGAAG	CTTCAACATCC**G**CAGCCGAATG
Asp 431	CGGCTGAGG**C**TGTTGAAGG	CCTTCAACA**G**CCTCAGCCG
Glu 433	GAGGATGTTG**C**AGGAAAGCACC	GGTGCTTTCCT**G**CAACATCCTC
His 436	GTTGAAGGAAAG**G**ACCATACCAATCC	GGATTGGTATGGT**C**CTTTCCTTCAAC
His 437	GAAGGAAAGCAC**G**ATACCAATCCTTAC	GTAAGGATTGGTAT**C**GTGCTTTCCTTC
Thr 438	GGAAAGCACCAT**G**CCAATCCTTAC	GTAAGGATTGG**C**ATGGTGCTTTCC
Asn 439	CACCATACC**GC**TCCTTACGTG	CACGTAAGGA**GC**GGTATGGTG
Ser 487	GAAGTGCTG**GC**CACCTCTTC	GAAGAGGTG**GC**CAGCACTTC
Ser 489	TGAGCACC**G**CTTCCAGGATAG	CTATCCTGGAAG**C**GGTGCTCA
Glu 499	TTGCATCCCAAGG**C**AACACTG	CAGTGTT**G**CCTTGGGATGCAA

Cloning

SYTA$^{\Delta TM}$ mutants were used to subclone each mutation into pTEX-SYTA-GFP, which had been created previously by cloning the *SYTA* coding sequence into pTEX-GFP (Lewis & Lazarowitz, 2010). Cloning SYTA$^{\Delta TM}$ mutants directly from pET28 would not have allowed for expression of full length SYTA because of the TM deletion in SYTA$^{\Delta TM}$. The entire domain containing each mutation (in C_2A or C_2B) was cloned from the corresponding pET28a-SYTA$^{\Delta TM}$ mutant. *E. coli* DH5α

cells containing pET28- SYTA$^{\Delta TM}$ mutants were grown to high density in LB culture media at 37°C, and plasmid DNA was purified with the QIAamp DNA Mini Kit (Qiagen) and digested with restriction enzymes BamHI and SalI (C_2A mutants) or SalI and SphI (C_2B mutants) (New England Biolabs). The pTEX-SYTA-GFP was digested with the same pair of enzymes as the insert sequence. Both insert and vector were gel purified using the QIAEX II Gel Extraction Kit (Qiagen). The plasmid and insert were ligated together with T4 DNA Ligase (Invitrogen) and the resulting pTEX-SYTA-GFP vector was transformed into DH5α competent cells. Each pTEX-SYTA-GFP mutant construct (Table 3-1) was confirmed by sequencing with an Applied Biosystems 3730xl capillary system (Cornell BRC Genomics Lab).

Protoplasts

SYTA-GFP constructs (wild-type and mutants), each driven by the 35S promoter in pTEX, were PEG transfected into mesophyll protoplasts isolated from *Nicotiana benthiana* leaves as described (Carvalho & Lazarowitz, 2004), with the exception that all buffers were used at room temperature (~23°C) instead of 4°C.

Protoplasts were isolated from the leaves of ~6-week-old *N. benthamiana* plants. The leaves were cut into strips and digested overnight in 0.2% cellulase, 0.05% macerozyme, 0.66 M mannitol, and 8 mM $CaCl_2$ to release the cells. Protoplasts were filtered through miracloth and layered on 21% sucrose so debris could be

removed by centrifugation (8 minutes at 437 g). Protoplasts that formed a band and remained above the sucrose solution were collected by pipetting, washed, and collected again by gentle centrifugation (2 minutes at 70 g) in the following buffers in order: 0.66 M mannitol/8 mM $CaCl_2$, 0.53 M mannitol/8 mM $CaCl_2$, 0.46 M mannitol/8 mM $CaCl_2$, 0.25 M mannitol/77 mM NaCl/62.5 mM $CaCl_2$/2.5 mM KCl/2.5 mM glucose/0.75 mM MES, and 154 mM NaCl/125 mM $CaCl_2$/5 mM KCl/5 mM glucose/1.5 mM MES. Protoplasts were resuspended and maintained in 400 mM mannitol, 15 mM $MgCl_2$, and 5 mM MES.

Protoplasts (300 µL), 40% polyethylene glycol (PEG) (300 µL) and 20-30 µl plasmid DNA (1 mg/ml) were mixed to transfect the protoplasts. In the co-localization studies, plasmids encoding PM (pBIN20-PM-rb), Golgi (pBIN20-G-rb), ER (pBIN20-ER-rb), and peroxisome (pBIN20-PX-rb) compartment markers fused with the mCherry fluorophore (Nelson *et al*, 2007) (ABRC) were co-transfected with SYTA-GFP constructs. The “rb” in each plasmid name indicates that the plasmid has an mCherry flurophore (r) and Basta resistance (b). For each co-localization experiment 15 µl of SYTA DNA (1 mg/ml) and 15 µl marker DNA (1 mg/ml) were co-transfected.

Imaging

Confocal Laser Scanning Microscopy (CLSM) was used to image protoplasts using a Leica SP2 microscope employing a 20x water immersion

objective lens. Individual images were collected in Z-series with ~0.8 µm interval between each image. Z-series were projected from 3 consecutive images from within the Z-series and scale bars were added using Leica SP2 software (Leica Microsystems).

WORKS CITED:

Carvalho, M. F. & Lazarowitz, S. G. “Interaction of the movement protein NSP and the *Arabidopsis* acetyltransferase *At*NSI is necessary for Cabbage leaf curl *geminivirus* infection and pathogenicity.” *J. Virol.* **78,** 11161–11171 (2004).

Chatellier, J. *et al.* “Codon-based combinatorial alanine scanning site-directed mutagenesis: design, implementation, and polymerase chain reaction screening.” *Anal. Biochem.* **229,** 282–290 (1995).

Frederick, R. D. *et al.* “Recognition specificity for the bacterial avirulence protein AvrPto is determined by Thr-204 in the activation loop of the tomato Pto kinase.” *Mol. Cell* **2,** 241–245 (1998).

Gaffaney, J. D. *et al.* “Synaptotagmin C_2B domain regulates Ca^{2+}-triggered fusion in vitro: critical residues revealed by scanning alanine mutagenesis.” *J. Biol. Chem.* **283,** 31763–31775 (2008).

Kindl, H. “Fatty acid degradation in plant peroxisomes: function and biosynthesis of the enzymes involved.” *Biochimie* **75,** 225–230 (1993).

Kunkel, T. A. “Rapid and efficient site-specific mutagenesis without phenotypic selection.” *Proc. Natl. Acad. Sci. U.S.A.* **82,** 488–492 (1985).

Lewis, J. D. & Lazarowitz, S. G. “*Arabidopsis* synaptotagmin SYTA regulates endocytosis and virus movement protein cell-to-cell transport.” *Proc. Natl. Acad. Sci. U.S.A.* **107,** 2491–2496 (2010).

Littleton, J. T. *et al.* “Synaptotagmin mutants reveal essential functions for the C_2B domain in Ca^{2+}-triggered fusion and recycling of synaptic vesicles *in Vivo*.” *J. Neurosci.* **21,** 1421–1433 (2001).

Mehler, E. L. & Solmajer, T. “Electrostatic effects in proteins: comparison of dielectric and charge models.” *Protein Eng.* **4,** 903–910 (1991).

Nelson, B. K. *et al.* “A multicolored set of in vivo organelle markers for co-localization studies in *Arabidopsis* and other plants.” *Plant J.* **51,** 1126–1136 (2007).

Rosenberg, A. H. *et al.* “Vectors for selective expression of cloned DNAs by T7 RNA polymerase.” *Gene* **56,** 125–135 (1987).

Sambrook, J. & Russell, D. W. “*Molecular Cloning: A Laboratory Manual.*” (Cold Spring Harbor Laboratory Press, Cold Spring Harbor, NY, 2001).

Schapire, A. L. *et al.* "*Arabidopsis* synaptotagmin 1 is required for the maintenance of plasma membrane integrity and cell viability." *Plant Cell* **20,** 3374–3388 (2008).

Viotti, C. *et al.* "Endocytic and secretory traffic in *Arabidopsis* merge in the trans-Golgi network/early endosome, an independent and highly dynamic organelle." *The Plant Cell Online* **22,** 1344–1357 (2010).

Xue, M. *et al.* "The Janus-faced nature of the C_2B domain is fundamental for synaptotagmin-1 function." *Nat. Struct. Mol. Biol.* **15,** 1160–1168 (2008).

Yao, J. *et al.* "Uncoupling the roles of synaptotagmin I during endo- and exocytosis of synaptic vesicles." *Nat. Neurosci.* **15,** 243–249 (2012).

CHAPTER 4
Biochemical Analysis of Synaptotagmin A

Introduction:

The hypothesis that synaptotagmins act in a homomultimeric complex is based upon four principal pieces of evidence: the characterization of a dominant-negative SYTA mutant (Lewis & Lazarowitz, 2010), the 3-D structural modeling of the C_2B domain of SYTA, the functional significance of that modeling as demonstrated in protoplasts, and the research on animal synaptotagmins. However, before my study the formation of this complex, and whether the complex would be a dimer or tetramer, had not been directly delineated. Experiments on animal SYTs have come closest to showing complex formation when using assays of denatured SYT protein or atomic force microscopy with SYT protein fragments (Vrljic *et al*, 2010; Perin *et al*, 1991; Shahin *et al*, 2008). The experiments that used denatured protein were found to be unreliable because denatured proteins can aggregate through interactions that do not occur in natively folded proteins (Alberts *et al*, 2002). When proteins aggregate after being denatured, they can be observed as being multimers in sizing experiments. Atomic force microscopy experiments lack the resolution to distinguish between dimers and conformational changes because they only measure size in one dimension and do not consider particle density. In atomic force microscopy experiments, empty space that is shielded by a protein cannot be observed and will appear to be included in the volume of the protein. To test the hypothesis that individual SYTA proteins form a dimer or tetramer, I purified SYTA protein and

measured the size of a complex through direct observation in an *in vitro* assay. Observing a SYTA complex is an important advance in the understanding of both SYTA and the whole synaptotagmin family of proteins.

SYTA expression and purification:

Researchers purifying SYT proteins have been challenged by their relative insolubility in aqueous solutions. Because SYTs contain both a transmembrane domain and lipid binding domains, insolubility is likely to be a general feature of synaptotagmins (Groer *et al*, 2009). A possibility exists that the formation of a higher order protein complex enhances solubility positively by shielding some hydrophobic residues from the surrounding media. No direct evidence thus far has suggested that this complex forms because neither the existence of higher order structures has been demonstrated nor has the solubility of any SYT complexes been compared to a SYT monomer. Problems with protein solubility are one of the reasons why animal SYT research is often focused on the C_2 domains in *in vitro* studies (Vrljic *et al*, 2010).

To study SYTA protein *in vitro*, I optimized a standard metal affinity purification protocol to reliably produce purified SYTA in sufficient quantities for my biochemical assays. I accomplished this process by optimizing many steps in the procedure, including protein expression, cell lysis, buffer composition, resin washing, protein elution, and protein concentration. I expressed SYTA and its

mutants from pET28 in Rosetta(DE3)™ *E. coli* cells. Rosetta(DE3)™ cells carry an extra plasmid that corrects for the codon usage bias of *E. coli* and allows for the expression of proteins with a eukaryotic codon bias (Novagen, 2011; Baca & Hol, 2000). When the lactose analog IPTG binds with the *lac* repressor, SYTA expression from pET28 is driven by inducible expression of a T7 RNA polymerase and the encoded SYTA (Rosenberg *et al*, 1987). To express a soluble SYTA from the Rosetta(DE3)™ cells, I used a SYTA mutant ($SYTA^{\Delta TM}$) that had the N-terminal signal peptide and overlapping transmembrane domain (residues 1–32) deleted and replaced with a histidine tag (6xHis) for metal affinity purification (Figure 3–2). Lewis and Lazarowitz have shown that expression of $SYTA^{\Delta TM}$ does not disrupt native SYTA function when assayed, indicating this mutant is not toxic to cells (Lewis & Lazarowitz, 2010). Because it retains over 90% of the length of the native SYTA, I expected the $SYTA^{\Delta TM}$ mutant to form a complex equivalent to that of wild-type SYTA. This was working under the assumption that the transmembrane domain is not essential for dimer formation. When I expressed $SYTA^{\Delta TM}$ protein at 37°C, a large fraction of the expressed protein was insoluble and likely sequestered in *E. coli* inclusion bodies. This sequestration resulted in low yields of soluble $SYTA^{\Delta TM}$ protein (less than 0.1 mg/ml in a volume of 2 ml) from 1-liter cultures grown to high density (OD_{600} of ~0.7).

I optimized the expression of SYTA$^{\Delta TM}$ to retain more SYTA protein in a soluble form by expressing SYTA$^{\Delta TM}$ at different temperatures and inducing its expression with decreasing concentrations of IPTG (Figure 4–1). By reducing the

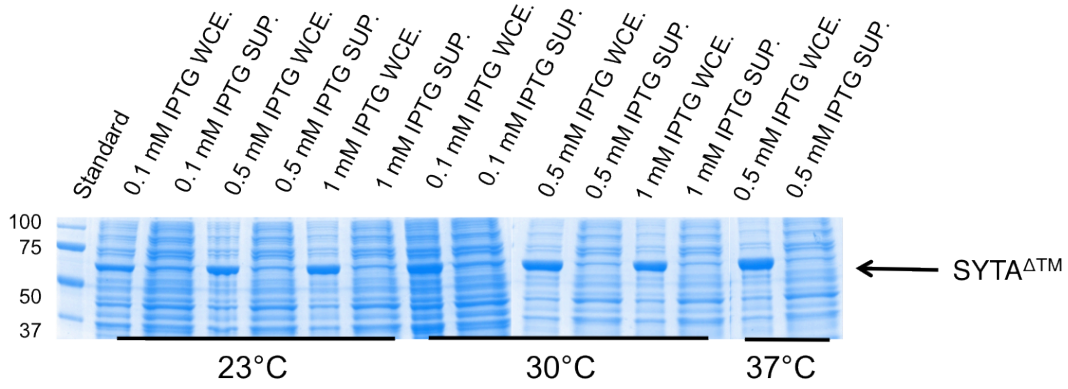

Figure 4-1: **Optimization Of SYTA$^{\Delta TM}$ Expression**. SDS-PAGE gel of SYTA$^{\Delta TM}$ expression in Rosetta(DE3) *E. coli* competent cells. Protein expressed at 23°C, 30°C or 37°C. Expression was induced with 0.1 mM, 0.5 mM, or 1 mM IPTG. After 3 hours of expression, the cells were collected and lysed to produce the whole cell extract (WCE). Centrifugation removed non-soluble proteins and cellular debris from the WCE. The soluble proteins remained in the supernatant (SUP). The WCE and SUP were loaded on a SDS-PAGE gel at a ratio of 1:2 (WCE:SUP). 60 ng of total protein was loaded in each SUP lane. The relative quantities of SYTA$^{\Delta TM}$ between the WCE and SUP were used to determine the conditions under which the greatest fraction of SYTA$^{\Delta TM}$ was soluble.

concentration of IPTG, I expected to reduce the rate of protein production, which put less stress on the protein synthesis machinery in *E. coli* cells. By reducing the expression temperature from 37°C to 23°C, a greater percentage of the total SYTA$^{\Delta TM}$ remained in the soluble fraction of the lysed cells (supernatant) instead of being found in the inclusion bodies (Figure 4-1). Decreasing the temperature likely increased the percentage of soluble SYTA both by slowing the rate of protein synthesis and SYTA protein accumulation. Since *Arabidopsis* normally grows between 18°C and 25°C, its proteins, including SYTA, and the interactions

between these proteins are be likely to be optimized for expression and folding at temperatures that are biologically relevant for the plant. Rapidly synthesized and accumulating protein is often less soluble and necessitates an *E. coli* cell sequester the protein in inclusion bodies rather than allowing it to be free within the cytosol. Both the concentration of IPTG, which is used to induce expression, and the temperature of the media, had a significant influence on the relative amount of soluble SYTA$^{\Delta TM}$ protein. Among the conditions I tested, 100 µM IPTG at 23°C had the greatest ratio of soluble SYTA$^{\Delta TM}$ protein to total protein (Figure 4-1). Given this optimization, the majority of the SYTA$^{\Delta TM}$ protein that I expressed in every condition was insoluble. My observation that native SYTA$^{\Delta TM}$ is generally insoluble is not surprising given that the same observation holds true with animal SYTs (Groer *et al*, 2009). By adapting the standard Rosetta(DE3)™ expression conditions recommended by the manufacturer (Qiagen, 2003), conditions were produced that favored the expression of soluble SYTA$^{\Delta TM}$. As a result, I realized an increased amount of soluble protein in the supernatant when the cells were lysed. I used these expression conditions for all subsequent protein preparations of SYTA$^{\Delta TM}$ and its mutants.

My purification of SYTA$^{\Delta TM}$ was optimized to improve yield without denaturing the protein. Because of the possibility of free Ca^{2+} ions promoting SYTA$^{\Delta TM}$ activity and, potentially, interactions with cellular membranes, I purified the protein with a standardized buffer in the presence of either 8 mM $CaCl_2$ (High

Ca^{2+}) or 0.2 mM EGTA (Ca^{2+} depleted). These concentrations were chosen based upon liposome binding studies with animal SYTs that showed clear preferences for either binding (8 mM $CaCl_2$) or not binding (0.2 mM EGTA) (Bhalla *et al*, 2008; Xu *et al*, 2009). The maximum protein yield after concentration (~0.8 mg/ml in a volume of 2 ml) was comparable in each condition. Purification in the presence of $CaCl_2$ was designed to provide an excess amount of Ca^{2+} ions. Purification in the presence of EGTA was designed to remove all free Ca^{2+} from the purification buffers by chelation. My procedure followed the general protocol for metal affinity purification, except for having a greater imidazole concentration in my elution buffer (Qiagen, 2003). I raised the imidazole concentration from the suggested 150 mM to 250 mM based on the

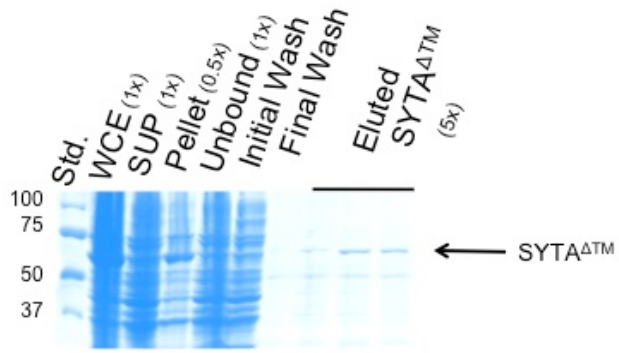

Figure 4-2: **Protein purification of SYTA$^{\Delta TM}$ by metal affinity purification**. SDS-PAGE of SYTA purification with TALON™ metal affinity resin in the presence of Ca^{2+}. After expression, competent cells were collected and lysed to create the whole cell extract (WCE). Centrifugation removed insoluble proteins resulting in supernatant (SUP) and pellet. Supernatant was applied to Co^{2+} resin. Resin was washed and proteins with low binding affinity were removed from the resin. Once the wash was protein free, enriched SYTA$^{\Delta TM}$ was eluted in fractions with 250 mM imidazole buffer; three of six fractions are shown. Relative volumes are indicated on the gel. After the eluted fractions were concentrated, the protein concentration was 0.8 mg/ml and the SYTA$^{\Delta TM}$ yield was 1.5% of total protein. Full details in materials and methods.

manufacturer's suggestion that proteins with low solubility elute more effectively with higher concentrations of imidazole. With this elution buffer, SYTA$^{\Delta TM}$ was eluted from the affinity resin in 6 ml of buffer (Figure 4–2). The SYTA$^{\Delta TM}$ enriched effluent could then be concentrated by centrifugal filtration to a volume of 2 ml.

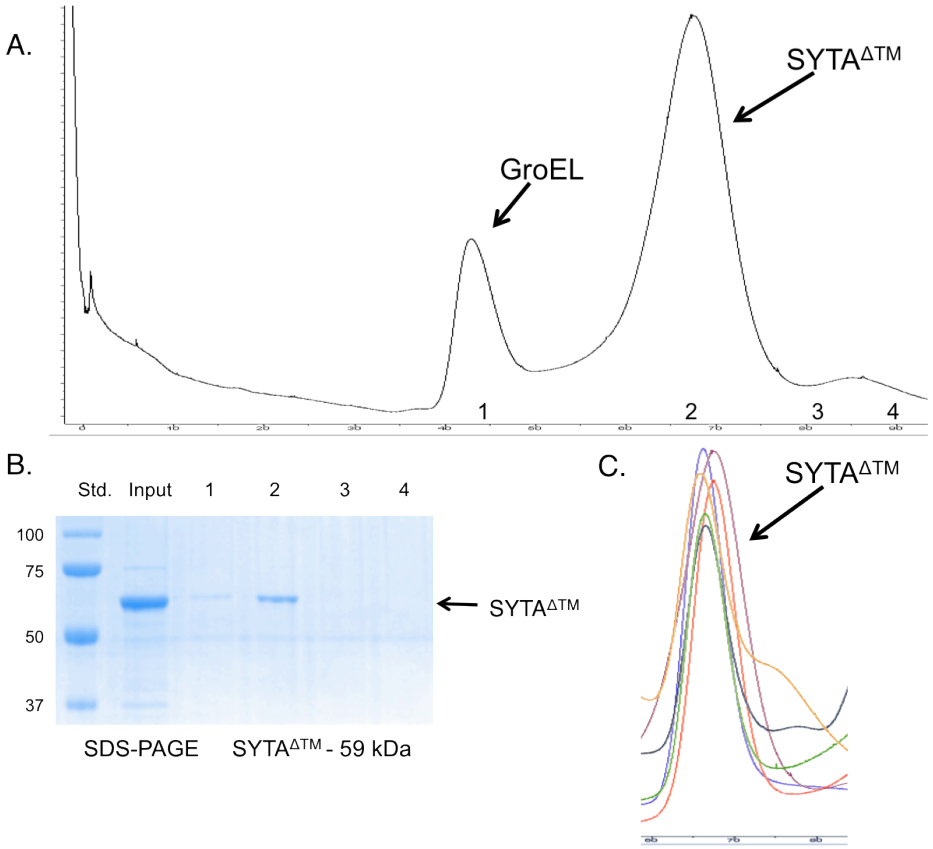

Figure 4-3: **Fast Protein Liquid Chromatography (FPLC) of SYTA$^{\Delta TM}$**. (A) FPLC effectively separated SYTA$^{\Delta TM}$ from its primary containment, GroEL from *E. coli*, based on the difference in size between the proteins. The SYTA$^{\Delta TM}$ protein flowed over the FPLC size-exclusion column at a rate consistent with being a dimer. Fractions were collected as they were eluted from the instrument. (B) The purity of SYTA$^{\Delta TM}$ protein was demonstrated with an SDS-PAGE gel where each of the numbers on the X-axis of the plot (A) corresponds to lane numbers on the gel. SYTA$^{\Delta TM}$ is a 59 kDa protein. (C) SYTA migrated consistently between individual FPLC purifications. The migration of the protein was not affected by Ca^{2+} availability or the presence of missense mutations. The FPLC runs overlaid here are WT + calcium (orange), WT + EGTA (green), E430A + calcium (violet), E430A + EGTA (blue), E433A + calcium (red), and E433A + EGTA (black).

My metal affinity purification, while effective in eliminating most contaminates, did not eliminate all of the contaminating proteins from SYTA$^{\Delta TM}$. To further purify SYTA$^{\Delta TM}$, I subjected the concentrated SYTA$^{\Delta TM}$ protein to gel filtration in order to separate and remove the contaminants. I selected fast protein liquid chromatography (FPLC) because its computer control allows for better repeatability between runs when compared to a bench-based gel filtration and because the system would allow me to track SYTA through the added purification. The repeatability allowed me to make qualitative comparisons between the individual samples. The *E. coli* GroEL protein was among the contaminants I separated from SYTA$^{\Delta TM}$ by FPLC (Figure 4–3A). I ran SYTA$^{\Delta TM}$ and each of the alanine missense mutants on the FPLC column under the same conditions, and I observed that protein was eluted with the necessary purity for subsequent assays (Figure 4-3B). Because FPLC is generally consistent between samples with similar molecule shape, the relative sizes of protein complexes can be compared in a related way, but the FPLC does not have a high enough resolution to allow one to make definitive conclusions about complex size quantitatively. Based upon comparison with other peptides utilizing the same FPLC program, the time at which the SYTA$^{\Delta TM}$ was eluted from the FPLC column was consistent with it having a molecular weight of approximately 120 kDa. This observation, while not conclusive, supports the hypothesis that SYTA$^{\Delta TM}$ forms a dimer. SDS–PAGE analysis indicates that fractions

corresponding to the FPLC peak, which is proposed to be SYTA$^{\Delta TM}$, do indeed contain SYTA protein (Figure 4–3 B).

SYTA forms a dimer:

I utilized native gel electrophoresis to test whether SYTA$^{\Delta TM}$ forms a dimer. However, purified SYTA$^{\Delta TM}$ protein did not migrate in the electric field. The protein failed to migrate because it has an isoelectric point of 7.18. Because the SYTA$^{\Delta TM}$ protein's charge is almost neutral (neutral isoelectric point is 7.0), the electric field pulls with near identical force in both positive and negative directions, which holds the protein in place (Bjellqvist *et al*, 1993). Given that the charges canceled each other out and that SYTA$^{\Delta TM}$ did not move, my native gel electrophoresis experiment did not provide any useful insight into the oligomerization of SYTA.

The isoelectric point limited the use of native gel electrophoresis as a method to study complex size. Instead, I employed laser light scattering to observe the oligomeric state of SYTA$^{\Delta TM}$. Two nearly identical experimental light scattering approaches are used to determine the size of particles that are either dissolved or suspended in solution: dynamic light scattering and static light scattering. The only distinction between dynamic light scattering and static light scattering is that the static approach collects light at fixed angles relative to the light source, whereas the dynamic approach can collect light at many angles. The

reason to select one over the other is that dynamic light scattering can compensate for destructive interference more effectively. Destructive interference is the effect where the opposing waveforms of two photons cancel each other out. When this occurs, light intensity is greatly diminished (Latimer & Pyle, 1972; Mullaney & Dean, 1970). The quantity of diffracted photons observed correlates to the angle of observation, the sample concentration, and the size of the particle being observed. When applied to protein studies, scattered photons can be used to study complex stability, nucleation, and size (Wilson, 2003; Nobbmann *et al*, 2007). When employing light scattering, laser light is applied to the sample and, in passing through the sample, some of the light is scattered out of the beam and can be detected at an angle off the line of the beam. The Rayleigh equation defines the relationship between these experimental variables and, in doing so, allows both the diameter and the volume of the particle to be derived. As structured globular proteins with molecular weights of at least 20 kDa generally have consistent densities (Fischer *et al*, 2004), average protein densities can be used to extrapolate accurate molecular weight observations from light scattering experiments. Using this assumption introduces error into the model; the standard deviation of molecular weights is estimated to be about 1% (Fischer *et al*, 2004).

The modified Rayleigh equation, as delineated below, includes the common density in lieu of solving for the density of SYTA$^{\Delta TM}$. The density ultimately is reflected in the values of the coefficients in the equation used with

proteins. This equation is solved based upon experimental data to calculate a molecular weight for each sample.

$$\frac{KC}{R_\theta} = \left(\frac{1}{M} + 2A_2C\right)P(\theta)$$

R_θ is the ratio of scattered to non-scattered light at a specific angle, which is the direct observation of the experiment. K is an optical constant specific to the solvent and wavelength of light used experimentally. C is the protein concentration. A_2 is the second virial coefficient, which quantifies the favorability of the solvent-solute interaction, and, specifically, the ability of the particle to become and remain suspended in solution. $P(\theta)$ is the angular scattering intensity and is a measure of how photons will scatter at a given angle. M is the molecular weight of the protein sample (Malvern, 2004).

This approach does make some assumptions, the most important of which is that the protein being sampled is a globular protein as opposed to being filamentous or any other shape. The protein being sampled should be as pure as possible to produce clear and defined peaks in the resulting data plots. Light scattering can be used to analyze the purity of protein for crystallization trials (Wilson, 2003). Because the molecular weight of SYTA$^{\Delta TM}$ expressed in *E. coli* is known to be 59.47 kDa, the anticipated size of both monomer and dimer can be predicted. The monomer should have a diameter of 6.8 nm (radius 3.4 nm) whereas the dimer should have a diameter of 9.2 nm (radius 4.6 nm) and a

molecular weight of 118.94 kDa. Further, because SYTA$^{\Delta TM}$ is larger than 20 kDa, the aforementioned density assumptions can reasonably be applied to SYTA$^{\Delta TM}$.

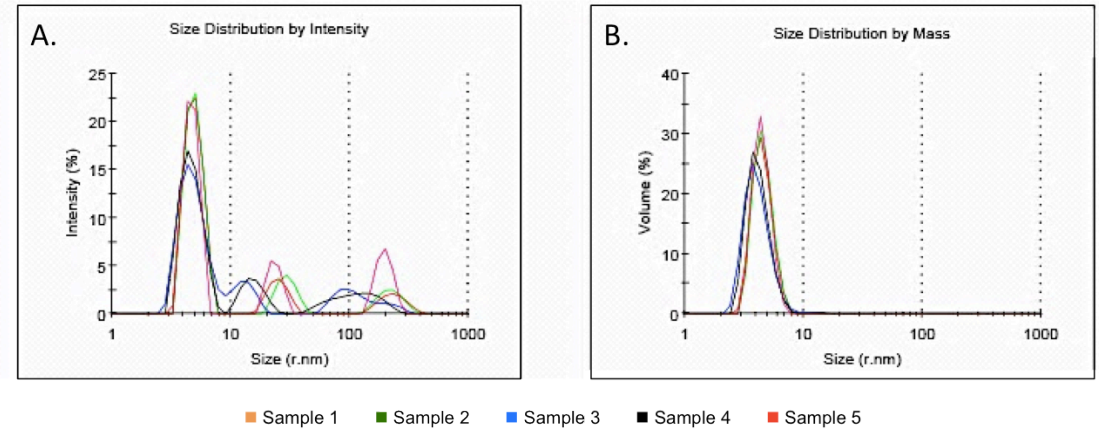

Figure 4-4: **Wild type SYTA$^{\Delta TM}$ size**. The radii of purified wild type SYTA$^{\Delta TM}$ protein complexes calculated from static light scattering measurements. (A) The plot of relative intensity has its largest peak at ~5 nm and some less voluminous peaks of greater radii. These large radii peaks are not consistent in size among all five samples. Because scattering is a property of particle volume, larger particles, presumably dust and aggregates, are over represented in peaks with larger radii on the intensity plot. (B) The distribution by mass plot corrects for the exponential relationship between scattered light and radius. This plot reveals a homogeneous population of particles of ~5 nm. These plots are the aggregated data of over 35,000 individual counts. Sample numbers correspond to samples in Table 4-1. SYTA$^{\Delta TM}$ is the predominant component of both plots as summarized in Table 4-2.

When I fired the laser at SYTA$^{\Delta TM}$ purified in the presence of Ca^{2+} using the static light scattering approach, I observed that SYTA$^{\Delta TM}$ had a radius that was measured to be about 4.8 nm and that this measurement remained unchanged regardless of the concentration at which the protein was sampled (Figure 4–4, Table 4-1). I scaled the light intensity output by particle mass because the relationship between light scattering and size is nonlinear and increases exponentially with size. I observed that nearly the entire sample, 99.8% by mass, was in a single population with a ~4.8 nm radius. This radius indicates that all of the protein in the sample was homogenous and had a single structural

arrangement. The molecular weight of SYTA$^{\Delta TM}$ is calculated to be 127 ± 18 kDa and represents 99.8% of the sample based on mass (Table 4–2). These results, derived from thousands of data points collected, indicated that purified SYTA$^{\Delta TM}$ forms a stable dimer.

Table 4-1: **Wild type SYTA$^{\Delta TM}$ size**. Calculated size of purified wild type SYTA$^{\Delta TM}$ protein at various concentrations. Sample numbers correspond to Figure 4-4. Calculated radii are all within 5% regardless of concentration tested.

Figure 4-4 Sample Number	[SYTA] (mg/ml)	Mean Particle Radius (nm)
1	0.82	4.93
2	0.55	4.96
3	0.41	4.91
4	0.27	4.71
5	0.16	4.72

Table 4-2: **Wild type SYTA$^{\Delta TM}$ is a dimer based on molecular weight**. Based upon the radii determined for SYTA$^{\Delta TM}$ (Figure 4–4, Table 4-1), the molecular weight of the purified SYTA$^{\Delta TM}$ can be determined. The percent intensity is a measure of the relative amount of light scattering in the sample caused by the SYTA. Because scattering is a property of volume of a particle, larger particles are overrepresented by intensity. The relative proportion of SYTA is calculated to correct for the large particle bias. The molecular weight is consistent with the predicted molecular weight of the SYTA$^{\Delta TM}$ dimer, thereby confirming that SYTA$^{\Delta TM}$ is a dimer.

Molecular Weight	Percent by Intensity	Percent by Mass	Total Counts	Oligimeric Structure
127 ± 18 kDa	64.0 %	99.8 %	35,125	Dimer

SYTA and SYTA missense mutants form Ca^{2+}-independent dimers:

With my prior findings in mind, I thought it would be important to demonstrate that the SYTA$^{\Delta TM}$ mutants that were targeting residues in the predicted SYTA C_2B Ca^{2+}-binding site could or could not form a dimer. Testing

whether the dimerization of SYTA is dependent on association with free Ca^{2+} ions was also important. Based on previous data, specifically the dominant-negative effect exhibited by $SYTA^{\Delta C2B}$, my hypothesis was that, like wild type $SYTA^{\Delta TM}$, point mutants in the C_2B domain would still form stable dimers. Such an outcome would fit this project's overarching hypothesis that dimerization, and the creation of a Ca^{2+} binding site in C_2B domain that results, is necessary for the endogenous function of SYTA. This hypothesis suggests that dimer formation does not depend upon Ca^{2+} binding between the two C_2B domains. Instead, the SYTA variable domain and/or C_2A domain are likely to be important in the formation of the dimer. A role for C_2B in dimer formation cannot yet be excluded. Any role the SYTA-C_2A domain has in dimer formation should be independent of the predicted C_2A Ca^{2+}-binding function because stable dimers can be purified in the absence of Ca^{2+} (in EGTA-containing buffers).

Based upon the calculated molecular weights of the $SYTA^{\Delta TM}$ proteins from my light scattering assay, the functionally defective SYTA missense mutants, E430A and E433A, form dimers (Table 4-3). In the case of the wild-type $SYTA^{\Delta TM}$, as well as the $SYTA^{\Delta TM}$ E430A and E433A mutants, dimers formed both in the presence of Ca^{2+} and in the presence of the chelating agent, which demonstrated that $SYTA^{\Delta TM}$ dimerization is a Ca^{2+}-independent event (Table 4–3). Regardless of the form of $SYTA^{\Delta TM}$ I tested in my assay or the availability of Ca^{2+} to it, $\geq$95% of the all particles observed in each sample were categorized as *in vitro*

dimerized SYTA$^{\Delta TM}$. My findings indicated the strength of the dimer interaction and showed that the defects in mutant SYTA function are not caused by a failure to dimerize.

Table 4-3: **SYTA$^{\Delta TM}$ mutants dimerize independent of Ca^{2+}**. When the SYTA missense mutants are sized by static light scattering, each has a size consistent with a SYTA$^{\Delta TM}$ dimer. The average particle radius of each sample and the mean molecular weight of each SYTA$^{\Delta TM}$ peak was independent of mutation introduced. At least 95% of every sample by mass is in the dimer population. Dimerization occurs in both the presence and absence of Ca^{2+}. Each sample reflects at least twelve separate measurements of >2000 individual counts (observed scattering events) each.

SYTA Mutant	Buffer Modification	Average Diameter	Molecular Weight (Mean ± SD)	Percent by Mass	SYTA$^{\Delta TM}$ Structure	Protoplast Localization
Wild Type	+ $CaCl_2$	9.431 nm	126.8 ± 17.7 kDa	99.8 %	Dimer	Endosomes
	+ EGTA	9.725 nm	137.2 ± 21.9 kDa	99.4 %	Dimer	
E430A	+ $CaCl_2$	8.792 nm	107.6 ± 16.8 kDa	97.8 %	Dimer	Plasma Membrane + ER
	+ EGTA	9.012 nm	122.3 ± 12.2 kDa	95.2 %	Dimer	
E433A	+ $CaCl_2$	8.984 nm	113.2 ± 19.5 kDa	99.9 %	Dimer	Delayed (>24h) to endosomes
	+ EGTA	9.122 nm	125.4 ± 13.9 kDa	98.0 %	Dimer	

SYTA dimer stability:

Demonstrating that the dimer exists under more biologically relevant conditions is essential to being confident in the functional relevance of the dimer. One of these biologically relevant conditions is the temperature. Using a dynamic light scattering system allowed me to change sampling temperatures without changing or disturbing the sample being sized. As a result, I could demonstrate that SYTA$^{\Delta TM}$ disassociated as temperature increased by comparing data from before and after the temperature change. At a low temperature (15°C), the dimer is clearly favored over the monomer and other oligomers (Figure 4–5). At plant

growth temperature (~20°C), the dimer is still favored, although to a much lesser extent. At 30°C, the dimer is more likely to disassociate. At a higher temperature (40°C), the monomer is favored. This difference between temperature-based samples may partly explain why expressing the SYTA$^{\Delta TM}$ in cells at 37°C results in the majority of the protein expressed being localized to inclusion bodies (Table 4-4).

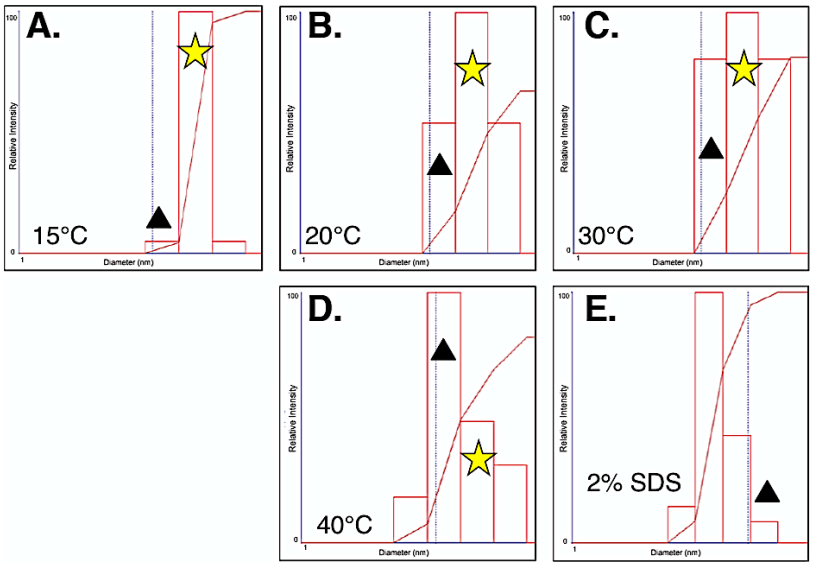

Figure 4-5: **Denaturation of SYTA$^{\Delta TM}$ dimer**. Dynamic light scattering protein radius of SYTA$^{\Delta TM}$ wild type at temperatures of (A) 15°C, (B) 20°C, (C) 30°C, and (D) 40°C shows that the relative amount of scattering due to the dimer form of SYTA$^{\Delta TM}$ (★) is greater than that of a disassociated SYTA$^{\Delta TM}$ monomer (⏏) at lower temperatures (15°C - 30°C). This includes at a biologically relevant temperature for *Arabidopsis* (B). When the temperature of the sample is 40°C, the monomer is favored. The vertical line indicates a diameter of 6 nm, roughly equivalent to the predicted diameter of a SYTA$^{\Delta TM}$ monomer. Histograms are plotted on a logarithmic scale and the largest column is normalized to 100%. Relative amounts of dimer and monomer are quantified in Table 4-4. When 2% SDS is added, the SYTA$^{\Delta TM}$ is fully denatured and appears much smaller than the monomer (E). As with static light scattering experiments, dust particles and other solids look large (in terms of quantity of light scattered) in dynamic light scattering experiments because the ability to scatter light goes up exponentially as radius increases. The formula for surface area of a sphere ($A=4\pi r^2$) is a can be taken as a simplified mathematical explanation of the effect of increasing particle radius on the ability of a particle to scatter light, a feature of a particle's surface area.

I demonstrated that the dimer is most strongly favored in lower temperature environments (20°C), the preferred temperature environments for *Arabidopsis*. Because the dimer is favored at ~20°C, a temperature at which *Arabidopsis*' can grow, my hypothesis, that this dimer is of functional significance, was confirmed. Complete denaturation of the purified SYTA$^{\Delta TM}$ dimer with 2% SDS demonstrated that the unstructured protein appeared smaller in size than even the monomeric SYTA (Figure 4-5E), which shows that high temperature does not fully denature individual SYTA$^{\Delta TM}$ proteins.[4]

Table 4-4: **Stability of SYTA$^{\Delta TM}$ dimer.** Comparison of relative light scattering intensities of wild type SYTA$^{\Delta TM}$ dimer and monomer at different temperatures as observed by dynamic light scattering (Figure 4-5). Too few trials of this experiment were completed to demonstrate statistical significance.

Temperature	Ratio of SYTA$^{\Delta TM}$ Dimer to SYTA$^{\Delta TM}$ Monomer
15°C	24
20°C	1.8
30°C	1.2
40°C	0.5

Membrane interaction:

As with all synaptotagmins, SYTA is predicted to be a Ca^{2+}-binding protein and phospholipid-binding protein (Craxton, 2004). A membrane binding assay with SYTA$^{\Delta TM}$ should demonstrate whether or not SYTA is capable of interacting

[4] It is important to present this result with the caveat that too few samplings were collected with the DLS instrument to calculate the statistical significance of this result. The DLS instrument operated and maintained by the Cornell Center for Materials Research was removed from the facility in early 2012 because "the instrument was no longer a good match for the mission and resources of the Center."

with membranes. The effect of the predicted SYTA C_2B Ca^{2+}-binding missense mutations on membrane interaction could detect whether defects of the mutants are related to impaired membrane binding by SYTA. This finding could reveal whether this site was important for SYTA-membrane interaction and whether the membrane interaction was dependent on Ca^{2+}, as is proposed to be the case for many synaptotagmin proteins.

To address this question, I attempted a membrane flotation assay. Initially, I used enriched membranes, which were derived from *Nicotiana benthamiana* leaves, as a model membrane for $SYTA^{\Delta TM}$ binding in this assay. The purified membranes were slightly opaque and could be seen with the naked eye in the reaction tubes. My expected result was that $SYTA^{\Delta TM}$ would bind to the membrane and float up in a high-density sucrose solution after centrifugation because of the low density of the lipid. However, this assay failed because it was ineffective in causing the floatation of SYTA above the densest highest percentage sucrose fraction. The opaque enriched membranes, having a tendency to precipitate in this assay, were visible as pellets at the bottom of the centrifuge tubes. In this assay, $SYTA^{\Delta TM}$ protein (both wild type and mutant) was retained in the bottom fraction (Figure 4-6). Because $SYTA^{\Delta TM}$ did not float, I could reach no meaningful conclusions about the protein-membrane interaction.

To optimize my assay, I experimented with changing several variables, which included the input concentration of $SYTA^{\Delta TM}$ protein, the input

concentration of membrane, the duration for which SYTA$^{\Delta TM}$ and the membranes could react before the addition of the sucrose, the reaction temperature, the primary antibody used in blotting, and the secondary antibody used in blotting. Each attempt at optimizing my assay was ineffective and not conclusive; therefore, I decided to use commercially available lipids instead of plant-derived membranes. Lipids derived from *Glycine max* (soy bean) extracts, with individual lipid compositions representative of plant total membrane composition (~20% phosphatidylcholine) and cellular membrane composition exempting large organelles (~40% phosphatidylcholine) (Li-Beisson *et al*, 2013), were substituted for the enriched membranes.

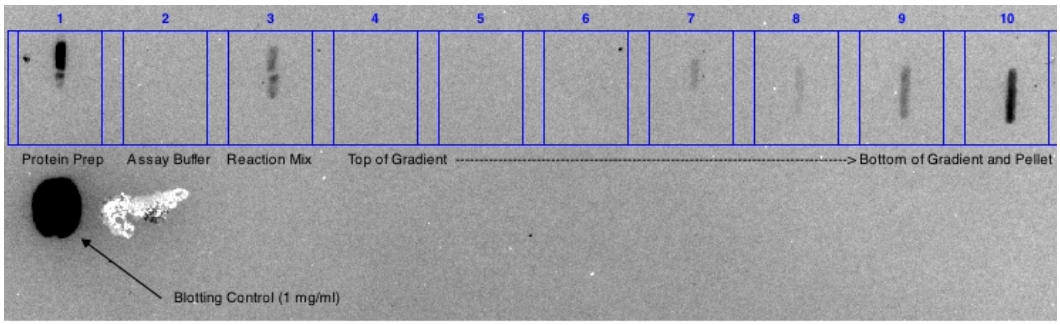

Figure 4-6: **SYTA flotation assay**: Dot blot of fractions collected from membrane flotation assay of SYTA$^{\Delta TM, E430A}$. The dots contained (l-r): purified protein (dot 1), assay buffer (dot 2), reaction mix (1/5 total reaction volume) (dot 3), and gradient fractions from top to bottom (dots 4-10). Protein purified in the presence of Ca^{2+} (dot 1) was combined with purified membranes to react (dots 3). The reaction was loaded at the bottom of a 4 - 40 - 67% (w/v) sucrose gradient and centrifuged. Bound protein was expected to float to the top of the gradient (dots 4 and 5) and unbound protein was expected in the pellet (dots 10). Instead, no protein floated to the top of the gradient (dot 4-6). The majority (61%) of the protein was in the pellet (dot 10). The remaining protein (39%) was distributed between the 40%-67% interface (dot 7) and the 67% sucrose layer (dots 8 and 9). Another 6xHis tagged protein was used as a control for the antibody (bottom). The blot was probed with anti-6xHis mouse antibody an anti-mouse secondary antibody conjugated to horseradish peroxidase (HRP). The chemiluminescence of HRP was detected with film for 1 minute.

I performed this assay twice, once with each of the two derived lipids. In each assay, as was the case with the plant-derived membranes, the SYTA$^{\Delta TM}$ protein remained predominantly in the highest density sucrose fraction. The expected outcome was that lipid bound SYTA$^{\Delta TM}$ would float and that unbound SYTA$^{\Delta TM}$ would pellet. My assumption was that by removing the added density in the membranes due to integral membrane proteins, vesicles would be more likely to float in the high-density sucrose solution. Even with this modification, the approach failed to yield any conclusive preference for a SYTA-lipid interaction.

Summary:

My work presents the first case of an assay demonstrating a synaptotagmin forming a stable dimer. This SYTA dimer exists at temperatures where *Arabidopsis* can grow, which, along with previous work, including the protoplast localization assay, supports my hypothesis that the dimer is functionally relevant. The formation of a SYTA dimer does not require free Ca^{2+} to be present. It may still require Ca^{2+} in order to be functional.

Mapping of the specific interactions between the two SYTA proteins that form the dimer has not yet been undertaken, but it is probable that such interactions involve the variable domain and the C_2A domain. Additional interactions may occur between C_2B domains. These interactions between C2B domains are not solely responsible for dimerization given that SYTA$^{\Delta C2B}$ is a

dominant negative and that a dimer forms even when SYTA C_2B is not functional in protoplasts. The VD may play an important role in dimer formation, specificity, and stability. The VD is the least well conserved domain across the synaptotagmin gene family in animals (Craxton, 2004). This variation could serve to guarantee that each synaptotagmin forms only homodimers. Because the SYTA dimer is formed independent of the predicted Ca^{2+} binding site of SYTA C_2B, and because it is favored at biological temperatures, it is likely that SYTA acts as a dimer during endosome formation at the plasma membrane and in recycling endosomes to the plasma membrane. Mutants that disrupt dimer formation or stability are required to test this possibility. If the interactions are mapped and such missense mutants are created, it may be possible to uncouple the specific functions of SYTA (both known and still unknown) if SYTA were to cycle into and out of being a dimer.

Utilizing a different approach to address the question of the role of Ca^{2+} and the dimer model in membrane interaction may be the best course of action considering the inability of the membrane/liposome flotation assay to be optimized and produce informative data. More fruitful approaches could include a liposome-pelleting assay or a mica-binding assay. A risk exists that the liposome-pelleting assay may be no more effective than the flotation assay due to the limited solubility of $SYTA^{\Delta TM}$. While setting up a liposome-pelleting assay, the protein-lipid complex would not be mixed with high-density sucrose buffer

solution. Instead, after being allowed to bind, the lipid and protein are loaded directly onto the top of a sucrose gradient and spun immediately after loading (Wang *et al*, 2009). Perhaps optimizing the pelleting assay could make a natural starting point for future related projects. However, because of the low solubility of SYTA, this assay would entirely miss any SYTA binding should the protein precipitate out of solution.

Another possible approach, preferred for animal SYTs, to optimizing either the flotation or pelleting assay is to only focus on the SYTA C_2A-C_2B fragment (Zhang *et al*, 2009). The mica-binding assay exploits the ability of mica to fracture into slightly negative charged, near perfect sheets. The negative charge attracts molecules, such as membrane interacting proteins, with affinity for negative charge, to bind. Binding can be observed by atomic force microscopy. This method has been successfully employed with animal SYT models (Shahin *et al*, 2008) and may be less prone to problems caused by the solubility of SYTA. The mica binding method is controversial because it is not biologically relevant. The charge density on the mica may not replicate that of the membrane one may want it to substitute for. Also, in the case of synaptotagmins, the C_2 domains need to insert a few residues into and possible induce the curvature of the target membranes to bind effectively (Paddock *et al*, 2011). Saludes *et al*. have shown that a fragment of rat SYT1 is correlated with high membrane curvature *in vitro* (Saludes *et al*, 2012).

Perhaps the most significant challenge limiting the success of the pelleting and flotation assays is the current understanding of plant membrane composition. Flotation assays with animal SYTs reveal that phosphotidylserine (PS) had to be a component of synthetic vesicles to observe protein-lipid binding (Bhalla *et al*, 2008). These experiments utilized vesicles that were 15% PS, whereas, PS represents only about 3% of the phospholipids in 7-week-old leaf extracts (Li-Beisson *et al*, 2013). Understanding the SYTA target membrane composition may be necessary to optimize these assays.

METHODS

Protein Expression

Rosetta™ (DE3) competent *E. coli* cells (EMD Millipore) containing pET28a-SYTA$^{\Delta TM}$ (or mutant variants) were grown at 37°C to OD_{600} of ~0.7 in LB media (10 g/L NaCl, 10 g/L tryptone, 5 g/L yeast extract) and protein expression was induced with 0.1 mM isopropyl 1-thio-β-D-galactopyranoside (IPTG) at 23° C. Three hours after induction the cells were collected by centrifugation (Qiagen, 2003).

Protein Purification

SYTA$^{\Delta TM}$ was purified as described (Qiagen, 2003) with TALON™ metal affinity resin (Clontech). All buffers included 50 mM NaH_2PO_4, 300 mM NaCl, 0.05% Tween 20 detergent, and 1 mM PMSF; only the imidazole concentration changed in each buffer. The imidazole used was 10 mM in cell lysis buffer, 20 mM in wash buffer and 250 mM in elution buffer. The three standard buffers were modified to include either 0.8 mM $CaCl_2$ or 0.2 mM EGTA, the concentration of each remaining constant throughout the purification. Cells were resuspended in lysis buffer (20 ml per 1 L of *E. coli* culture in LB media) and lysed by lysozyme digest (30 min, 50 mg/l lysozyme) and sonication (6 x 10 sec, intensity 4, Misonix Sonicator). Soluble compounds in the whole cell extract was separated from the insoluble compounds by centrifugation (10,000 x g for 20 min at 4°C). On average, 40-45% of SYTA$^{\Delta TM}$ expressed was soluble based on gel quantification

with Image Lab™ software (Bio-Rad). Soluble protein was applied to TALON metal affinity resin (Clontech), a Co^{2+} resin, according to the manufacturer's guidelines (1 ml per 20 ml lysis buffer) and washed with buffer by gravity flow. Wash volume was 100 ml per 1 ml of metal affinity resin. Protein was eluted in 6 x 1ml fractions. Eluted SYTA protein was concentrated by a factor of ~5 to the desired volume (~1.25 ml) with Amicon Ultra-4 protein MWCO 30K protein concentrators (Millipore). Protein concentrations of ~0.8 mg/ml were normal. This represents a yield of about 1 mg per 1 L of culture. The yield represented about 2-3% of total $SYTA^{\Delta TM}$ expressed and 5-6% of soluble $SYTA^{\Delta TM}$ based on gel quantification with Image Lab™ software (Bio-Rad). As figure 4-2 suggests, a significant majority of the $SYTA^{\Delta TM}$ protein was lost to the insoluble fraction that was removed by centrifugation. A significant quantity of $SYTA^{\Delta TM}$ protein was also lost in the course of washing the Co^{2+} resin.

The concentrated protein (~1.2 ml) was loaded and separated by size on the ÄKTA Fast Protein Liquid Chromatography system with 100 mM NaCl and 25mM HEPES buffer pH 7.0 (Hsu *et al*, 2012). FPLC runs were analyzed using UNICORN software (GE Healthcare Life Sciences). FPLC fractions were concentrated with Amicon Ultra-4 protein MWCO 30K protein concentrators to concentrations of ~0.5 mg/ml in 100 mM NaCl and 25 mM HEPES buffer for subsequent applications; 20% glycerol was added when long term storage (-80°C) was desired.

Native Gel Electrophoresis

Native PAGE was conducted with the Mini-PROTEAN® Tetra Cell system (Bio-Rad) using 8% acrylamide gels run in 25 mM Tris and 52 mM glycine buffer as described in the product manual (http://www.bio-rad.com/webroot/web/pdf/lsr/literature/10007296D.pdf)

Static Light Scattering

Proteins were sized with a Zetasizer Nano-ZS with a ZEN2112 cuvette (Malvern). The Zetasizer instrument was standardized with first toluene and then 100 mM NaCl and 25mM HEPES controls at 20°C as recommended by the facility manager. Scattering angle (θ) was fixed at 178° as described (Malvern, 2004). Zetasizer software was used to analyze the data. A minimum of 12 trials were conducted on each sample.

Dynamic Light Scattering

Protein was sampled with a BI-200SM dynamic light scattering system (Brookhaven Instruments). Light scattering angle was set to 90°. Proteins were sampled at different temperatures with the aid of the BI-200SMPt module in 100 mM NaCl and 25mM HEPES buffer. Counts were processed with the BI-200SM software.

Membrane Purification

Cellular membranes from homogenized *Nicotiana benthamiana* leaves were isolated, separated, and enriched by centrifugation as described (Ward *et al*, 1997). Fresh leaves from 6-8 week old plants were homogenized on ice with a Polytron homogenizer (3000 rpm for 3 min) in 10 ml grinding buffer (230 mM sorbitol, 50 mM HEPES, 10 mM KCl, 3 mM EGTA, 3 mM DTT, 1% BSA, and 1 mM PMSF). Homogenate was filtered with Miracloth and centrifuged (1000 x g for 15 min) to separate subcellular membranes (supernatant) from large organelles, cell wall, and other insoluble cellular contents. Centrifugation (5200 x g for 80 min) separated ER membranes (pellet) from other subcellular membranes (supernatant).

The yields of cellular lipids were quantified by phospholipid ashing. Determination of yield is based on comparison of each membrane sample to an inorganic phosphate standard (Kingsley & Feigenson, 1979). Membrane samples (0.5 µL to 5.0 µL) were heated at 200°C with 200 µL 10% (v/v) sulfuric acid and 20 µL 30% H_2O_2 for 1 hour or until all carbon was oxidized. Samples were hydrated with 480 µL of H_2O at 45°C. 0.5 ml Color reagent (0.05 mL 5% ammonium molybdate in H_2O (w/v), 0.45 mL H_2O and 0.01 gm ascorbic acid) was added, and after 20 min, absorbance (abs_{800}) was measured and plotted against the phosphate standard.

Lipid/Membrane Flotation

Lipids, either from enriched membrane or soybean leaf membrane extracts (Avanti Polar Lipids) were suspended in flotation buffer (100mM NaCl and 25mM HEPES at pH 7.4). SYTA$^{\Delta TM}$ (10 µl of 0.5 mg/ml) and lipid (15 µL of ~2 mg/ml) were incubated together at room temperature. The presence of soluble protein was confirmed with Bradford reagent (Bio-Rad). 75 µL of 67% sucrose (w/v) in flotation buffer was added to the reaction after 1 hour. In a 250 µl ultracentrifuge tube, 80 µl of the reaction was layered beneath 90 µl of 40 % sucrose in flotation buffer and 40 µl of 4 % sucrose in flotation buffer. The tubes were centrifuged at 87,000 rpm (325,000 x g) for 1 hour at 20° C in a TLA-100 rotor (Beckman) (Kaan, 2007). Fractions were collected after centrifugation and analyzed by immunoblotting.

Immunoblotting

Flotation samples were blotted onto nitrocellulose with a dot blot apparatus (Bio-Rad), probed with anti-6xHis mouse monoclonal antibody (Invitrogen), and detected by horseradish peroxidase activity using the ECL Advance Western Blotting Detection Kit (GE Healthcare Life Sciences).

WORKS CITED:

Alberts, B. *et al.* "*Molecular Biology of the Cell*." (Garland Science, New York, 2002).

Baca, A. M. & Hol, W. G. "Overcoming codon bias: a method for high-level overexpression of *Plasmodium* and other AT-rich parasite genes in *Escherichia coli*." *Int. J. Parasitol.* **30,** 113–118 (2000).

Bhalla, A. *et al.* "Analysis of the synaptotagmin family during reconstituted membrane fusion. Uncovering a class of inhibitory isoforms." *J. Biol. Chem.* **283,** 21799–21807 (2008).

Bjellqvist, B. *et al.* "The focusing positions of polypeptides in immobilized pH gradients can be predicted from their amino acid sequences." *Electrophoresis* **14,** 1023–1031 (1993).

Craxton, M. "Synaptotagmin gene content of the sequenced genomes." *BMC Genomics* **5,** 43-56 (2004).

Fischer, H. *et al*. "Average protein density is a molecular-weight-dependent function." *Protein Sci.* **13,** 2825–2828 (2004).

Groer, G. J. *et al.* "Expression and purification of soluble E-Syt2: low protein stability impedes tag removal." *J. Chromatogr. B Analyt. Technol. Biomed. Life Sci.* **877,** 1643–1650 (2009).

Hsu, F. *et al.* "Structural basis for substrate recognition by a unique *Legionella* phosphoinositide phosphatase." *Proc. Natl. Acad. Sci. U.S.A.* **109,** 13567–13572 (2012).

Kaan, H. Y. "Structure of BAR and PX domains of sorting nexin 9 reveals cooperativity in membrane binding." Cornell College of Agriculture and Life Sciences Honors Thesis (2007). at <http://hdl.handle.net/1813/7893>.

Kingsley, P. B. & Feigenson, G. W. "The synthesis of a perdeuterated phospholipid: 1,2-dimyristoyl-sn-glycero-3-phosphocholine-d72." *Chemistry & Physics of Lipids* **24,** 135–147 (1979).

Latimer, P. & Pyle, B. E. "Light scattering at various angles. Theoretical predictions of the effects of particle volume changes." *Biophys. J.* **12,** 764–773 (1972).

Lewis, J. D. & Lazarowitz, S. G. "*Arabidopsis* synaptotagmin SYTA regulates endocytosis and virus movement protein cell-to-cell transport." *Proc. Natl. Acad. Sci. U.S.A.* **107,** 2491–2496 (2010).

Li-Beisson, Y. *et al.* “Acyl-Lipid Metabolism.” in *The Arabidopsis Book* e0161 (2013). doi:doi: 10.1199/tab.0161

Mullaney, P. F. & Dean, P. N. “The small angle light scattering of biological cells. Theoretical considerations.” *Biophys. J.* **10,** 764–772 (1970).

Nobbmann, U. *et al.* “Dynamic light scattering as a relative tool for assessing the molecular integrity and stability of monoclonal antibodies.” *Biotechnol. Genet. Eng. Rev.* **24,** 117–128 (2007).

Paddock, B. E. *et al.* “Membrane penetration by synaptotagmin is required for coupling calcium binding to vesicle fusion *in vivo*.” *J. Neurosci.* **31,** 2248–2257 (2011).

Perin, M. S. *et al.* “Structural and functional conservation of synaptotagmin (p65) in *Drosophila* and humans.” *J. Biol. Chem.* **266,** 615–622 (1991).

Rosenberg, A. H. *et al.* “Vectors for selective expression of cloned DNAs by T7 RNA polymerase.” *Gene* **56,** 125–135 (1987).

Saludes, J. P. *et al.* “Detection of highly curved membrane surfaces using a cyclic peptide derived from synaptotagmin-I.” *ACS Chem. Biol.* **7,** 1629–1635 (2012).

Shahin, V. *et al.* “Synaptotagmin perturbs the structure of phospholipid bilayers.” *Biochemistry* **47,** 2143–2152 (2008).

Vrljic, M. *et al.* “Molecular mechanism of the synaptotagmin-SNARE interaction in Ca^{2+}-triggered vesicle fusion.” *Nat. Struct. Mol. Biol.* **17,** 325–331 (2010).

Wang, Q. *et al.* “Molecular mechanism of membrane constriction and tubulation mediated by the F-BAR protein Pacsin/Syndapin.” *Proc. Natl. Acad. Sci. U.S.A.* **106,** 12700–12705 (2009).

Ward, B. M. *et al.* The *geminivirus* BL1 movement protein is associated with endoplasmic reticulum-derived tubules in developing phloem cells.” *J. Virol.* **71,** 3726–3733 (1997).

Wilson, W. W. “Light scattering as a diagnostic for protein crystal growth: a practical approach.” *J. Struct. Biol.* **142,** 56–65 (2003).

Xu, J. *et al.* “Synaptotagmin-1 functions as a Ca^{2+} sensor for spontaneous release.” *Nat. Neurosci.* **12,** 759–766 (2009).

Zhang, Z. *et al.* “Phosphatidylserine regulation of Ca^{2+}-triggered exocytosis and fusion pores in PC12 cells.” *Mol. Biol. Cell* **20,** 5086–5095 (2009).

CHAPTER 5
Conclusions and Discussion

The *Arabidopsis thaliana* synaptotagmin SYTA was identified previously by its interactions with plant virus cell-to-cell movement proteins. Subsequent investigation revealed that SYTA regulates viral MP-directed cell-to-cell movement (Lewis & Lazarowitz, 2010). In plant cells, SYTA regulates endocytosis at the plasma membrane. In addition, and likely as a result of this function, SYTA has also been demonstrated to play roles in plant responses to both biotic stresses (Lewis & Lazarowitz, 2010) and abiotic stresses (Schapire *et al*, 2008; Yamazaki *et al*, 2008). SYTA$^{\Delta C2B}$ is a mutant form of the protein from which the predicted C_2B domain is deleted. The deletion of the C_2B domain abolishes SYTA function in endocytosis and inhibits MP cell-to-cell movement through the plasmodesmata in the presence of endogenous SYTA (Lewis & Lazarowitz, 2010). Analogous to animal synaptotagmins, the conclusion that the SYTA C_2B domain is dominant in relation to the C_2A domain and is essential for function in endocytosis was derived from the loss of function in SYTA$^{\Delta C2B}$. When investigated, such dominance is also observed in the exocytic function of animal synaptotagmins known to be involved in exocytosis (Lewis & Lazarowitz, 2010; Littleton *et al*, 2001; Südhof, 2013; Lee *et al*, 2013).

Arabidopsis SYTA and rat SYT1 are generally similar to each other, but there are several functional differences that exist between them. When endocytosis and exocytosis are uncoupled, either of the two SYT1 C_2 domains

can function as the Ca^{2+} sensor in endocytosis (Yao *et al*, 2012). Despite some similarity between the C_2 domains, evidence that both C_2A and C_2B domains are necessary for specific functions is growing (Lee *et al*, 2013). Interestingly, the C_2A domain of rat SYT7 has been demonstrated to be essential for asynchronous release of neurotransmitters when SYT1 is knocked out (Bacaj *et al*, 2013). Because SYT7 is anchored to the plasma membrane, the SYT7 C_2A domain is possibly adapted to specifically bind synaptic vesicle membranes. Based upon this model, one possible requirement for SYT function would involve each of the two C_2 domains having a specific membrane target. Because it is possible that some similar function exists between the SYTA C_2 domains and the equivalent domains from animal SYTs, the functional significance of SYTA C_2A may be revealed through membrane/compartment dynamics studies occurring at a distance from the plasma membrane. Any similar functions remain unknown because SYTA$^{\Delta C2A}$ and similar mutants have yet to be assayed for function (with the exception of some point mutants in this study). The possibility that the two domains could have different Ca^{2+}-lipid binding arrangements is in accord with my model of SYTA C_2A and C_2B (Figure 2-3) because this model predicts that the domains stabilize Ca^{2+} differently.

The ability of SYTA$^{\Delta C2B}$ to act as a dominant-negative mutant and, therefore, inhibit MP cell-to-cell movement in the presence of endogenous wild-type SYTA suggested that SYTA forms a dimer, or perhaps a tetramer, *in vivo*,

which has also been proposed for animal synaptotagmins. Supporting this conclusion, FM4-64 labeling studies and RabF1-GFP expression studies in *N. benthamiana* leaf cells showed that transient expression of SYTA$^{\Delta C2B}$ inhibited the formation of plasma membrane-derived endosomes (Lewis & Lazarowitz, 2010). In the presence of endogenous functional SYTA, the transient expression of SYTA$^{\Delta C2B}$ inhibited SYTA function in these assays, indicating that SYTA$^{\Delta C2B}$ functions as a dominant-negative mutant in endocytosis.

Researchers who have studied the related animal synaptotagmin proteins have postulated that those synaptotagmins function as either dimers or multimers in relevant systems (Perin *et al*, 1991). While some researchers have seen artifacts when working with full-length proteins, they have not shown conclusively that the animal SYTs form dimers or higher order complexes (Vrljic *et al*, 2011). Plant and animal researchers can learn from and be informed by each other in regards to their respective synaptotagmins, which are, in fact, similar. The demonstration in this report that *Arabidopsis thaliana* SYTA forms a dimer advances the understanding of the synaptotagmin family of proteins. At the very least, this study should encourage groups studying synaptotagmins to ask if deficiencies in dimer formation may account for defective mutant phenotypes.

The hypothesis that SYTA has a functional C_2B domain, and that SYTA forms a homoligomeric complex in order to function, was not universally accepted

(Schapire *et al*, 2008) regardless of how it functions in animals (Gaffaney *et al*, 2008). A competing hypothesis, which was based upon simple sequence alignments, argued that because the SYTA C_2B domain lacks the predicted residues necessary for a Ca^{2+}-binding site, plant SYTs are fundamentally different and do not have a functional C_2B domain. In this alternate hypothesis, SYTA C_2B is treated as being a monomer, but this hypothesis is the result of a far too simplistic analysis (Yamazaki *et al*, 2010). The model for SYT function in animal systems, as demonstrated in several studies, remains simple (Bacaj *et al*, 2013). Animal synaptotagmin publications often focus on only the C_2 domains and not the variable domain. The latter is, however, likely an important domain for dimerization (Gauer *et al*, 2012; Diao *et al*, 2009; Striegel *et al*, 2012). *In vitro* biochemical experiments tended to focus on just the C_2 domains. Up to the present time, many synaptotagmin experiments could not or would not distinguish between monomeric and oligomeric complexes as a consequence of SYT constructs and/or experimental design (Bhalla *et al*, 2008). A review of this research, where SYT fragments are treated as solitary units and free in solution, can give the impression that synaptotagmins function as monomers.

The goals of my project were to model how SYTA C_2B might bind Ca^{2+} in the case of a SYTA dimer, to test the dimer model for functional significance *in vivo* and to demonstrate the relevance of the dimer model by directly showing that $SYTA^{\Delta C2B}$ forms a dimer. Using threading model analysis of the SYTA C_2B

domain, I hypothesized that a Ca^{2+}-binding site would be created between both C_2B domains when the protein dimerized. The core of this site is comprised of two acidic residues, E430 and D431, which are capable of providing a sufficient localized negative charge for stable Ca^{2+} cation binding. In the primary sequence, one position removed from this pair of residues is a third acidic residue, E433, which could be expected to provide an additional negative charge to the site (Figure 2-4, Table 3-1, Figure 3-1). The dimer model predicted how the C_2B domain could bind Ca^{2+} to function as a regulator of endocytosis. Given that Yamizaki *et al*. predicted that monomeric SYTA C_2B was not capable of binding Ca^{2+} (Yamazaki *et al*, 2010), the dimer model provided a testable alternative to explain how the C_2B domain could bind Ca^{2+} ions.

Creating a series of alanine missense mutants that targeted the residues implicated as part of the proposed Ca^{2+}-binding site in a SYTA dimer allowed me to test this model. When expressed in transfected *Nicotiana benthamiana* protoplasts, all three missense mutants were found to localize to the plasma membrane rather than to endosomes after approximately 20 hours. After approximately 40 hours, only the two core binding site mutants, $SYTA^{E430A}$-GFP and $SYTA^{D431A}$-GFP, localized to the plasma membrane. At the 40-hour time, the $SYTA^{E433A}$-GFP mutant had localized to endosomes. The $SYTA^{E433A}$-GFP mutant changed a residue that was two amino acid residues away from the core of the proposed Ca^{2+}-binding site in the primary sequence of SYTA. Given my

hypothesis, that SYTA^{E433A}-GFP was not fully defective is not surprising. As the protoplast-based transient expression assay had previously been shown to correlate localization and function in endocytosis (Lewis & Lazarowitz, 2010), I was able to utilize it as a functional assay for SYTA in endocytosis. The failure of the SYTA^{E430A}-GFP and SYTA^{D431A}-GFP mutants to localize to plasma membrane-derived endosomes indicated that these key mutants are not functional in endocytosis. Showing that my missense mutants targeting the predicted Ca^{2+} binding site were either not functional or partially functional agreed with my hypothesis that the encoded residues (E430, D431 and E433) all have an important role in SYTA function in endocytosis. I found that SYTA^{E430A}-GFP and SYTA^{D431A}-GFP were not functional and that SYTA^{E433A}-GFP was partially functional. In accord with my threading model, mutants to the region of the C_2B domain aligning with the active site of the animal synaptotagmin C_2B domain (Set C, Table 3-1, Figure 3-1), all localized to endosomes, retaining wild-type function, which indicated that these residues and this site were not required for endocytosis from the plasma membrane.

The SYTA^{E433A}-GFP mutant was only delayed and not fully defective in function, which makes it an interesting case. The most likely scenario to aid in the recruitment of Ca^{2+} to the binding site is that only the E430 and D431 residues of SYTA bind Ca^{2+} and that the two E433 residues, one from each protein in the dimer, provide additional localized negative charge near this binding site. This

arrangement would be expected to increase the Ca^{2+} binding affinity of SYTA C_2B (Mehler & Solmajer, 1991).

Having tested my predictive model of SYTA C_2B as a dimer and observing similar results *in vivo*, my hypothesis that SYTA forms a dimer should be confirmed through direct observation. The flow rate of purified SYTA over an FPLC column was compatible with the formation of a dimer. While native gel electrophoresis would have been a simple method to demonstrate the dimer had formed, $SYTA^{\Delta TM}$ lacks a sufficient net charge to migrate in an electric field. Instead, I utilized laser light scattering to determine the size of purified $SYTA^{\Delta TM}$ and then calculated the corresponding molecular weight. The molecular weight measured for each $SYTA^{\Delta TM}$ mutant (wild-type and point mutants) was twice the molecular weight of an individual $SYTA^{\Delta TM}$ protein monomer, showing conclusively that purified SYTA exists as a dimer *in vitro*. This observation applied to both the predicted Ca^{2+}-binding site ($SYTA^{\Delta TM,E430A}$) and to its peripheral site ($SYTA^{\Delta TM,E433A}$). The $SYTA^{\Delta TM}$ dimers form independent of the availability of Ca^{2+} ions, the SYTA transmembrane domain, or the key C_2B domain residues for endocytosis. The formation of a dimer under the conditions of my assay suggests that some combination of the variable domain and the C_2A domain are essential for dimer formation. Both domains may play essential roles in dimer formation. The SYTA dimer is favored over the monomer at a biologically relevant temperatures (15-20°C), which suggests that the SYTA

dimer is the functionally active form of SYTA instead of the monomer. If the monomer is functionally relevant, or if it even exists at all, it should have been detectable by light scattering. However, every sample of $SYTA^{\Delta TM}$ that I tested *in vitro* was at least 95% dimer by mass at a temperature of 20°C in the static light scattering experiments; I did not detect any $SYTA^{\Delta TM}$ monomer. Some of the observable difference between the ratio of SYTA dimer in static and dynamic light scattering may be due to the absence of added Ca^{2+} or EGTA in the dynamic light scattering buffer. It is possible that binding of Ca^{2+} in the proposed C_2B binding site may add stability to the dimer.

My research is the first direct demonstration of any synaptotagmin forming a dimer. This conclusion, that SYTA forms a dimer, is important because it explains how $SYTA^{\Delta C2B}$ is able to act as a dominant-negative mutant to interfere with SYTA activity. Other *Arabidopsis* synaptotagmins may function as dimers similarly to SYTA. My primary sequence alignment between the five *Arabidopsis* SYTs indicates that at least two of the three acidic residues are conserved as acids in each SYT protein. Specifically, E430 is conserved in every SYT, D431 is conserved in SYTB, SYTD and SYTE, and E433 is conserved in SYTB and SYTC. Primary sequence alignments indicate that SYTD and SYTE have additional aspartic acid residues in their canonical Ca^{2+} binding site. However, SYTD and SYTE still have fewer acidic residues in this site than the animal synaptotagmins and are not expected to be capable of Ca^{2+} binding.

Alternative splicing in the gene that encodes the synaptotagmin SYTC produces two isoforms of the protein being translated. One isoform is a full-length SYTC protein (Uchiyama *et al*). The second is truncated after the variable domain and, consequently, lacks both Ca^{2+}-binding domains. SYTC is specifically found in "guard" cells where Ca^{2+} has been shown to play an important role in stomatal function (Uchiyama *et al*). The model for SYTC function, that the truncated isoform regulates SYTC activity by means of a direct interaction between variable domains of each isoform, is analogous to the effect of the dominant negative $SYTA^{\Delta C2B}$ mutants on SYTA function. This effect has been observed for other proteins involved in the reaction of plants to environmental stresses (Mastrangelo *et al*, 2012; Dubrovina *et al*, 2013) indicating a precedent for that similar regulation of SYTC. Having confirmed that a dimer is formed with a protein with 50% sequence similarity to SYTC, the dimer model likely applies to SYTC as well.

Localization of the more distantly related *Arabidopsis* SYTE protein in protoplasts is similar to that of SYTA (Figure 5–1). While the precise function of SYTE remains unknown, the comparable localization, the conservation of some key residues, and 31% sequence similarity support a correspondence in the functional mechanism at the molecular level. Future colocalization studies will reveal the extent to which SYTA localization and SYTE localization are similar.

My conclusion, that SYTA protein forms a dimer to function, will provide support for hypotheses related to SYTE function and the mechanism by which it functions in more thorough SYTE studies because the two are related.

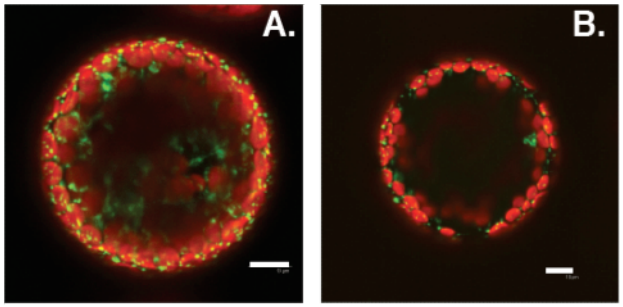

Figure 5-1: **Protoplast localization of *Arabidopsis* SYTE**. Projected CLSM Z-series of *Arabidopsis* SYTE-GFP in *N. benthamiana* protoplasts. When expressed in protoplasts, SYTE–GFP localizes to endosomes at both ~20 hours (A) and ~40 hours (B) post-transfection. Chlorophyll autofluorescence is shown in red in both panels. Scale bars 10 µm.

By broadening the understanding of plant SYTs, my conclusion that SYTA forms a dimer will be relevant to the understanding of animal synaptotagmins as well. Even though the consensus is that animal synaptotagmins likely function as dimers or tetramers, a significant faction of SYT researchers consider only C_2 domains from a single peptide. The direct demonstration of a plant synaptotagmin as being a dimer likely means that, in animals, synaptotagmins also function as dimers. This presumption would have to be tested on a case-by-case basis. Because dimerization is likely, the models of SYTs being studied can be refined. The more important realization that arises from this work is that the C_2B domains may act synergistically to carry out their function in Ca^{2+}-binding, as is proposed to be the case with SYTA C_2B from *Arabidopsis*. This synergistic

action could play a role in the interactions between mammalian SYT1 and the SNARE complex.

Studies of the SYT1-SNARE interaction in animals yield varying conclusions about the nature of the interaction, how SYT1 may coordinate docking and Ca^{2+} sensing, and the order in which the steps of exocytosis occur (Lai *et al*, 2011; Vrljic *et al*, 2010). Because of this uncertainty, multiple models for the mechanism of exocytosis, including the mechanism diagramed in Figure 1-5, have been proposed. Evidence exists that SYT1-SNARE interactions occur between C_2B and SNAP-25 (Choi *et al*, 2010), and for both SYT1 C_2 domains with the SNARE 4-helix bundle (Lai *et al*, 2011). Because many animal SYT studies on fusion and SNARE interactions use soluble C_2 domains in their assays, the effects of multiple identical C_2 domains interacting with a SNARE, as would be favored in the case of a dimer, may only be observed when a high concentration of protein fragments drive the binding equilibrium from unbound to bound states. The results of my project should encourage researchers to consider the synergistic effects that are created between domains as a consequence of dimer formation.

My results, as detailed and discussed in this study, should spur future synaptotagmin research. By establishing that SYTA functions as a true synaptotagmin, future experiments may be able to delineate further the

connections between plant and animal SYTs. Recent studies of yeast tricalbin proteins (Schulz & Creutz, 2004; Manford *et al*, 2012) show that those proteins may be able to be grouped with the synaptotagmins as a part of a family of SYT-like proteins. With the discovery of more shared properties between plant synaptotagmins, animal synaptotagmins, and yeast tricalbins, the probability that research on one protein can be used to create informative and predictive models of the others becomes higher. Considering this presumed similarity, tests on both plant and non-plant synaptotagmins are necessary to connect the understandings of both.

For the plant synaptotagmins, a few experiments could be initiated as a result of my research. Perhaps the best question to address is whether or not the SYTA point mutants that are defective in endocytosis are also defective in viral MP-directed cell-to-cell trafficking. If MPs depend on endosome recycling to function, testing the alanine missense mutants that I created based upon my SYTA C_2B dimer model should show that disrupting the site can inhibit MP activity. Testing this hypothesis with the MP cell-to-cell trafficking assay used by Lewis and Lazarowitz should reveal the frequency with which MPs can spread locally in the presence of SYTA mutants (Lewis & Lazarowitz, 2010). Second, to better understand how SYTA and different viral movement proteins interact, future projects may consider mapping the interactions between SYTA and viral movement proteins. Understanding these interactions may reveal strategies to

disrupt or inhibit a necessary interaction specific for some viruses. Third, one could map the residues involved in the native SYTA dimer formation to show definitively that a single domain or multiple domains catalyze the dimerization. Understanding the features involved in SYTA dimer formation and stability can also be used to help predict which other synaptotagmins may form dimers. In conjunction with an appropriate Ca^{2+} binding assay, mapping these residues may also reveal additional residues involved in Ca^{2+} binding by SYTA. Fourth, using light scattering, the other four synaptotagmins from plants can be tested to demonstrate that they form dimers as well. This experiment could provide evidence that supports the model that the truncated isoform of SYTC regulates SYTC activity through direct interaction. The observation of interactions between SYTC isoforms with the light scattering assay could be possible.

Animal synaptotagmin research might also benefit from testing for dimerization of the full-length SYTs outside of the transmembrane domain. This research could refine the models and consider more thoroughly the interactions between C_2 domains and any effects that interactions may have on protein function. With the assumption that animal synaptotagmins are dimers, as is predicted, research into the biochemistry and, perhaps, the structure of the proteins could lead to a significant enhancement in the understanding of both the SYTs and the proteins that complement their functions.

The tricalbins may also function as dimers. If both the plant and animal synaptotagmins dimerize, the probability that the tricalbins dimerize is quite high. Phylogenetic analysis of the C_2 domains of SYTs and SYT-like proteins reveals that both animal and plant synaptotagmins have more similarities to tricalbins than they do to each other (Craxton, 2004). The implication of the phylogenetic analysis is that the tricalbins can represent something of an intermediary in connecting plant and animal synaptotagmin research.

The diversity of the many eukaryotic synaptotagmins and extended synaptotagmins (tricalbins and E-SYTS) is likely to become more apparent in the future. Despite sharing the common architecture of signal peptide, transmembrane domain, variable domain, and C_2 domains, these proteins seem to have great specificity in where and how they function. These different functions have been observed for the *Arabidopsis* (Lewis & Lazarowitz, 2010; Uchiyama *et al*); with very similar structures, SYTA and SYTC have significantly different functions at the organismal level. Future studies may reveal the mechanistic similarities between these proteins, and the differentiation between them may be where and when they function in a cell. In accord with this hypothesis, synaptotagmins and extended synaptotagmins have been found to function at ER-PM contact sites, plasma membrane, endosomes, secretory vesicles, Golgi, and other organelles. (Giordano *et al*, 2013; Manford *et al*, 2012; Bacaj *et al*,

2013; Min *et al*, 2007; Lewis & Lazarowitz, 2010; Südhof, 2013; Yeo *et al*, 2012; Wakana *et al*, 2012; Zhang *et al*, 2011).

The results of my project, which have increased the understanding of SYTA function, could impact the real world. New and potentially important targets for the development of an antiviral strategy or a virus-resistant plant should result from greater knowledge of which residues of a regulator of virus cell-to-cell movement proteins are essential for the function of that movement protein. Because SYTA is able to regulate MP function for a spectrum of unrelated viruses, SYTA has the potential to become a viral control site. Because of the broad relevance of the SYTA C_2B domain and, by extension, because of the residues I identified in this project, this site may be more economically feasible to target than other viral targets. In the future, factors such as global population growth and climate change will necessitate increased crop yields. Additionally, inefficient agricultural processes, such as those currently in use in many developing nations, will see a greater strain from growing demand. Reducing the negative impact of plant viruses on crops is an obvious means by which agricultural productivity can expand. With the costs of agricultural products expected to rise as a result of this greater demand, research on techniques that could increase crop yields, including research into the function of SYTA, is likely to attract further consideration from scientists, policy makers, and investors.

WORKS CITED

Bacaj, T. *et al.* “Synaptotagmin-1 and synaptotagmin-7 trigger synchronous and asynchronous phases of neurotransmitter release.” *Neuron* **80,** 947–959 (2013).

Bhalla, A. *et al.* “Analysis of the synaptotagmin family during reconstituted membrane fusion. Uncovering a class of inhibitory isoforms.” *J. Biol. Chem.* **283,** 21799–21807 (2008).

Choi, U. B. *et al.* “Single-molecule FRET-derived model of the synaptotagmin 1-SNARE fusion complex.” *Nat. Struct. Mol. Biol.* **17,** 318–324 (2010).

Craxton, M. “Synaptotagmin gene content of the sequenced genomes.” *BMC Genomics* **5,** 43-56 (2004).

Diao, J. *et al.* “C_2AB: a molecular glue for lipid vesicles with a negatively charged surface.” *Langmuir* **25,** 7177–7180 (2009).

Dubrovina, A. S. *et al.* “The role of canonical and noncanonical pre-mRNA splicing in plant stress responses.” *Biomed Res. Int.* **2013,** (article 264314) 1-14 (2013).

Gaffaney, J. D. *et al.* “Synaptotagmin C_2B domain regulates Ca^{2+}-triggered fusion in vitro: critical residues revealed by scanning alanine mutagenesis.” *J. Biol. Chem.* **283,** 31763–31775 (2008).

Gauer, J. W. *et al.* “Mechanism for calcium ion sensing by the C_2A domain of synaptotagmin 1.” *Biophys. J.* **103,** 238–246 (2012).

Giordano, F. *et al.* “PI(4,5)P(2)-dependent and Ca^{2+}-regulated ER-PM interactions mediated by the extended synaptotagmins.” *Cell* **153,** 1494–1509 (2013).

Lai, A. L. *et al.* “Synaptotagmin 1 and SNAREs form a complex that is structurally heterogeneous.” *J. Mol. Biol.* **405,** 696–706 (2011).

Lee, J. *et al.* “Genetic analysis of synaptotagmin C_2 domain specificity in regulating spontaneous and evoked neurotransmitter release.” *J. Neurosci.* **33,** 187–200 (2013).

Lewis, J. D. & Lazarowitz, S. G. “Arabidopsis synaptotagmin SYTA regulates endocytosis and virus movement protein cell-to-cell transport.” *Proc. Natl. Acad. Sci. U.S.A.* **107,** 2491–2496 (2010).

Littleton, J. T. *et al.* “Synaptotagmin mutants reveal essential functions for the C_2B domain in Ca^{2+}-triggered fusion and recycling of synaptic vesicles *in vivo*.” *J. Neurosci.* **21,** 1421–1433 (2001).

Manford, A. G. *et al.* “ER-to-plasma membrane tethering proteins regulate cell signaling and ER morphology.” *Dev. Cell* **23,** 1129–1140 (2012).

Mastrangelo, A. M. *et al.* “Alternative splicing: enhancing ability to cope with stress via transcriptome plasticity.” *Plant Sci.* **185-186,** 40–49 (2012).

Mehler, E. L. & Solmajer, T. “Electrostatic effects in proteins: comparison of dielectric and charge models.” *Protein Eng.* **4,** 903–910 (1991).

Min, S. W. *et al.* “E-Syts, a family of membranous Ca^{2+}-sensor proteins with multiple C_2 domains.” *Proc. Natl. Acad. Sci. U.S.A.* **104,** 3823–3828 (2007).

Perin, M. S. *et al.* “Structural and functional conservation of synaptotagmin (p65) in *Drosophila* and humans.” *J. Biol. Chem.* **266,** 615–622 (1991).

Schapire, A. L. *et al.* “Arabidopsis synaptotagmin 1 is required for the maintenance of plasma membrane integrity and cell viability.” *Plant Cell* **20,** 3374–3388 (2008).

Schulz, T. A. & Creutz, C. E. “The tricalbin C_2 domains: lipid-binding properties of a novel, synaptotagmin-like yeast protein family.” *Biochemistry* **43,** 3987–3995 (2004).

Striegel, A. R. *et al.* “Calcium binding by synaptotagmin's C_2A domain is an essential element of the electrostatic switch that triggers synchronous synaptic transmission.” *J. Neurosci.* **32,** 1253–1260 (2012).

Südhof, T. C. “Neurotransmitter release: the last millisecond in the life of a synaptic vesicle.” *Neuron* **80,** 675–690 (2013).

Uchiyama, A. *et al.* “*Arabidopsis* SYTC.” *In preparation*

Vrljic, M. *et al.* “Molecular mechanism of the synaptotagmin-SNARE interaction in Ca^{2+}-triggered vesicle fusion.” *Nat. Struct. Mol. Biol.* **17,** 325–331 (2010).

Vrljic, M. *et al.* “Post-translational modifications and lipid binding profile of insect cell-expressed full-length mammalian synaptotagmin 1.” *Biochemistry* **50,** 9998–10012 (2011).

Wakana, Y. *et al.* “A new class of carriers that transport selective cargo from the trans-Golgi network to the cell surface.” *EMBO J.* **31,** 3976–3990 (2012).

Yamazaki, T. *et al.* “Calcium-dependent freezing tolerance in Arabidopsis involves membrane resealing via synaptotagmin SYT1.” *Plant Cell* **20,** 3389–3404 (2008).

Yamazaki, T. *et al.* “Arabidopsis synaptotagmin SYT1, a type I signal-anchor protein, requires tandem C_2 domains for delivery to the plasma membrane.” *J. Biol. Chem.* **285,** 23165–23176 (2010).

Yao, J. *et al.* “Uncoupling the roles of synaptotagmin I during endo- and exocytosis of synaptic vesicles.” *Nat. Neurosci.* **15,** 243–249 (2012).

Yeo, H. *et al.* “Developmental expression and subcellular distribution of synaptotagmin 11 in rat hippocampus.” *Neuroscience* **225,** 35–43 (2012).

Zhang, H. *et al.* “Golgi apparatus-localized synaptotagmin 2 is required for unconventional secretion in Arabidopsis.” *PLoS ONE* **6,** e26477 (2011).